Stability of the Thermohaline Circulation in analytical and numerical models

Stabilität der thermohalinen Zirkulation in analytischen und numerischen Modellen

---

Gerrit Lohmann

Ber. Polarforsch. 200 (1996)
ISSN 0176 - 5027

Gerrit Lohmann
Max-Planck-Institut für Meteorologie
Bundesstraße 55
D-20146 Hamburg

Die vorliegende Arbeit ist die inhaltlich unveränderte Fassung einer Dissertation, die 1995 dem Fachbereich Physik/Elektrotechnik der Universität Bremen vorgelegt wurde.

Contents

Zusammenfassung

Störungen im Oberflächensaltzgehalt des Nordatlantiks können eine drastische Veränderung des großskaligen ozeanischen Wärmetransports und damit des globalen Klimas zur Folge haben. Die Stabilität der ozeanischen thermohalinen Zirkulation im Hinblick auf diese Störungen wird mit Hilfe von gekoppelten Ozean-Atmosphäre (-Meereis) Modellen unterschiedlicher Komplexität untersucht.

Als atmosphärisches Modell dient hierzu ein Energiebilanzmodell (EBM), das die Süßwasser- und Wärmeflüsse an der Ozeanoberseite vorraussagen kann. Es zeigt sich, daß dieses Modell eine geeignete obere Randbedingung für den Ozean darstellt. Ein gekoppeltes atmosphärisches EBM-ozeanisches Zirkulationsmodell zeigt, daß der atmospärische Wärmetransport eine wichtige destabilisierende Rolle für die Zirkulation darstellt, während die anomalen Süßwasserflüsse von untergeordneter Bedeutung für die Zirkulation sind. Um die Sensitivität der thermohalinen Zirkulation für eine ganze Reihe von Randbedingungen zu verstehen, ist ein Boxmodell entwickelt worden, das als einfachstes gekoppelte System angesehen werden kann. Die lineare Stabilitätsanalyse zeigt, daß unter Berücksichtigung der atmosphärischen Transportprozesse die Sensitivität der Zirkulation gegenüber Störungen neu beurteilt werden muß.

Sich selbsterhaltende Oszillationen werden in einem atmosphärischen EBM-ozeanischen Zirkulationsmodell beobachtet, in dem der meridionale Salzgradient relativ stark ist. Es zeigt sich, daß dieser Zustand wesentlich empfindlicher auf Störungen reagiert als Zustände mit kleinerem meridionalen Salzgehaltsgradienten, was auch mit dem analytischen Modell im Einklang steht.

Die Rückkopplungseffekte im gekoppelten Atmosphäre-Ozean-Meereissystem werden mit Hilfe eines gekoppelten Modells, das ein thermodynamisches Meereismodell, obiges EBM und ein ozeanisches Zirkulationsmodell enthält, herausgearbeitet. Es zeigt sich, daß durch eine Störung im Oberflächensalzgehalt ein anderer Zustand des Modells entsteht, in dem die Atmosphäre kälter, die Meereisbedeckung und der atmosphärische Wärmetransport zugenommen haben, hingegen der nordwärtige ozeanische Wärmetransport und die Konvektionstiefe des Nordatlantischen Tiefenwassers reduziert sind. Dieser Zustand ist konsistent mit Zuständen, die nach dokumentierten Klimaveränderungen durch Süßwassereinträge gefunden wurden.

Abstract

Freshening of high latitude surface water in the North Atlantic can change the poleward oceanic transport of heat and salt with drastic effects on the global climate. The sensitivity of the thermohaline circulation is analyzed with respect to these perturbations. The study is based on coupled ocean-atmosphere (-sea ice) models with different levels of complexity in idealized geometries of the Atlantic ocean.

An atmospheric energy balance model (EBM) is constructed which predicts the heat and fresh water fluxes at the surface. The response of the EBM to sea surface temperature anomalies and radiative forcing is consistent with complex atmospheric models.

For a range of coupled models it is shown that the atmospheric transport affects the stability of the thermohaline circulation (THC). Coupled atmosphere EBM-ocean circulation model experiments show that the atmospheric heat transport is an important destabilizing effect while changes in fresh water flux are of minor importance for the THC. To understand the sensitivity of the THC for a range of atmospheric boundary conditions, a box model is designed, as it is considered the most simple atmosphere-ocean system. The analytical investigation shows how the stability of the THC is affected by the representation of the atmospheric transport of heat and moisture and the basic state.

Depending on the strength of the meridional salinity gradient, self-sustained oscillations do appear in a coupled atmosphere EBM-ocean circulation model. It was found that the oscillatory state is more sensitive to perturbations than basic states with moderate meridional salinity gradients which is consistent with the analytical model.

The sensitivity and feedback mechanisms affecting the THC are examined in a coupled ocean-atmosphere-sea ice system. The EBM is coupled with an ocean circulation model which includes a thermodynamic sea ice model. Due to a perturbation in high latitude salinity, the THC evolves into another steady state with decreased atmospheric temperature, more sea ice, enhanced atmospheric heat transport, and decreased oceanic heat transport. The formation of intermediate water and cessation of deep convection in the northern North Atlantic is consistent with well documented paleoclimatic climate shifts caused by a fresh water release.

Chapter 1

Introduction

The oceanic thermohaline circulation (THC) is a major component of the climate system, transporting heat and salt poleward. The sensitivity of today's THC, which is characterized by strong poleward heat and salt transports in the North Atlantic, has motivated the presented work. The deep water formation in the northern North Atlantic seems to be a sensitive part affecting the large-scale thermohaline driven circulation.

In the regions of deep water formation in the North Atlantic relatively small amounts of fresh water added to the surface can stabilize the water column to the extent that convection is prevented from occurring. Such interruption decreases the poleward mass transport in the ocean. Furthermore, perturbations of the meridional transport in the ocean can be amplified by positive feedback in the salt transport. A weaker northward salt transport brings less dense water to high latitudes, which further reduces the meridional transport.

The conveyor belt can turn on and off within decades influencing local and global climate. The younger dyras cooling about 11,000 years B.P. broke into the Holocene with about 3 degrees colder global mean temperature. This intermediate cold period lasted hundreds of years and is thought to be associated with a slowed down thermohaline circulation.

Paleoclimate studies show that changes in the THC are linked to meltwater events originating from retreating glaciers of the Barents shelf and North America (Keigwin et al., 1991) or from calving icebergs in the North Atlantic (Bond, 1995 and references therein). High-resolution records from the deep western basin of the North Atlantic suggest that an absence of North Atlantic deep water formation was associated with a meltwater input $16,900 - 17,100$ years B.P. (Sarntheim et al., 1994). These intermediate cold periods began with abrupt warming within a few decades due to external forcing followed by cooling which may be linked to a reduction of the THC. Variations in solar radiation due to orbital parameters (Berger, 1978) may trigger changes in atmospheric and oceanic conditions. Indeed, foraminiferans in sediment cores indicate ocean circulation changes occurring synchronously with

terrestrial climate changes (Boyle and Keigwin, 1987).

During these different climatic states, modified atmospheric conditions (e.g. the hydrological cycle) are expected (Broecker et al., 1990). It it therefore natural to ask which processes in the climate system affect the stability of the conveyor belt. The sensitivity of the large-scale thermohaline driven circulation is strongly determined by fluxes at the upper ocean surface. Therefore, correct physical representations of these fluxes are required in models.

A range of climate models with different levels of complexity are used to isolate the relevant sources of feedback of the coupled system. The study presented here is based on coupled ocean-atmosphere (-sea ice) models in idealized geometries of the Atlantic ocean. The results may be helpful to understand climate variations induced by changes in the THC.

Previous numerical studies (e.g. Bryan, 1986; Marotzke and Willebrand, 1991; Stocker and Wright, 1991) show that the deep water formation could be halted if the surface water became capped by low salinity water, thereby leading to a "polar halocline catastrophe" (Bryan, 1986). Another stable state of the thermohaline circulation evolves under nearly identical surface forcing. These different steady states have been connected to the different roles of the Atlantic and Pacific ocean (Stocker and Wright, 1991) or to a different balance between thermal and haline effects driving the present day conveyor.

The THC in the North Atlantic is characterized by deep water formation, transporting warm and salty surface water poleward which is sometimes called "salinity conveyor belt" (Broecker and Peng, 1989). Therefore, the THC gives rise to high surface salinities and warm water which pushes, on annual average, the ice margin to about 70^0 N. The high latitude Atlantic ocean releases enormous amount of heat to the atmosphere as the surface water cools. In contrast to the Atlantic, the THC in the North Pacific is characterized by a wind driven circulation combined with intermediate water formation (Warren, 1983). These different parts of the present conveyor belt do strongly affect characteristic climatic conditions, e.g. the relative mild climate in northern Europe. A changed oceanic circulation would therefore influence the regional climatic conditions and would probably lead to a climate shift.

A complete breakdown of the circulation induced by a perturbation in surface salinity at high latitudes, however, did not take place even when a large input of melt water entered the northern North Atlantic during the last deglaciation (Lehmann and Keigwin, 1992; Sarntheim et al., 1994; Bond, 1995). The THC cell in the northern North Atlantic was shallower and the sites of deep water formation have shifted southward. These different modes which occurred in the past are related to climatic changes observed in Greenland ice-core records (Broecker et al., 1985).

The models showing a complete breakdown of the THC use too idealized boundary conditions (prescribed fresh water flux and fixed atmospheric temperature). Because atmospheric processes are neglected, these models cannot correctly describe the sensitivity of the coupled atmosphere-ocean system. Experiments with changed heat flux parameterizations (e.g. Stocker et al., 1992; Zhang et al., 1993; Rahmstorf and Willebrand, 1995; Lohmann et al., 1995 a) show a more stable THC. It is only recently that coupled models, including atmospheric transport of heat and moisture, have been analyzed to understand stability and variability of the THC (Delworth et

al., 1993; Nakamura et al., 1994; Lohmann et al., 1994, 1995 a b).

In this thesis it will become apparent that the sensitivity of the coupled system strongly depends on the large-scale feedback processes included, some of them are explored in chapter 2. A priori it is not obvious which of the mechanisms included will dominate the response of the system which strongly depends on the physical representation of the climatic components.

Furthermore, the theoretical and numerical analysis will indicate that the stability and variability of the circulation is strongly affected by its own characteristics, for example the strength of the mass transport, the relative roles of meridional salinity and temperature gradients and the strength of the hydrological cycle. The basic methods used in the presented work and the structure of the thesis will be described in the next paragraph.

Methods and Strategy

To explore the physical feedback related to the thermohaline circulation, a physically based theory is required. Continuum mechanics as a non-relativistic, macroscopic field theory are applied to the media water, air, snow and ice. The governing equations of the theory is the balance of mass, momentum, angular momentum and energy (Landau and Lifschitz, 1970). The set of equations are closed with assumptions about the considered materials. For the media air and water isotropic Newton fluids are assumed. The governing momentum equations for isotropic Newton fluids are the Navier-Stokes equations.

Considering the interactions of thermohaline circulation with the other climate components would require a fully coupled atmosphere-ocean-ice model. However, such a model is too costly for computers of the present generation to perform several runs with hundreds of years of integration. Furthermore, even today's highly complex coupled circulation models (GCMs) do not describe the coupled system without ad hoc (and rather unphysical) flux corrections. It is useful to understand and to extract the involved feedback mechanisms with simplified components (e.g. the atmosphere) in a coupled model.

The analytical and numerical studies will show that the formulation of boundary conditions for the upper ocean implies an atmospheric model. The sensitivity of the thermohaline circulation is strongly affected by the kind of boundary conditions used. Therefore, it is obvious to look for simple atmospheric models which adequately describe the sensitivity of the coupled atmosphere-ocean system.

Recently, energy balance models (EBMs) with variable meridional atmospheric transports have been coupled to ocean models (among others Stocker et al., 1992; Rahmstorf and Willebrand, 1995; Lohmann et al., 1995 a). EBMs are computationable inexpensive models and their effects on the coupled system can be easily understood. Furthermore, coupling a carefully tuned EBM to an ocean model, unphysical flux corrections can be avoided which may have a strong influence on the sensitivity of the coupled system (Marotzke and Stone, 1995).

The EBM, used for most experiments as an upper ocean boundary condition, will be presented in chapter 3. Neither the vertical nor the longitudinal structure in the atmospheric model are resolved. The energy balance model explores some sources of feedback in the climate system, but should be seen as a first step to understand features of the highly complex climate system. In a stand alone mode, the atmospheric model is tested in response to sea surface temperature anomalies and radiative forcing (chapter 4). Features seen in GCMs can be qualitatively reproduced.

An ocean circulation primitive equation model is described in chapter 5. The numerical model with the acronym MOM is a standard model solving the primitive equations (Bryan, 1969; Cox, 1984). Therefore, only a short description is given in section 5.2 of this ocean general circulation model (OGCM).

Experiments with a coupled ocean circulation-atmospheric energy balance model (OGCM-EBM) are presented in chapter 6. These experiments provide some insight into the relative role of atmospheric transports and fresh water flux for the sensitivity of the THC. The experiments show that the total heat transport (atmosphere+ocean) is nearly unaffected by a perturbation of the fresh water flux. Atmospheric heat transport destabilizes the THC in the coupled system since enhanced atmospheric heat transport is associated with less oceanic heat transport and vice versa. Depending on the formulation of the boundary conditions transitions to other stable states are observed.[1]

The stability of the THC in the North Atlantic is assessed by a linear stability analysis of a simple coupled model (chapter 7 [2]). A box model approach is used, as it is considered the most simple atmosphere-ocean system. A range of climate models with different assumptions about the atmospheric transport are used to isolate the relevant feedback of the system.

Box models are a useful tool for studies of the stability and variability of the THC. These models have no zonal and only crude vertical and meridional resolution. In chapter 8 the time dependent response of a coupled box model to additional forcing is considered. The model is forced by additional radiation which may come from increased tracer gas concentrations in the atmosphere. Furthermore, the variability of the stochastically driven box model shows the integrating effect of the ocean circulation (typical red-noise spectrum). The oceanic heat transport in this coupled model shows a variability about the deterministic stable steady state on decadal time scale excited by purely random weather fluctuations.

To detect climate warming trends, it is an important issue to estimate natural variations within the Earth's climate system. Therefore, mechanisms relevant for natural variability should be considered in coupled models with different levels of complexity. The variability of a coupled oceanic circulation - atmospheric energy balance model is investigated in chapter 9. The mechanism of such variability is explored which seems to be mainly an oceanic phenomenon. The horizontal distribution of high latitude salinity leads to horizontal density gradients and therefore to motion which itself influences the density field.

---

[1] Part of this chapter will appear in the journal "Climate Dynamics" (Lohmann et al., 1995 a).

[2] A great part of this chapter is identical to a publication of Lohmann et al. (1995 b) which will appear in the journal "Tellus".

Sea ice significantly alters the sensitivity of the coupled system. Only few studies (Yang and Neelin, 1993; Zhang et al., 1994; Lohmann et al., 1994) employ the feedback mechanisms including sea ice. A thermodynamic sea ice model is coupled to the atmosphere-ocean system (chapter 10). The experiments in chapter 10 indicate that the stability of the THC depends on the chosen boundary conditions and feedback mechanisms included (e.g. the representation of the atmospheric heat transport) in the coupled ice-ocean-atmosphere system. The analysis may be a good starting point to understand more complex coupled models including sea ice.

Conclusions are given in chapter 11.

Chapter 2

Looking for adequate boundary conditions

In the coupled ocean-atmosphere system the fluxes of heat and fresh water affect the oceanic surface salinity and temperature in different ways. Local sea surface temperature anomalies are damped by a coupling between the ocean surface and the atmospheric boundary layer through sensible and latent heat fluxes, whereas there is no corresponding fast mechanism for sea surface salinity anomalies. A recent anomaly of surface salinity in the northern North Atlantic, the Great Salinity Anomaly (GSA), thus persisted for more than a decade (Dickson et al., 1988).

A common technique to get a realistic oceanic circulation in numerical models is to restore the sea surface temperature T and salinity S to fixed climatological values T^* and S^*:

$$A_{HV}\,\partial_z T = -\frac{\Delta z}{\tau_T}(T - T^*) = -\frac{\gamma}{\rho_0 c_p}(T - T^*) \tag{2.1}$$

$$A_{HV}\,\partial_z S = -\frac{\Delta z}{\tau_S}(S - S^*) = Q_s^* \quad . \tag{2.2}$$

The time constant τ_T is chosen such that the heat flux rate γ is about $50\,Wm^{-2}K^{-1}$ (Haney, 1971). The depth of the upper ocean layer is denoted by Δz. Furthermore, ρ_0 and c_p are the density and heat capacity of sea water ($10^3 kg\,m^{-3}$, $4.210^3 Jkg^{-1}K^{-1}$) and A_{HV} is the vertical diffusivity for the tracers. The time τ_S is usually chosen to be equal to τ_T.

For salinity there is no physical basis for restoring the surface salinity to S^*. The most simple physically reasonable boundary condition is to prescribe the salt flux Q_s^* and calculate the heat flux at the ocean-atmosphere interface (2.1). The virtual salt flux Q_s^* can be diagnosed under steady state conditions and is required to maintain the sea surface salinities to observed values S^*. Specification of the fresh water flux $-Q_s^*/S_0$, where S_0 is a reference salinity, allows the sea surface salinity to evolve freely. It is assumed that any change in evaporation is compensated locally

by precipitation.

This boundary condition (mixed boundary condition) was used for sensitivity studies (among others Bryan, 1986) instead of prescribing both temperature and salinity. A system under mixed boundary conditions is very sensitive to perturbations in salinity (Bryan, 1986; Marotzke and Willebrand, 1991; Stocker and Wright, 1991).

We will see that this system does not correctly describe the sensitivity of the climate system because changes of atmospheric temperature and fresh water flux are neglected. To look for appropriate boundary conditions at the upper ocean surface, conceptual understanding is necessary about the mechanisms affecting the surface heat and fresh water flux and thus the sensitivity of the THC. This will be explored in the next paragraph.

Which processes affect the stability of the THC ?

In this section the feedback mechanisms affecting the THC are discussed. A positive feedback tends to destabilize, a negative to stabilize the system. The mechanisms are schematically drawn in figure 2.1 with plus and minus signs denoting positive and negative feedback. Positive (+) and negative (−) feedback must be multiplied to get the effective negative or positive feedback mechanism.

Today's North Atlantic circulation is characterized by strong northward salt transport in contrast to the Pacific. A reduced transport of salinity to high latitudes decreases the high latitude density. The reduced density stabilizes the water column, and convection is reduced. The reduction of mass transport further reduces the transport of salinity. This mechanism represents a strong positive feedback. The fresh water flux is independent of the sea surface salinity (SSS). Therefore, the positive loop (SSS, density, vertical mixing, poleward transport of salt) is mainly an internal mechanism of the ocean. The persistence of salinity anomalies is largely caused by the lack of a mechanism removing anomalies as effectively as the surface flux for SST anomalies.

The other active tracer determining the mass transport is temperature. A reduced mass transport brings less heat to high latitudes which cools the sea surface temperature (SST). The density of surface water is therefore increased and the water column is destabilized (negative feedback: SST, density, vertical mixing, poleward transport of heat). These large-scale advective transport processes of heat and salt compete about the stability of the circulation (figure 2.1).

Under mixed boundary conditions the stabilizing heat transport mechanism is underestimated because air temperature and thus SST are not free to develop. A variable atmosphere will allow SST variations and the stabilizing heat transport mechanism of the ocean.

Changes in the surface water properties will affect the air-sea heat flux, which influences the local air temperature and radiation balance. This in turn causes changes in the atmospheric transports of heat and moisture.

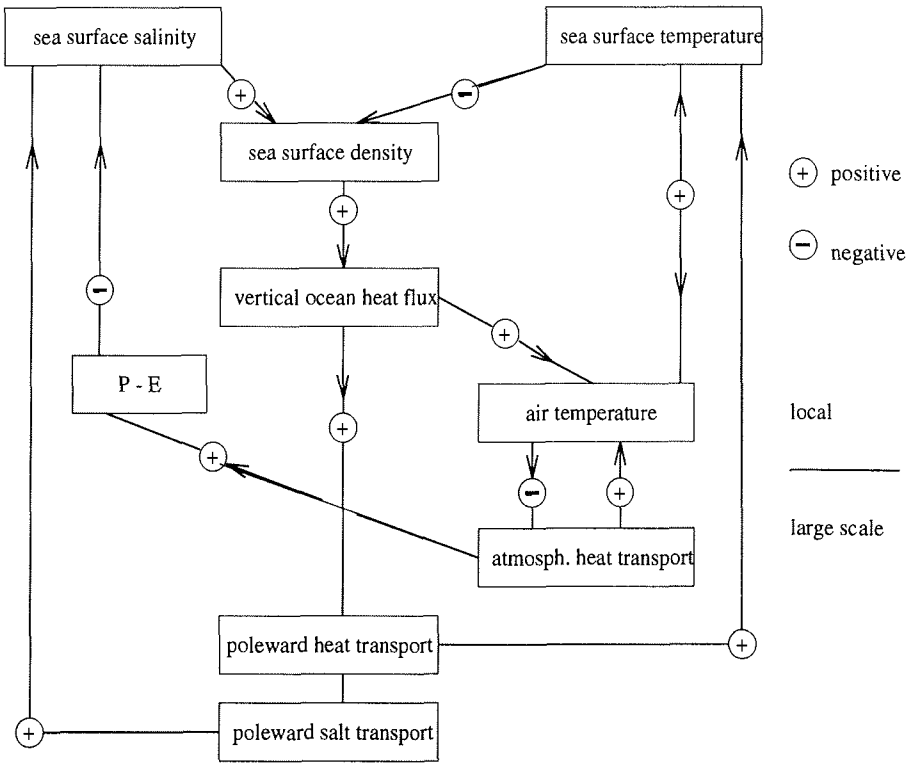

Figure 2.1: Feedback mechanisms in the coupled ocean-atmosphere system. Positive (+) and negative (−) feedback must be multiplied to get the effective negative or positive feedback mechanism.
On a large scale the oceanic heat and salt transport determines sea surface temperature and salinity. The conveyor belt depends strongly on the positive loop (SSS, density, vertical mixing, poleward transport of salt) because salinity at high latitudes is relatively weakly influenced by the surface fluxes. In contrast, the SST at high latitudes is strongly coupled to the air temperature. For the THC this is a stabilizing feedback because the air temperature decreases when the overturning is weakened. Enhanced eddy activity warms the air and reduces the effect mentioned above (positive destabilizing feedback). One further positive feedback destabilizing our climate system is through the fresh water flux (SSS, density, vertical mixing, poleward transport of moisture).

The atmospheric heat transport will increase if the meridional temperature gradient increases. The atmospheric temperature at high latitudes will increase through increased poleward heat transport due to enhanced eddy activity (traveling highs and lows). This warms the ocean surface layer and leads to a reduced density. Therefore, the atmospheric transport is a destabilizing, positive feedback (in figure 2.1: SST, density, vertical mixing, local air temperature, atmospheric heat transports, changed air temperature).

Changes in fresh water fluxes affect the density and thus vertical mixing. The atmospheric transport of moisture increases through enhanced eddy activity. Therefore, the hydrological cycle is a positive feedback through increased poleward moisture transport and fresh water flux (SSS, density, vertical mixing, poleward transport of moisture).

In chapter 10 we will see that the coupled system including sea ice changes the sensitivity of the THC and that the feedback schematically drawn in figure 2.1 must be modified.

A simple diagnostic atmospheric model is required which has the potential to respond to a changed oceanic circulation. Such a model should include a variable atmospheric temperature and fresh water flux. Therefore, the transport of heat and moisture must be treated in the model. Energy balance models of the sixties and seventies (Sellers, 1969, 1973; Budyko, 1969; North, 1975 a b; Ghil, 1976; Nicolis, 1979; Warren and Schneider, 1979) have been rediscovered to study the sensitivity of the THC (Stocker et al., 1992; Chen et al., 1995; Rahmstorf and Willebrand, 1995; Kleeman and Power, 1995; Lohmann et al., 1995 a). EBMs work with physical approximations of governing processes where the transport terms are usually parameterized as diffusion. However, only few EBMs include a hydrological cycle (Jentsch, 1989 a b; Chen et al., 1995; Chu and Ledley, 1995; Lohmann et al., 1995 a).

The EBM presented in the next chapter is a one dimensional climate model including heat and moisture transport and thus allowing variable fluxes at the ocean-atmosphere interface. This simplified atmospheric model will be used to study the sensitivity of the coupled atmosphere-ocean (-sea ice) system.

Chapter 3

Energy Balance Model

A one dimensional atmospheric energy balance model used as a boundary condition for the oceanic thermohaline circulation is presented in this chapter. The model considers a zonally and annually averaged circulation of the atmosphere and calculates surface fresh water fluxes and surface heat fluxes along with sea surface temperatures. Additionally, a change of the wind stress is predicted. In the unperturbed system the modelled surface boundary fluxes for the ocean reproduce present values.

In section 3.1 the basic energy equations of the EBM are presented. The poleward transport of heat at low latitudes is primarily through the Hadley circulation whereas the meridional transport poleward of 30^0 latitude is dominated by eddies generated by baroclinic instability (Oort and Peixoto, 1983). The eddy transport parameterization is based on the theory of baroclinic instability (section 3.2). The EBM treats the transport processes as diffusion.

Variable surface wind stress is based on a scheme for angular momentum balance (section 3.3). The parameterization of surface wind stress and the Hadley circulation is based on earlier work (Lindzen and Ferrel, 1980; Held and Hou, 1980; Lindzen and Hou, 1988). Their theories are adopted to develop a scheme for prediction of wind stress for the EBM. In section 3.4, the turbulent transfer formulas for heat flux for zonally averaged and time mean conditions are explored. The effect of the Hadley heat transport on the atmospheric temperature is estimated in section 3.5.

It is useful to discuss other diagnostic atmospheric models in the context of the presented EBM (section 3.6). The numerical scheme to solve the equations are shortly described in section 3.7.

3.1 Energy Balance

The balances of energy will be used to derive equations for the atmospheric temperature and fresh water flux. The thermodynamic equation (internal plus potential energy) in the atmosphere in isobaric coordinates reads

$$\partial_t(C_p T_a) + \nabla \cdot (C_p\, v\, T_a) + \partial_p(C_p\, \omega\, T_a) = \partial_p Q_R + Q_L + \partial_p Q_S + \frac{RT_a}{p}\omega \quad (3.1)$$

where v and ∇ are the horizontal vector of wind and gradient operator, T_a atmospheric temperature, t time, p pressure, $\omega = \frac{d}{dt}p$ vertical wind, and C_p specific heat at constant pressure ($1004\, J\, kg^{-1}\, K^{-1}$). Q_R and Q_S are the radiative and sensible heat fluxes, respectively.

Q_L denotes the latent heat release due to phase transitions in the air. This term includes condensation of water vapour ($c > 0$), evaporation of cloud water ($c < 0$), evaporation in unsaturated air ($e > 0$) :

$$Q_L = L_v\,(c - e) \quad ,$$

where L_v is the latent heat of condensation ($L_v = 2.5 \cdot 10^6\, J\, kg^{-1}$). The last term on the right hand side of equation (3.1) is the buoyancy-change term which is responsible for the exchange between kinetic and potential energy of the system.

Additionally to (3.1), the budget equations for the mass mixing ratio of water vapour q_v and cloud water q_w are used:

$$\partial_t q_v + \nabla \cdot (v\, q_v) + \partial_p(\omega\, q_v) = e - c + E \quad (3.2)$$

$$\partial_t q_w + \nabla \cdot (v\, q_w) + \partial_p(\omega\, q_w) = c - \wp \quad , \quad (3.3)$$

where $\wp$ denotes the formation of precipitation and E denotes the evaporation from the ground (ocean and land).

The budget equations (3.1, 3.2) and (3.3) are now vertically integrated and zonally averaged. It is assumed that in the vertically integrated left hand side of (3.3) the first two terms vanish (stationarity, small horizontal transports). Furthermore, the vertically integrated last term on the right hand side of (3.1) is neglected. With $\omega = 0$ at the top and bottom, (3.3) reduces to

$$\int \frac{dp}{g}\, c = \int \frac{dp}{g}\, \wp \quad ,$$

where g is the gravitational acceleration ($9.81\, m\, s^{-2}$). The net precipitation P on the ground ($p = p_0 = 10^5 N m^{-2} = 1000\, mb$) is defined by

$$P = \int \frac{dp}{g}\,(\wp - e) \quad .$$

This yields the vertically integrated balances for the mixing ratio of water vapour and the atmospheric temperature

$$\int \frac{dp}{g}\,\partial_t(C_p T_a) + \int \frac{dp}{g}\nabla \cdot (C_p\, v\, T_a) = Q_R^{top} - Q_R^{bottom} + L_v\, P + Q_S^{bottom} \quad (3.4)$$

$$\int \frac{dp}{g}\,\partial_t(L_v q_v) + \int \frac{dp}{g}\nabla \cdot (L_v\, v\, q_v) = L_v\,(E - P) \quad . \quad (3.5)$$

The one dimensional atmosphere EBM prognoses the vertically integrated mixing ratio of water vapour and atmospheric temperature along with (3.4, 3.5). To evaluate the effective change of the vertically integrated humidity and temperature in equations (3.4, 3.5) the height distribution of humidity and temperature must be taken into account. Most energy balance models (e.g. North, 1975 b; Stocker et al., 1993) consider the energy balance at the surface only, neglecting a coupling of surface air temperature and lapse rate. In the atmosphere, the lapse rate is maintained by two principal mechanisms:

- The vertical transfer of heat by convection which is the dominant mechanism in the tropics. The vertical temperature distribution is quite sensitive to surface temperature changes.
- The vertical heat transport by large scale eddies coming from baroclinic instability which is important mainly in middle latitudes. This process stabilizes the vertical temperature distribution, and, therefore, the distribution is rather insensitive to surface temperature changes.

Rennick (1977) related empirically the lapse rate to the surface temperature including implicitly the above mentioned effects. Based on that finding, Chen et al. (1993) found that the change of vertically averaged temperature $\delta \int dp\, g^{-1}\, T_a(p)$ can be expressed in terms of the change of surface air temperature δT_A at p_0 through two constants globally:

$$\delta \int \frac{dp}{g} T_a(p) = \beta_1 \quad \delta T_A \quad \text{with} \tag{3.6}$$

$$\beta_1 = \begin{cases} 5708\ kg\, m^{-2} & \text{for } T_A \geq 275\ K \\ 3966\ kg\, m^{-2} & \text{for } T_A < 275\ K \end{cases} \quad . \tag{3.7}$$

The mixing ratio of water vapour q_v is expressed by the product of relative humidity $rh(p)$ and the saturation mixing ratio of water vapour q_s. For the change of humidity with surface temperature, three empirical relations are used: The lapse rate of Rennick (1977), the empirical function of saturation mixing ratio of water vapour (Bolton, 1980, "Clausius-Clapeyron Equation") on temperature (in ^0C) and pressure (in $10^2 Nm^{-2}$):

$$q_s(T_a, p) = 6.112 \cdot \exp\left(\frac{17.67\ T_a}{T_a + 243.5}\right) \cdot 0.622/p$$

and an empirical, linear vertical profile of the relative humidity depending on pressure (Manabe and Wetherald, 1969):

$$rh(p) = \max\left[0.0, 0.77\, \frac{(p/p_0 - 0.02)}{(1.0 - 0.02)}\right] \quad . \tag{3.8}$$

A parameter β_2 represents the effective change of the humid atmospheric interiors varying with surface temperature T_A:

$$\delta \int \frac{dp}{g} rh(p) q_s(T_a(p), p) \;=\; \int \frac{dp}{g} rh(p) \frac{\partial q_s(T_a(p), p)}{\partial T_a} \quad \delta T_A \;=\; \beta_2 \quad \delta T_A \tag{3.9}$$

The slope β_2 in equation (3.9) can be expressed by

$$\beta_2 = T_A^{-2} \exp\left(\frac{-5222.71}{T_A + 30.0989}\right) \quad , \tag{3.10}$$

where the surface temperature T_A is measured in Kelvin.

Combining equations (3.4, 3.5) yields one vertically integrated energy equation:

$$(C_p\beta_1 + L_v\beta_2)\ \partial_t T_A + \int \frac{dp}{g} \nabla \cdot (C_p v T_a) + \int \frac{dp}{g} \nabla \cdot (L_v v q) = Q_R^{top} - F_{oa} \quad , \tag{3.11}$$

where $F_{oa} = Q_R^{bottom} - L_v E - Q_S^{bottom}$ denotes the ocean-atmosphere heat flux calculated by bulk formulas (section 3.4). The net radiation on top of the atmosphere Q_R^{top} is the difference between net solar radiation and net outgoing longwave radiation Q_{LW}^{top}. The longwave radiation Q_{LW}^{top} is approximated by a linear law:

$$Q_{LW}^{top} = A + B\ T_A \quad \text{with} \quad A = 213.2\ W\,m^{-2} \text{ and } \quad B = 2.2\ W\,m^{-2}K^{-1} \tag{3.12}$$

The planetary albedo α is parameterized in terms of the surface air temperature (Sellers, 1969; Chen et al., 1993). A feedback factor (chosen as $ff = 0.006$ in Chen et al., 1993) represents the non-linear change of the planetary albedo α due to snow and ice:

$$ff = \frac{\partial \alpha}{\partial T_A} \quad \text{for} \quad T_A < 283\,K\ .$$

Due to the non-linear ice-albedo-feedback in the presented EBM, an additional solution (besides the present climate) appears if the initial conditions are strongly perturbed (Chen et al., 1995). This solution may be associated with an ice-covered earth solution (North, 1975 b).

Alternatively, an albedo parameterization of Griffel and Drazin (1981) has been used in the EBM:

$$\alpha(T_A) = 0.42 - 0.20 \cdot \tanh\left[0.052\,(T_A - 276.15)\right] \quad .$$

This parameterization incorporates high albedos of snow and ice in terms of the surface temperature (T_A in Kelvin).

Some EBMs (e.g. Stocker et al., 1993) overestimate the effective change of the heat capacity of the atmosphere by assuming that the total heat content of the air column changes. The term $(C_p\beta_1 + L_v\beta_2)$ in (3.11) together with the strength of atmospheric transports determine the adjustment time scale of the EBM. The effective heat capacity that interacts with the underlying ocean is about half of the heat capacity of the troposphere.

With equation (3.11) the surface temperature T_A is calculated prognostically, while the fresh water flux for the ocean surface is given by the right hand side of equation (3.5) by evaluating the left hand side of the water vapour budget. The transport parameterizations will be discussed in the next section.

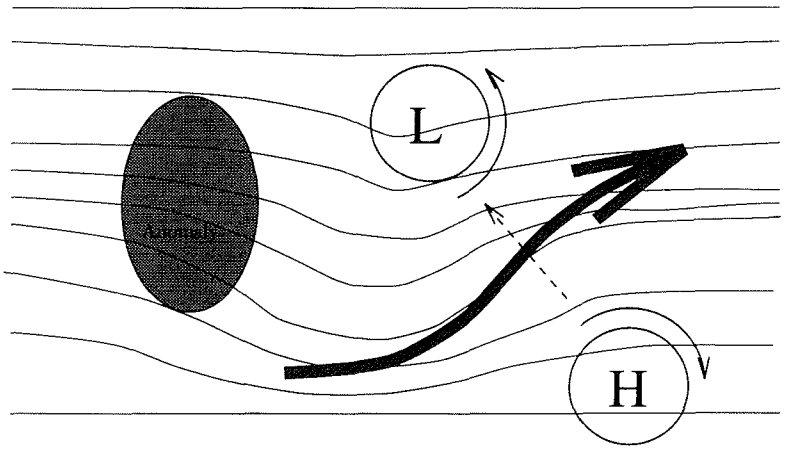

Figure 3.1: Schematic representation of enhanced baroclinic instability due to a negative temperature anomaly (shaded area). The black arrow illustrates the storm track. Heat is transported from the high to the low, schematically drawn by the dashed arrow.

3.2 Eddy transport parameterization

The mechanism of heat and moisture transport in middle and high latitudes by baroclinic instability is the most important mechanism in the atmospheric energy balance model. Therefore, the process of baroclinic instability will be schematically described for one weather pattern. Consider an atmospheric condition with isotherms coincident with latitude circles. A cold anomaly, which could be thought of as a cold air outbreak from the North American continent, results in a changed surface heat flux from the ocean (figure 3.1). Alternatively, the change in heat flux may be caused by a stable stratification of the water column due to fresh water or by anomalous sea ice extent.

In the region of strong temperature gradient cyclones (low pressure) and anticyclones (high pressure on the northern hemisphere) are formed. These traveling weather systems move north-eastward defining the major storm track (in figure 3.1 the black arrow). Both, heat and vorticity is transported down the temperature gradient (dashed arrow). The scale over which this process is important is about 1000 km.

This process is the main source of meridional heat transport in middle and high latitudes. The balances of heat (3.4) and moisture (3.5) are averaged over a length scale of synoptic scale disturbances of O(1000) km and a time scale longer than

the life time of such disturbances (e.g. two weeks). The variables can be splitted into a large scale, long term quantities ($\overline{T_a}, \overline{q_v}, \overline{v}$) and the deviations ($T_a', q_v', v'$). The moments $\overline{v'T_a'}$ and $\overline{v'q_v'}$ are connected mainly with transient processes in the atmosphere. The transients act as diffusion in a statistical sense bringing warm and moist air poleward due to individual high and low pressure contributions.

3.2.1 Transient eddy transport

The parameterization of large scale transient eddies in the troposphere is based on the theory of baroclinic instability (Green, 1970; Stone, 1972; Held, 1978; Branscone, 1983; Peng et al., 1987; Stone and Yao, 1990). In this parameterization the meridional heat transport is expressed in terms of the mean temperature gradient.

A scaling analysis is used to determine the formulation of the transient eddy transport $\overline{v'T_a'}$. The relevant velocity scale is taken to be that determined by the vertical shear of the zonal wind $\overline{u}_z$:

$$V = d\frac{\partial \overline{u}}{\partial z} = -d\left(\frac{g}{f\overline{T_a}}\frac{\partial \overline{T_a}}{\partial y}\right) \quad , \tag{3.13}$$

where d is an unspecified vertical scale and $\overline{T_a}$ is the mean potential temperature and $f = 2\Omega\sin\phi$ is the Coriolis parameter, where Ω is the angular velocity of the earth. For the second equality in (3.13) the thermal wind relation is used. The characteristic length scale for the baroclinic waves L is taken to be the Rossby radius of deformation corresponding to the vertical scale d:

$$L = L_d = \frac{N\,d}{f} \quad . \tag{3.14}$$

where H is the density scale height in the troposphere and $N^2 = g\overline{T_a}^{-1}\partial_z\overline{T_a}$ the static stability. The deformation radius is chosen as the meridional scale because this scale is responsible for conversion from potential to kinetic energy in the Eady model (Branscome, 1983). From that follows that the eddy diffusivity K scales linearly with the temperature gradient:

$$K \sim VL = -\frac{d^2 gN}{\overline{T_a}f^2}\left(\frac{\partial \overline{T_a}}{\partial y}\right) \quad . \tag{3.15}$$

The eddy fluxes in a statistically steady state of the atmosphere scale as:

$$\overline{v'T_a'} \sim -K\left(\frac{\partial \overline{T_a}}{\partial y}\right) \sim \frac{d^2 gN}{\overline{T_a}f^2}\left(\frac{\partial \overline{T_a}}{\partial y}\right)^2 \quad . \tag{3.16}$$

The remaining question is the height d above the surface up to which linear (quasi-geostrophic) waves, destabilized by a surface temperature gradient, can produce substantial eddy fluxes (Shutts, 1978). Following Branscome (1983), an expansion for short Charney waves (Charney, 1947) near the first neutral curve is made to

obtain the vertical structure of the first unstable mode. The first order equations in the Rossby number expansion, the conservation of quasi-geostrophic potential vorticity, is used in its linearized form.

In the linear stability analysis, the wavenumber k of the most unstable mode (Charney mode) is approximately

$$k = \frac{f}{NH} \frac{1+\gamma}{2} \quad .$$

The horizontal wavelength depends on the dimensionless parameter

$$\gamma = \frac{\beta N^2 H}{f^2 \bar{u}_z}$$

with $\beta = d_y f$. For the shear $\partial_z \bar{u}$ the thermal wind relationship is again assumed. The parameter γ determines the vertical scale of the meridional heat flux $\overline{v'T'_a}$ and is of the order of unity. The vertical scale d, according to the analysis of Branscome (1983), is given by:

$$d = \frac{H}{1+\gamma}$$

and the transient eddy heat transport can be parameterized by:

$$\overline{v'T'_a} = \aleph \frac{d^2 g N}{\overline{T_a} f^2} \left(\frac{\partial \overline{T_a}}{\partial y} \right)^2 \exp(-z\gamma/H) \quad . \tag{3.17}$$

The unknown parameter $\aleph$ is estimated from observed transport magnitudes (Green, 1970) or by relating wave amplitude and and mean flow energy (Stone, 1972) which is consistent with a finite-amplitude analysis (Shepherd, 1989, 1993). The eddy transport in equation (3.17) is always directed towards lower temperatures. The effective eddy diffusion coefficient in (3.17) is estimated as

$$\aleph \frac{d^2 N}{\overline{T_a}} \frac{\partial \overline{T_a}}{\partial y} \exp(-z\gamma/H) \approx 3.0 \cdot 10^6 \frac{m^2}{s} \quad .$$

This approach must be considered with caution because the system of linear differential equation is non-orthogonal (Trefethen, 1993). A good starting point for a better parameterization of baroclinic instability may be the spectrum analysis (Trefethen, 1993) or the non-linear analysis using a Lyapunovfunction (Shepherd, 1993). However, these theoretical parameterizations have been tested in statistical dynamical models by Vallis (1982) and Stone and Yao (1990) and can reproduce the zonally averaged state of the atmosphere. Stone and Miller (1980) derived an empirical relationship between the mean meridional temperature gradient and the sensible heat transport by stationary and transient eddies. They found an approximately quadratic power law for middle latitudes, which is consistent with the theoretical parameterizations.

The vertical structure of the transient eddy heat transport is neglected by assuming a constant lapse rate and fixed vertical stability. The vertical integrated sensible

eddy heat transport is calculated in terms of the surface temperature T_A and is tuned to reproduce the current climate (Oort, 1983; Oort and Peixoto, 1983).

$$\int \frac{dp}{g} \quad \overline{v'T'_a} \;=\; -\;\; K_s \quad \left(\frac{\partial T_A}{\partial y}\right)^2 \qquad . \tag{3.18}$$

The transient eddies and diffusivities are shown in figures 3.2 a, b. More recent data (Kann et al., 1994; Keith, 1995) of meridional energy transport and radiation would influence the coefficients in figure 3.2 only slightly.

3.2.2 Latent eddy heat transport

There are two different approaches in the literature to deal with latent eddy heat flux although in practice they are very similar. The first approach assumes that water vapour is treated much as a conservative variable for transport which gives reasonable realistic eddy fluxes of water vapour (e.g. Vallis, 1982). It is assumed that the eddy transfer coefficients for trace gas and water vapour are identical with those for heat. The eddy transfer scheme is applicable to tracers with lifetimes greater than the eddy transfer time scales (order of week). If life times of a constituent is less than the transport time then it will not reach its destination as assumed by the transfer theory.

The other approach assumes that eddy fluctuations in relative humidity are small compared to fluctuations in specific humidity, and that the Clausius-Clapeyron equation can be linearized (Leovy, 1973). Stone and Yao (1990) argue that the eddy fluxes arise from baroclinic instability and prefer this parameterization rather than a diffusive mixing length formulation of Vallis (1982). For the EBM, Stone and Yao's parameterization is adopted. Therefore, the latent eddy heat transport is parameterized as

$$\overline{v'q'_v} \;=\; rh(p) \quad \frac{\partial\, q_s}{\partial \overline{T_a}}(\overline{T_a}, p) \quad \overline{v'T'_a} \quad , \tag{3.19}$$

where rh is the relative humidity and q_s the saturation water vapour. The relative humidity is prescribed using (3.8). For the latent heat transport (3.19) the relative humidity, $\frac{\partial\, q_s}{\partial T}$ and the terms on the right hand side of (3.17) strongly decrease with height. Therefore, the surface values for the latent heat transport may be a good choice in the vertical integrated model.

$$\int \frac{dp}{g} \quad \overline{v'q'_v} \;=\; -K_l \quad rh(p_0) \quad \frac{\partial\, q_s}{\partial T_A}(T_A, p_0) \quad \left(\frac{\partial T_A}{\partial y}\right)^2 \qquad . \tag{3.20}$$

As for the sensible heat transport, the coefficient K_l is tuned to reproduce observed latent eddy heat transports of the current climate. The values for latent northward transport by transient eddies from Oort and Peixoto (1983) and the associated diffusivities are shown in figure 3.2. Note that the diffusivity is strongly temperature dependent due to the quadratic power law and the saturation water vapor at the

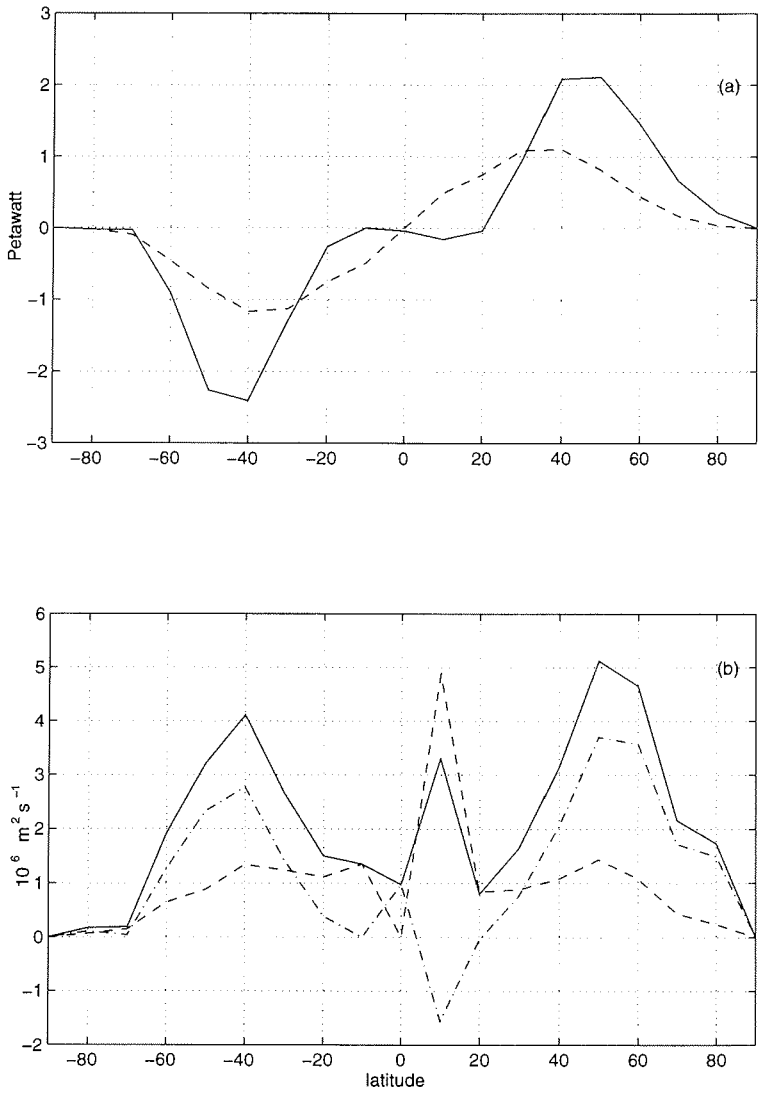

Figure 3.2: a) Sensible (solid) and latent (dashed) northward transport by transient eddies from Oort and Peixoto (1983).
b) Effective diffusivities for the total (solid), sensible (dashed) and latent (dash-dotted) heat transport calculated from observed temperatures and transport.

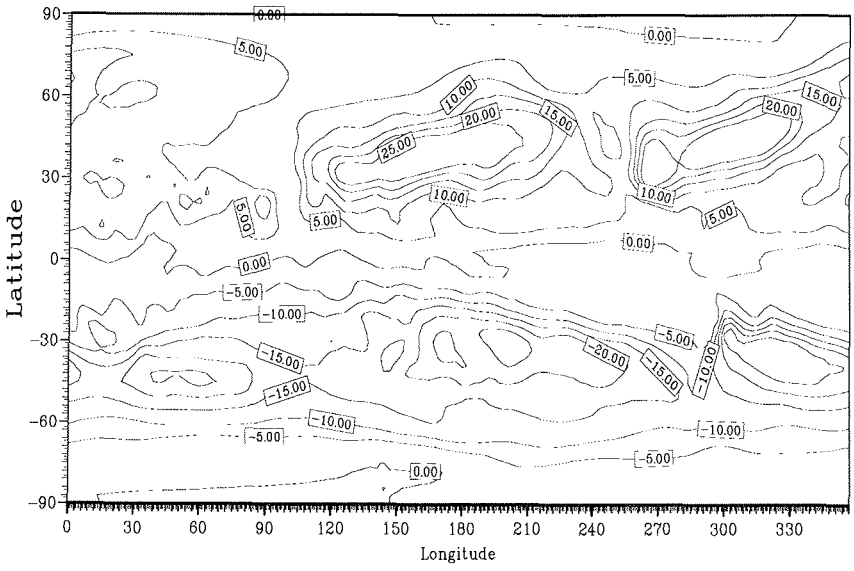

Figure 3.3: Meridional transport of moisture by transient eddies. For the analysis, ECMWF data for the years 1988-1992 are used to obtain the transient transport on annual average. Units are $kg\,m^{-1}\,s^{-1}$ with contour interval $5\,kg\,m^{-1}\,s^{-1}$.

surface.

The vertical integrated, meridional transport of moisture by transient eddies is shown in figure 3.3, where ECMWF data for the years between 1988 and 1992 are used.[1] The picture indicates that the eddy activity is greatly enhanced over the ocean surfaces as opposed to over land surfaces. In the northern hemisphere, two major storm tracks exists extending northeast across the Atlantic and Pacific oceans from the east coast of the major continents. It is along these tracks that the majority of eddy heat and vorticity transport takes place (figure 3.3 for the latent heat transport). In the southern hemisphere the transport is relatively homogeneous in the zonal direction. In the present model, however, longitudinal asymmetries in the atmosphere are neglected. Especially when modelling seasonal variations, the longitudinal distribution is essential for heat and moisture transport. Including these effects in a diagnostic model would be an important task for future work.

[1]Dr. James Dodd is acknowleged for providing the data

3.2.3 Stationary eddies

The heat transport by stationary baroclinic waves is large in winter on the northern hemisphere when the land-sea contrast is most pronounced. Green (1970) argued that stationary eddies are more transient phenomena which repeatedly occur at the same location. This happens due to fixed topographic effects providing perturbations upon which baroclinic waves can grow. These phenomena relating to stationary eddies are ultimately driven by the large scale baroclinicity of the atmosphere. Therefore, standing eddies could be parameterized as transient eddies.

It is interesting that the zonally averaged state may not depend on whether eddy kinetic energy is realized by transient or stationary eddy conversions. The removal of topography in an atmospheric circulation model (AGCM) by Manabe and Terpstra (1974) shows a relatively unchanged zonally averaged climate state. The total energy conversion from potential to kinetic energy is nearly the same because the contributions to energy conversion by transient eddies is increased, compensating almost fully for the loss of stationary eddies. This result is consistent with that of Stone and Miller (1980) who found that the variation of total eddy heat flux has a higher correlation with temperature gradient than either of the individual (transient and stationary) eddy components.

However, stationary eddies are not modeled in this EBM although they would respond to changed forcing. Especially, models including a seasonal cycle should resolve the stationary eddies.

3.3 Wind stress

For the calculation of the zonal wind stress, a balance of angular momentum is applied. The parameterization of the wind stress is based on the assumption of approximately conserving angular momentum M. Therefore, angular momentum M is a function of the zonal velocity u in the upper layers and latitude:

$$M = \Omega a^2 \cos^2\phi + ua\cos\phi = \Omega a^2 = M(\text{equator}) \quad . \tag{3.21}$$

The turbulent diffusivity of angular momentum at the surface has to be taken into account:

$$\nabla \cdot (\vec{u}M) = \nu\, \partial_z^2 M \quad . \tag{3.22}$$

With M from equation (3.21) and the vertically integrated equation (3.22) over the troposphere, $\tau_x = \nu\, \partial_z u(0)$ can be calculated:

$$\begin{aligned} \tau_x\, a\cos(\phi) &= \nu\, \partial_z u(0)\, a\cos(\phi) = \nu\, \partial_z M(0) \\ &= \frac{1}{a\cos(\phi)}\, \partial_\phi \left(a\cos^2(\phi) \int dz\, uv \right) \quad , \end{aligned} \tag{3.23}$$

where vanishing wind stress at the tropopause is assumed. The contribution of the so-called mountain torque (mountains intersect with isobaric levels) is left out. This

term balances probably with the mean transport $\int dz\bar{u}\bar{v}$ whereas the transient eddy term may provide the essential contribution to the surface stress (Oort and Peixoto, 1983, section 3.4.1). Therefore, only the contribution due to eddies will be considered.

Following Held and Hou (1980) it is further assumed that the momentum flux $\int dz\, uv$ can be expressed by the heat transport $\int dz\, vT_a$. This can be based on the assumption that the vertical profiles of u and T_a are self-similar:

$$\frac{u(z)-u(0)}{u(H)-u(0)} \approx \frac{T_a(z)-T_a(0)}{T_a(H)-T_a(0)} \quad .$$

Therefore,

$$\tau_x = \frac{1}{a\cos^2(\phi)}\partial_\phi\left(\cos^2(\phi)\frac{u(H)-u(0)}{T_a(H)-T_a(0)}\int dzvT(z)\right) \tag{3.24}$$

The term

$$\frac{\cos^2(\phi)}{a}\frac{u(H)-u(0)}{T_a(H)-T_a(0)}$$

is calculated using equation (3.24) with climatological τ_x by eddies and sensible heat transport by eddies (Oort and Peixoto, 1983) and is held fixed in the model. Figures 9 and 10 in Oort and Peixoto (1983) show that the zonal mean northward transport of momentum by transient eddies dominate over the transport by stationary eddies and mean meridional circulations.

It is assumed that direction of the surface wind does not change although the intensity may change. As a result, the angle α_w of the wind stress remains unchanged:

$$\tan(\alpha_w) = \frac{\tau_y}{\tau_x} = \text{const.} \quad . \tag{3.25}$$

and can be taken from climatology (Hellerman and Rosenstein, 1983), as shown in figure 3.4.

3.4 Heat flux

For the heat flux at the ocean-atmosphere interface the turbulent transfer formulas for zonally averaged and time mean conditions are simplified. In contrast to Haney (1971) variable atmospheric temperatures and wind are used. The atmosphere absorbs about 25% of the incoming solar radiation and about 75% of the short wave radiation $Q_{SW}^{top}(1-\alpha)$ reaches the ocean surface. The sensible and latent heat flux formula are linearized about the difference of the sea surface temperature and atmospheric temperature at 1000 mb:

$$Q_S = C_p\rho_a C_D|\mathbf{u}|\,(T_O - T_A) \tag{3.26}$$

$$\begin{aligned} Q_L &= L_v\rho_a C_D|\mathbf{u}|\,(q_s(T_O) - rh\; q_s(T_A)) \\ &\approx L_v\rho_a C_D\,|\mathbf{u}|\left([1-rh]q_s(T_A) + \frac{\partial q_s(T_A)}{\partial T_A}[T_O - T_A]\right) \quad , \end{aligned} \tag{3.27}$$

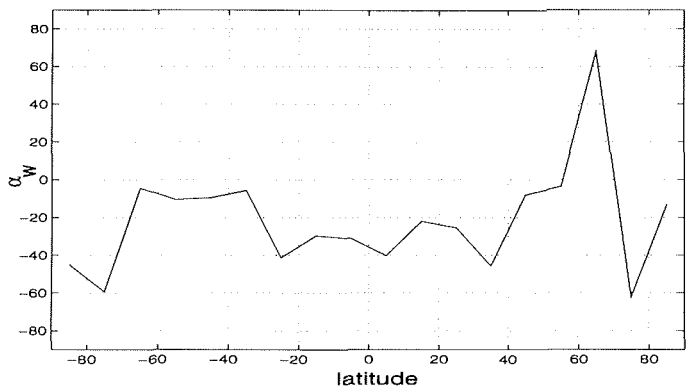

Figure 3.4: Angle α_w of the wind stress from zonal mean (global) wind stress (Hellerman and Rosenstein, 1983).

where $C_D = 1.4 \cdot 10^{-3}$ is a constant drag coefficient over ocean surfaces, $|\mathbf{u}|$ the wind speed at 1000 mb and ρ_a the air density ($1.225\, kg\, m^{-3}$). The surface wind speed determines the heat flux at the ocean-atmosphere boundary (3.26, 3.27) and the momentum balance at the interface. The momentum flux $\vec{\tau} = (\tau_x, \tau_y)$ can be written in terms of a surface drag coefficient C_D and surface velocities u, v:

$$\tau_x = C_D \rho_a |\vec{u}|\, u \cdot \vec{e}_x \tag{3.28}$$

$$\tau_y = C_D \rho_a |\vec{u}|\, v \cdot \vec{e}_y \tag{3.29}$$

From the wind stress $\vec{\tau}$ the absolute amount of velocity in the bulk formula is calculated as

$$|\mathbf{u}| = \sqrt[4]{(\tau_x^2 + \tau_y^2)(\rho_a C_D)^{-2}} \quad . \tag{3.30}$$

The net longwave radiation at the ocean surface is calculated by

$$Q_{LW}^{bot} = Q^*\, \sigma T_O^4 \quad ,$$

where σ is the Stefan-Boltzmann constant and Q^* is an empirical function for the reduction of radiation by clouds and water vapour (Haney, 1971). Therefore, the heat flux F_{oa} depends on $(T_A, T_O, \vec{\tau}, \alpha, Q_{SW}^{top})$ and is the sum of the above mentioned components:

$$F_{oa} = Q_s + Q_l + Q_{LW}^{bot} + 0.75 \cdot Q_{SW}^{top}(1 - \alpha) \quad . \tag{3.31}$$

3.5 Estimation of the Hadley Circulation

The effect of the Hadley circulation on the temperature distribution is estimated, based on the assumption of approximate conservation of angular momentum. For

simplicity it is assumed that the equator separates the two tropical Hadley cells which are supposed to be symmetric about the equator. Following Lindzen and Hou (1988), the zonal velocity u is assumed to be in cyclostrophic balance

$$fu + \frac{u^2 \tan\phi}{a} = -\partial_y \Phi \quad , \tag{3.32}$$

where $\Phi = p/\rho_0$ is the quasi geostrophic stream function. This balance is taken for height H which defines the topmost level of the troposphere and the ground. These equations are subtracted and the angular momentum balance (3.32) in the upper layers is used to obtain

$$u(H) = \Omega a \tan\phi \cdot \sin\phi \; = \; \frac{M}{a} \tan\phi \cdot \sin\phi \quad .$$

Surface winds are small compared to upper level winds $u(H)$ and are neglected. Furthermore, the hydrostatic and Boussinesq approximations are applied. Thus, the vertically integrated temperature gradient $\partial_y \int_0^H dz T_a$ is related to latitude and the total angular momentum per unit mass M only. It is postulated that the flow in the upper branch of the Hadley circulation conserves angular momentum which is in good agreement with observations (Oort and Peixoto, 1983). The vertically integrated temperature is linearly related to the surface temperature T_A (Rennick, 1977). The gradient of the surface temperature within the Hadley cells is therefore determined under the above assumptions by latitude and total angular momentum.

Peng et al. (1987) modified an approach originally suggested by Held and Hou (1980) and obtained a diffusive law for the sensible heat transport and a diffusive law with negative diffusivities for latent heat transport, depending on the vertically integrated moisture content.

The effect of the Hadley cell for the thermohaline driven ocean circulation is negligible small because the high latitude fluxes are mainly responsible for changes in the THC. Therefore, the mean transport is held fixed in most experiments while the response of the transient eddies is calculated.

3.6 Other diagnostic atmospheric models

In terms of the present EBM, other starting points for suitable boundary conditions can be easily understood. The heat flux at the atmosphere-ocean interface is approximated by

$$F_{oa} \; = \; -\gamma \quad (T_O - T_A) \quad . \tag{3.33}$$

Furthermore, stationarity of the atmospheric temperature balance (3.11) is assumed. Therefore, the atmospheric temperature T_A ca be expressed in terms of the atmospheric heat transport Q_a and ocean temperature T_O:

$$T_A \; = \; \frac{\gamma T_O \; + \; Q_a \; - A}{\gamma \; + \; B} \tag{3.34}$$

This model with fixed meridional heat transport Q_a is Schopf's model (1983) which was used by Zhang et al. (1993) as the thermal boundary condition for their ocean model. Changes of the oceanic temperature δT_O would result in a local change δT_A of the atmospheric temperature:

$$\delta T_A = \frac{\gamma}{\gamma + B} \delta T_O \approx \frac{50}{52.2} \delta T_O \quad . \tag{3.35}$$

Therefore, the heat flux (3.33) does not change much in this atmospheric model and the typical time scales τ_T over which SST-anomalies are removed is very long. Later on, we will see that the time scales τ_T strongly influences the stabilizing feedback of oceanic heat transport.

However, there is evidence (e.g. Frankignoul, 1985) that the rate at which SST-anomalies are damped is a function of its horizontal extent. The atmospheric heat transport can be included into the thermohaline boundary conditions through replacing the heat flux rate γ by a scale dependent coefficient (Willebrand, 1993):

$$\gamma = \gamma_0 - \gamma_1 \nabla^2 \quad , \tag{3.36}$$

where ∇ is the horizontal gradient operator. A scale dependent coefficient comes out from a diffusive formulation of the atmospheric heat transport ($Q_a \sim \nabla^2 T_A$) and putting of (3.34) in (3.33) (for more details: Marotzke, 1994; Rahmstorf and Willebrand, 1995). A diffusive atmospheric heat transport has been previously used in EBMs (e.g. Sellers, 1969; Budyko, 1969; North, 1975 a b; Stocker et al., 1992).

Alternatively, the response of an atmosphere could be measured by analyzing the statistics of atmospheric circulation experiments (Bretherton, 1982). For simulating variations of a coupled system the slower varying components could be taken as a boundary condition for a faster component. For ocean modeling, a problem is what should be done with the "fast" atmosphere ?

It is assumed that the ocean requires only the first statistical moments of an ensemble of atmospheric experiments. Bretherton (1982) suggested measuring the response of an atmospheric circulation model (e.g. the heat flux F_{oa}) to SST changes $\delta T_s(x)$. For sufficiently small variations in SST, the atmospheric variables vary linearly. A sensitivity coefficient or Green's function $\lambda(x, x')$ may be calculated, defined by:

$$\delta F_{oa}(x) = \int \lambda(x, x') \, \delta T_s(x') \, dx' \quad . \tag{3.37}$$

The sensitivity coefficient varies seasonally and spatially and therefore, a lot of experiments are necessary to calculate the statistical sensitivity matrix $\lambda_{i,j}$. Applying the ergodic hypothesis, mean values and variances could be calculated by time averaging. The statistics of the fluxes of heat, fresh water and momentum contain a complex atmospheric model, and therefore, the statistical moments might be very complicated. [2] The formulation (3.37) include formally the diffusive heat flux parameterization (3.36). This approach has been successfully applied to the variability

[2] To keep the investigation as simple as possible, one could neglect the variances and higher statistical moments of the atmospheric variables, though fluctuations may be important for the dynamics. In general, the ocean-atmosphere system is non-linear and the noise depends on the state of the system.

of the tropical Pacific (El Niño) replacing heat flux with wind stress (Barnett et al., 1993).

3.7 Numerics

The EBM is governed by a non-linear, parabolic partial differential equation for the temperature as a function of time and latitude.[3] The non-linearities are the ice-albedo parameterization and the temperature dependence of the latent and sensible heat transport. The latent and sensible heat transport are calculated by centered space differences for the meridional temperature gradient. The governing equation for the atmospheric temperature (3.11) is treated as an initial-value problem with boundary conditions such that the heat transport vanishes at the poles. The term $(C_p\beta_1 + L_v\beta_2)$ depending on temperature is calculated with the temperature from the previous time step while the time derivative of the humid interior $\int dp\, g^{-1}\, q_v$ in (3.5, 3.9) is diagnosed from $\partial_t T_A$. The meridional grid spacing is chosen to be 10^0 latitude from pole to pole. This coarse resolution is chosen because the diffusive parameterization of the heat transport (section 3.2.1) is valid for this scale. A forward Euler scheme is used to solve the equation numerically. The time step in this explicit numerical treatment is restricted (0.3 – 0.5 day) by the Courant-Friedrichs-Lewy criterium (Courant et al., 1928).

[3]The code of the model is based on the numerical implementation of the energy balance model (version 2) of Chen et al. (1993)

Chapter 4

The EBM in a stand alone mode

Experiments with prescribed sea surface temperature anomalies and perturbations in radiation can provide a qualitative understanding of important features of the atmospheric model. Perturbation experiments of sea surface temperature (SST) at mid-latitudes in section 4.1 indicate how the atmospheric temperature and fresh water flux are affected by the anomalous transport of heat and moisture.

The response of the EBM to a perturbation in radiation will be analyzed in section 4.2 in a stand alone mode. This may be useful to understand the different role of latent and sensible heat transport and the feedback mechanisms involved in the EBM.

4.1 Response to sea surface temperature anomalies

A negative SST anomaly of $-1K$ is posed at 40^0-50^0 N where the eastward traveling cyclones and anticyclones dominate the atmospheric transport of heat and moisture. In the SST-experiments documented here, the anomaly persists for the whole experiment and all properties of the mixed layer are left unchanged. A 70^0-wide Atlantic ocean sector is considered, ranging from 70^0 South to 70^0 North. Changes of heat fluxes over land areas and over other ocean basins are neglected. Since the atmospheric circulation generally have much less persistence time than SST anomalies, it is believed that such a situation can be compared to anomalies with shorter persisting times.

In the following, the effects of variable atmospheric temperature and heat transport on the response of the system are dicussed. The resulting heat and fresh water fluxes would affect the THC in the coupled mode which will be analyzed in the subsequent chapters.

One important input signal for the coupled ocean-atmosphere system is the local heat flux at the ocean-atmosphere interface. The change of the local heat flux at the ocean-atmosphere interface can provide a simple criterium to determine the stability in a coupled model (chapter 7).

To analyze the response for mixed boundary conditions (fixed atmospheric temperature and prescribed fresh water flux) and Schopf's model (1983), the simplified formula (3.35) for the heat flux at the atmosphere-ocean interface (3.33) is used. Under mixed boundary conditions the reduction of the heat loss for the ocean is

$$\delta F_{oa} = \gamma \quad \delta T_O \approx \quad -50 \quad Wm^{-2} \tag{4.1}$$

at 45^0 N whereas unchanged elsewhere. This local reduction is far too strong because a reduced heat loss of the ocean would diminish the local air temperature.

In Schopf's model (1983), the change in heat loss from the ocean is much smaller

$$\delta F_{oa} = \gamma \quad (\delta T_O - \delta T_A) = \gamma \frac{B}{\gamma + B} \delta T_O \approx -2.1 \ Wm^{-2} \tag{4.2}$$

at 45^0 N. Because this is a local model, the heat flux is unchanged elsewhere.

However, the meridional heat transport in the atmosphere will affect the change in heat flux which is included into our EBM of chapter 3. Two anomaly experiments of the EBM with fixed (solid lines in figures 4.1, 4.2, 4.3 and 4.4) and variable (dashed lines in the figures) wind stress are compared. The SST anomaly causes a cooling in the atmosphere where the local response at 45^0 N is the strongest (figure 4.1). Anomalous atmospheric transports of heat and moisture (figure 4.2) tend to warm the air and enhance the hydrological cycle. Both heat transport mechanisms cause a destabilizing feedback for the THC as described in chapter 2.

Figure 4.4 indicates that the anomalous heat flux δF_{oa} is $-32 \ Wm^{-2}$ for fixed wind and $-18 \ Wm^{-2}$ for variable wind at 45^0 N. Therefore, the EBM (with fixed and variable wind stress) lies between the two extremes of vanishing anomalous transport and fixed atmospheric temperature. This has also been seen in a SST anomaly experiment by an AGCM (Power et al., 1995).

The heat flux is reduced locally by a reduction of the temperature air-ocean difference. North of 50^0 N and south of 40^0 N, the SST is fixed and the atmosphere is cooled which lead to positive δF_{oa} (increase in oceanic heat loss). Furthermore, a cold anomaly reduces the latent heat flux out of the ocean which strongly depends on temperature. This was found in an AGCM experiment with a large SST anomaly in the North Atlantic simulating the Younger Dyras cooling (Rind et al., 1986).

The resulting change of fresh water flux changes sign near the imposed anomaly (figure 4.3). The average effect of changes in fresh water flux $\delta(P-E)$ between 30^0 and 60^0 N is less than $8\,mm/yr$ for both experiments which is rather small. This may lead to the speculation that changes of fresh water flux are of minor importance for the THC in the coupled mode as a destabilizing effect. The time depending response of fresh water flux due to the storage term (3.6) is very weak, a maximum of $13\,mm/yr$ is reached after 2 days, after a week the effect is negligably small.

In the experiment with variable wind, the negative SST-anomaly coincides with

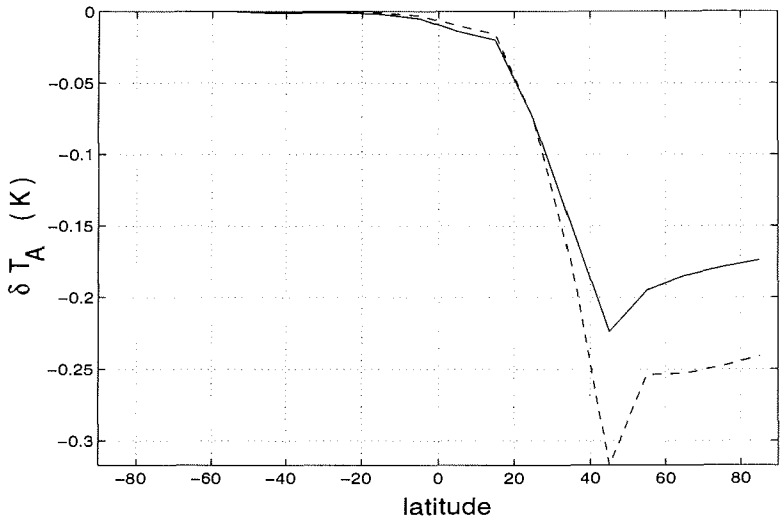

Figure 4.1: Reaction of the atmospheric temperature to a negative SST anomaly at 45^0 N of -1 K in a stand alone mode with fixed (dashed line) and variable (solid line) wind stress. For both experiments the change is smaller than the imposed SST anomaly at 45^0 N.

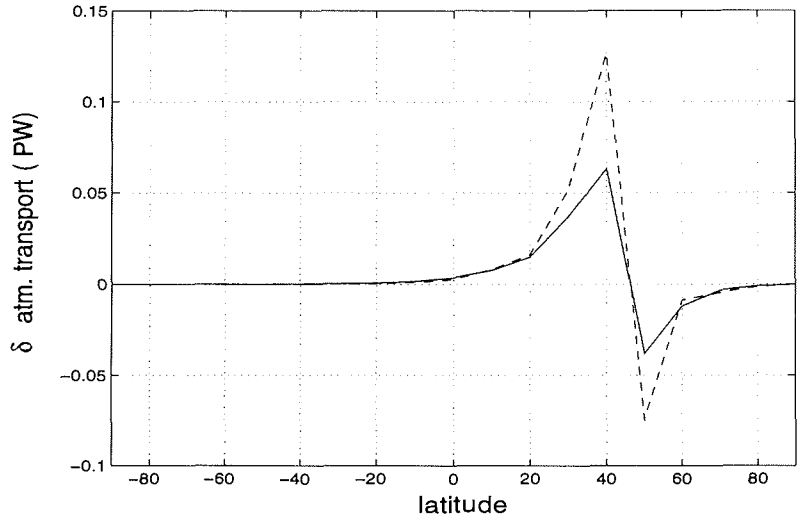

Figure 4.2: Reaction of total atmospheric heat transport ($PW = 10^{15}\,W$) to a negative SST anomaly at 45^0 N with fixed (dashed line) and variable (solid line) wind stress in equilibrium. The anomalous heat transport is enhanced equatorward of the anomaly and weakend poleward of it. This is due to different eddy activity.

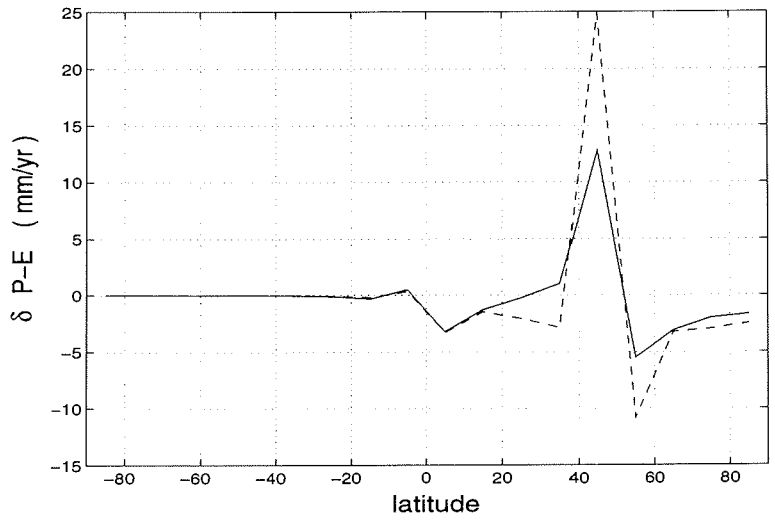

Figure 4.3: Change of fresh water flux with a negative SST anomaly at 45^0 N of -1 K in a stand alone mode with fixed (dashed line) and variable (solid line) wind stress. The pattern of $\delta(E-P)$ is spatially correlated to the anomalous heat flux in figure 4.4.

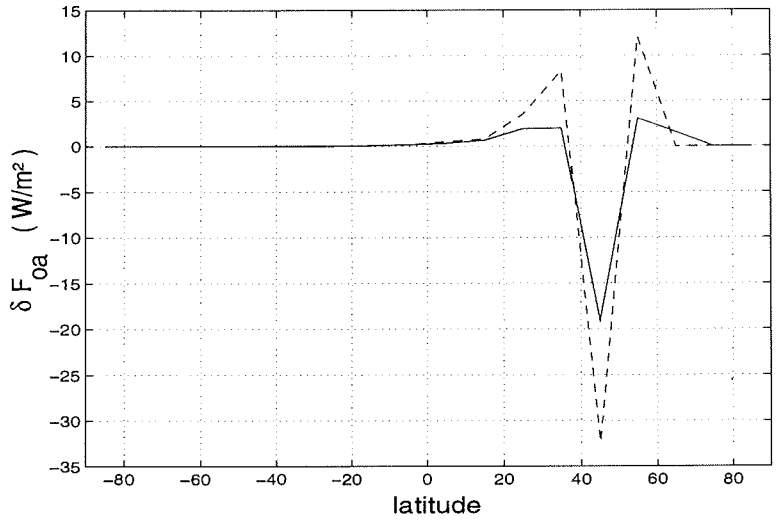

Figure 4.4: Reaction of the atmosphere-ocean heat flux to a negative SST anomaly at 45^0 N of -1 K with fixed (dashed line) and variable (solid line) wind stress. Negative values stand for a reduction of heat loss from the upper ocean.

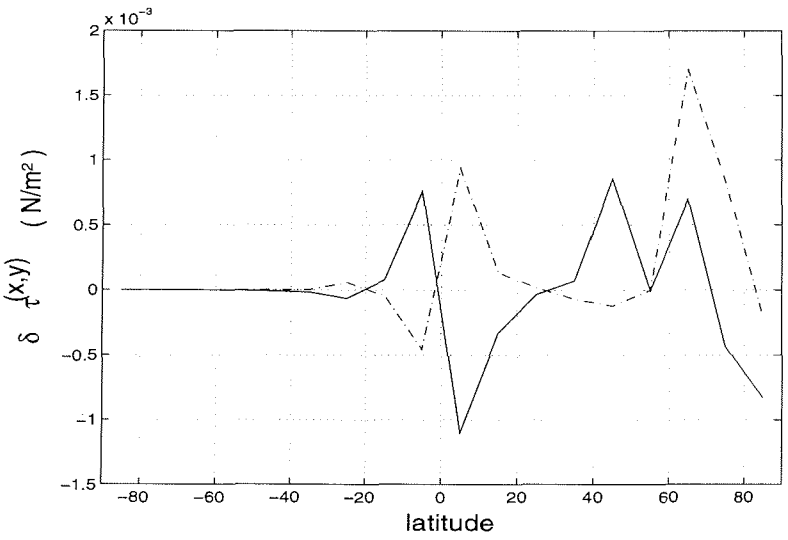

Figure 4.5: Equilibrium response of wind and wind stress to a negative SST anomaly at 45^0 N. The solid lines indicate the zonal direction, whereas the dashed dotted lines indicate the meridional direction.

stronger than normal winds towards west. However, the changes in wind stress are rather small (figure 4.5) and are typically less than 5% of the mean value. The mid-latitude ocean will respond to the changed wind stress with changes in oceanic velocity. This is consistent with findings of Frankignoul (1985) that the effect of changed wind is of less importance for large-scale anomalies. For the zonal component of wind stress on the northern hemisphere an enhancement of both westerlies and easterlies is observed. Both peaks of the meridional wind stress component in figure 4.5 can be explained by the fixed angle parameterization (figure 3.4). North of 55^0 N anomalous north-west wind corresponds to an enhanced storm track. The storm tracks are rather localized in the real atmosphere, therefore the zonally averaged change of wind stress is admittedly rather crude.

A positive feedback involving wind that amplifies the SST anomaly for middle latitudes can be seen from coupled GCM results of Latif and Barnett (1994). A negative SST anomaly enhances the storm track and the zonal wind. Therefore, the heat flux is enhanced due to diabatic heating at the surface. A further feedback connected to SST-anomalies is found by Deser and Blackmon (1993). They argue that the increased wind velocity and the changes in air-sea fluxes can contribute to the SST anomaly and reinforce it. Wind induced vertical mixing processes in the ocean that accelerate the entrainment of cooler water from below would further cool the SST. Therefore, the anomaly modifies the response in such a manner that the anomaly is strengthened. This may be a further argument for the experiment with a long lived SST anomaly imposed here.

The experiments show that a variable wind weakens the coupling between atmosphere and ocean because anomalous atmospheric temperatures and fresh water

fluxes are smaller (figures 4.3, 4.4). The heat flux change is rather non-linear because the coupling strength depends on the atmospheric temperatures itself. Later on we will see that the more decoupled the ocean is from the atmosphere, the more stable the THC in the coupled system becomes. This stand alone experiment is helpful in understanding the EBM, but should be interpreted with caution because an interactive ocean will change the response of the system.

4.2 Response of the atmospheric model to radiative forcing

The equilibrium response of the atmospheric model to a perturbation in radiation is investigated in a stand alone mode. This is useful in helping to understand the roles of latent and sensible heat transport included in the EBM. The model sensitivity is investigated under an external perturbation of an uniform increase in net radiation of $+4\,Wm^{-2}$. Such an increase is characteristic of the global warming due to a doubling of the atmospheric CO_2 (Lal and Ramanathan, 1984). For high latitudes this finding can be reproduced (Lohmann, 1995) by a one dimensional radiative scheme of Schmetz and Raschke (1979) and Schmetz (1984).

The downward terrestric radiation flux strongly increases whereas the upward flux is strongly reduced. the solar radiation flux diminishes in the troposphere (about $1Wm^{-2}$). The addition of CO_2 lifts the effective level of outgoing radiation, decreasing the radiation leaving the troposphere (Lal and Ramanathan, 1984).

Coupled GCM results of Manabe and Bryan (1985) show that the surface heat flux at the atmosphere-ocean interface remains almost constant under different CO_2 concentrations ($1 - 8 \times CO_2$, figure 17 therein). This will be also shown within a simple coupled model in section 8.1. Here, a fixed heat flux is used to look for the response of the EBM to perturbation in radiation.

The resulting anomalous atmospheric temperature is shown in figure 4.6. In this picture, the effect of the Hadley circulation (section 3.5) is included. Otherwise, the anomalous temperature would be colder and more smooth between 30^0 S and 30^0 N. The temperature change in figure 4.6 in this warmer climate is enhanced due sea ice melting, less snow and a reduction of surface albedo which is parameterized by the non-linear ice-albedo feedback.

Chen et al. (1995) checked the influence of the ice-albedo effect against the model climate associated with two versions of the model. The planetary albedo α depends on surface temperature T_A and an ice-albedo feedback factor $ff = \frac{\partial \alpha(y)}{\partial T_A}$. For both model versions, Chen et al. (1995) found an appropriate value of the feedback factor ff ($= 0.006$) by comparing the model sensitivity to external forcing to that of AGCMs. They found numerically that the system is very stable with respect to positive temperature anomalies whereas for negative perturbations in the initial conditions the stability depends on the ice-albedo feedback factor.

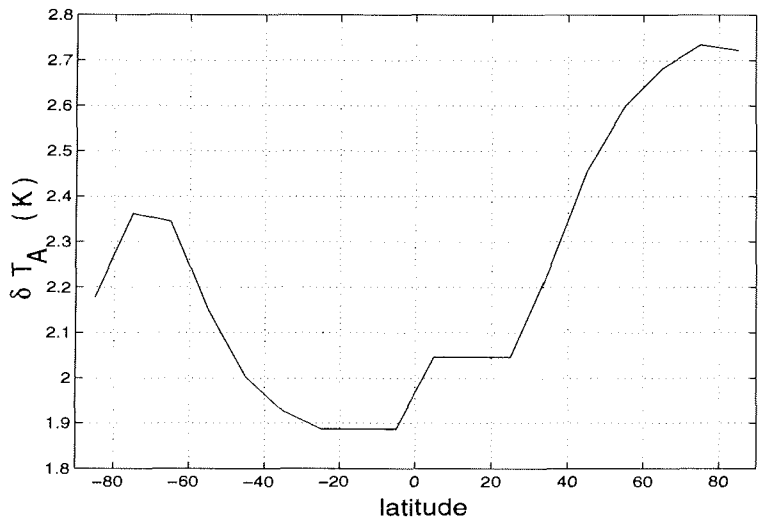

Figure 4.6: Anomalous surface temperature T_A under a perturbation in net radiation of $+4Wm^{-2}$.

If the whole heat transport (atmosphere and ocean) is held fixed (version 1) the stability of the atmosphere can be calculated analytically. From a linear stability analysis it follows that the system is stable if

$$ff \quad < \quad \frac{B}{\min\left[Q_R^{top}(y)\right]} \approx \frac{2.2}{180\,K} \approx 0.012\ K^{-1} \quad . \tag{4.3}$$

The choice of the ice-albedo factor is restricted because the solution is linearly unstable for $ff \geq 0.012\,K^{-1}$. Ice and snow are responsible for very low temperatures as a result of a strong destabilizing (positive) feedback. For stronger perturbations in the temperature initial conditions ($20\,K$ in Chen et al.) the critical ice-albedo feedback factor is much smaller ($ff_{crit} = 0.005\,K^{-1}$).

However, the restriction on ff can be relaxed if atmospheric heat can be transported in the meridional direction. In this case, the oversensitivity in the vicinity of the ice line disappears. Anomalous atmospheric heat transport is responsible for a non-local response to the radiative forcing. This mechanism, called transport-temperature feedback in Chen et al. (1995), cannot be neglected in climate studies (as e.g. in version 1 of Chen et al. and in Tang and Weaver, 1995).

Changes of sensible and latent heat transports in the atmosphere partly compensate each other (figure 4.7). Reduced sensible heat transport due to a reduction of meridional gradient of temperature is accompanied by enhanced latent heat transport due to increased temperature. This reflects the competing effects of latent and sensible heat transport in the atmosphere. The non-linear Clausius-Clapeyron equation plays the dominant part for the latent heat transport.

The different roles of sensible and latent heat transport have also been found by

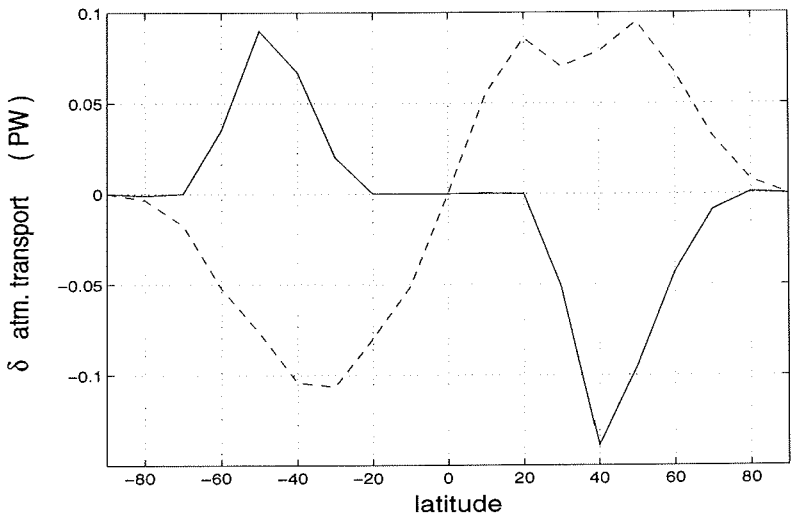

Figure 4.7: Anomalous eddy heat transport under a perturbation in net radiation which can be compared to a doubling of CO_2. The sensible heat transport $(-)$ is decreased whereas latent heat transport $(--)$ is increased.

Manabe and Bryan (1985) who studied the heat transport in atmosphere and ocean under different CO_2 forcings using a coupled circulation model. A reduced THC due to an enhanced hydrological cycle is left out in this stand alone experiment. This will be discussed in section 8.1 in a simple coupled model.

Chapter 5

Ocean Circulation Model

5.1 Primitive Equations

The equations of the ocean circulation model are the Navier-Stokes equations in spherical coordinates (λ, ϕ, z) , where λ and ϕ are longitude and latitude, respectively, and z is height relative to the mean radius of earth, a. Applying the hydrostatic and Boussinesq approximations, the momentum and continuity equations are

$$u_t + Adv(u) - \left(f + \frac{u \tan\phi}{a}\right) v = -\frac{1}{a\cos\phi}\left(\frac{p}{\rho_0}\right)_\lambda + A_{MV} u_{zz} + F^\lambda \quad (5.1)$$

$$v_t + Adv(v) + \left(f + \frac{u \tan\phi}{a}\right) u = -\frac{1}{a}\left(\frac{p}{\rho_0}\right)_\phi + A_{MV} v_{zz} + F^\phi \quad (5.2)$$

$$0 = -\left(\frac{p}{\rho_0}\right)_z - g\rho \quad (5.3)$$

$$Adv(1) = 0 \quad (5.4)$$

Here, u, v, and w are the longitudinal, latitudinal, and the vertical velocity components, respectively. ρ is the density while ρ_0 denotes the reference density. Adv represents the advection operator applied to a variable ξ :

$$Adv(\xi) = \frac{1}{a\cos\phi}\left[(u\xi)_\lambda + (v\xi\cos\phi)_\phi\right] + (w\xi)_z \quad . \quad (5.5)$$

F^λ and F^ϕ denote the horizontal, non-conservative terms, representing horizontal eddy stress divergence,

$$F^\lambda = A_{MH}\left[\nabla^2 u + (1 - \tan^2\phi)\frac{u}{a^2} - \left(\frac{2\tan\phi}{a^2\cos\phi}\right) v_\lambda\right] \quad , \quad (5.6)$$

$$F^\phi = A_{MH}\left[\nabla^2 v + (1 - \tan^2\phi)\frac{v}{a^2} - \left(\frac{2\tan\phi}{a^2\cos\phi}\right) u_\lambda\right] \quad . \quad (5.7)$$

Here, ∇^2 is the horizontal Laplacian operator in spherical coordinates:

$$\nabla^2\xi = \left(\frac{1}{a^2\cos^2\phi}\right)\left[(\xi)_{\lambda\lambda} + \cos\phi\,(\xi_\phi\cos\phi)_\phi\right] \quad . \tag{5.8}$$

To solve the equations numerically, the hydrodynamic equations are "coarse grained" in space and time. Subgrid scale processes are parameterized by diffusive mixing with horizontal and vertical eddy viscosity coefficients A_{MH} and A_{MV}. The horizontal eddy viscosity A_{MH} is artificially large to ensure that the western boundary currents have horizontal scales Δx that are resolved by the grid ($\beta v \sim A_{MH}\nabla^2 v_y \rightarrow A_{MH} = \beta\,\Delta x^3$). The vertical eddy viscosity coefficient A_{MV} has to be chosen such that the Ekman depth Δz_E does not exceed the depth Δz of the uppermost layer. The Ekman depth is defined by the Ekman balance ($fu \sim A_{MV}u_{zz} \rightarrow \Delta z_E = \sqrt{A_{MV}/f}$). Convection is parameterized implicitly as enhanced vertical diffusion according to the convective adjustment scheme implemented in Cox (1984) since the model cannot explicitly treat gravitational instabilities.

The equation for tracers χ, e.g. potential temperature Θ or salinity S, is

$$\chi_t + Adv(\chi) = A_{HH}\,\nabla^2\chi + A_{HV}\,\chi_{zz} \quad , \tag{5.9}$$

where A_{HH} and A_{HV} are the horizontal and vertical eddy diffusion coefficients. The potential temperature, salinity and depth determine the density of the ocean:

$$\rho = \rho(\Theta, S, z) \quad . \tag{5.10}$$

The vertical eddy diffusivity for tracers A_{HV} can be estimated from climatological hydrographic data (Olbers et al., 1985) and varies roughly between 10^{-5} and $10^{-4}\,m^2\,s^{-1}$ depending on depth and region. The vertical diffusivity of the tracers, A_{HV}, determines the intensity of the diabatic processes and thus influences the meridional mass transport (Bryan, 1987). However, the sensitivity of the THC with respect to subscale parameterizations is not considered here.

The horizontal eddy diffusivities for tracers are chosen to be artificially large so as to avoid computational errors in the chosen numerical scheme (leapfrog). The numerical algorithms for tracer advection (5.9) influence the behavior of the circulation (Gerdes et al., 1991), e.g. the meridional heat transport. The large value of A_{HH} produces an unrealistically strong upwelling at the western boundary layer of the subtropical gyre which reduces the amount of deep water carried from the formation areas towards low latitudes and across the the equator (Bryan, 1987; Danabasoglu and McWilliams, 1994). Improved parameterizations for mesoscale tracer transports, e.g. with mixing along isopycnals (Gent and McWilliams, 1990), have not been considered here.

Table 5.1: Coefficients parameterizing the subgrid scale processes along coordinate axis.

Parameter		$m^2\,s^{-1}$
horizontal viscosity (momentum)	A_{MH}	$2.0 \cdot 10^5$
vertical viscosity (momentum)	A_{MV}	$1.0 \cdot 10^{-3}$
hor. diffusion coeff. (tracer)	A_{HH}	$2.0 \cdot 10^3$
vert. diffusion coeff. (tracer)	A_{HV}	$1.0 \cdot 10^{-4}$

5.2 Numerical Model

The ocean model used is the 1991-version of the GFDL primitive equation model (Pacanowski et al., 1993, 1991) based on the work of Bryan (1969) and Cox (1984). The model with the acronym MOM (Modular Ocean Model) solves the primitive equations of section 5.1 with finite differences. For the numerics of this ocean model I refer to a detailed description by Cox (1984).

A rigid lid approximation is done, setting $w = 0$ at $z = 0$, to eliminate external gravity waves. With the rigid lid approximation the stream function of the vertically integrated mass transport Ψ is a prognostic variable of the model. Including external gravity waves would restrict the numerical computations to small time steps (Cox, 1984). Furthermore, the primitive equations were integrated with different time steps for the tracer and velocity. This asynchronous integration technique (Bryan, 1984) slows down the fast waves, the internal gravity waves and external Rossby waves, and makes numerical integration over hundreds of years possible. The improper representation of the fast waves is of no importance for the phenomena considered on a time scale of years. Internal Rossby and Kelvin waves accomplish the adjustment of the density field to changes in the forcing; they are hardly affected by that technique, because their wavelengths are large compared to the internal radius of deformation (Bryan, 1984).

In the following sections different idealized geometries of the Atlantic ocean are used. For all model representations a resolution of 2^0 in both the zonal and meridional directions is used. The model has 15 vertical levels with increasing grid size from 30 m to 836 m.

The east and west walls of the basin are insulating, non-slip, impermeable boundaries ($u = v = \Theta_\lambda = S_\lambda = 0$). The bottom is assumed insulating, free-slip and impermeable ($u_z = v_z = \Theta_z = S_z = 0$). The wind stress, applied to the surface, has a zonal and meridional component. Here, the wind stress is a function of latitude only where the zonal average has been taken over the Atlantic ocean.

$$\rho_0 A_{MV}\,(u_z, v_z) = (\tau^\lambda, \tau^\phi) \tag{5.11}$$

For all experiments, wind stress data of Hellerman and Rosenstein (1983) are used.

Chapter 6

Sensitivity of the oceanic circulation with respect to different boundary conditions

In the experiments documented here, the sensitivity of the THC is investigated for different types of boundary conditions to isolate the effects of the atmospheric heat transport and fresh water fluxes. Furthermore, systems with other boundary conditions used previously in the literature may be understood in terms of the coupled atmosphere-ocean system. The experiments give insight into the feedback processes of the coupled atmosphere-ocean system.

The ocean model is the primitive equation model of section 5.2 with a 70^0 wide sector from 66^0 S to 80^0 N representing the Atlantic. The model has a flat bottom of 5700 m everywhere. Because the non-linear terms in the momentum balance are small the steady state stream function of the vertically integrated transport Ψ is purely determined by the wind stress curl, giving the subtropical, subpolar and polar gyres in the ocean circulation. The integration is done with the distorted physics (Bryan, 1984) using a 8.6 h time step for the tracers and 0.5 h for the velocity fields.

The atmospheric model is the EBM described in chapter 3. Because an older version of the EBM was used here, wind stress τ^x is held fixed to climatological values (Hellerman and Rosenstein, 1983) and the meridional component τ_y is zero. Furthermore, the fresh water flux due to the storage term $(\partial_t q)$ is neglected and the heat flux is computed along with SST with a simplified version of the large-scale heat flux parameterization of section 3.4.

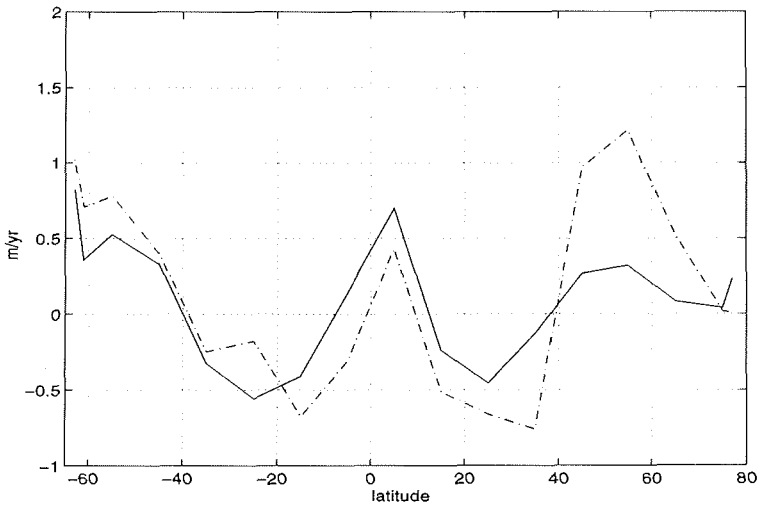

Figure 6.1: Comparison between fresh water fluxes from the spin up and climatology. The dashed line comes from a spin up with observed sea surface salinities whereas the solid line shows the climatological fresh water flux of Sellers (1969).

6.1 Experimental strategy and initial conditions

The spin up of the ocean is done from rest under restoring boundary conditions. Climatological salinities (Levitus, 1982) zonally averaged over the Atlantic basin and zonal mean atmospheric temperatures of Oort (1983) were used for the spin-up procedure. For the first 6800 yrs of integration, the surface fresh water flux is simulated by restoring law (2.2). Further 1380 yrs of integration used the zonal mean climatological fresh water flux of Sellers (1969). Integrating the model from the beginning with the climatological fresh water flux leads to a THC with sinking at both hemispheres which shows that the model has two different steady states under the same (mixed boundary) boundary conditions.

Both fresh water fluxes (precipitation - evaporation + runoff), shown in figure 6.1, qualitatively agree (positive fresh water in the equatorial region and middle to high latitudes). However, the diagnosed flux under restoring salinity to observed values strongly depends on the time constant τ_S in the spin up procedure (2.2). Larger relaxation times τ_S smooth out the diagnosed fresh water flux.

The ocean is in equilibrium with the boundary conditions if the oceanic heat and salt transport is equal to the same transport calculated by the fluxes F_{oa} and $(P-E)$ at the upper ocean surface:

$$WT_O(\phi) = \frac{1}{\cos(\phi)} \int_{-90^0}^{\phi} a\cos(\phi')\, F_{oa}(\phi')\, d\phi' \tag{6.1}$$

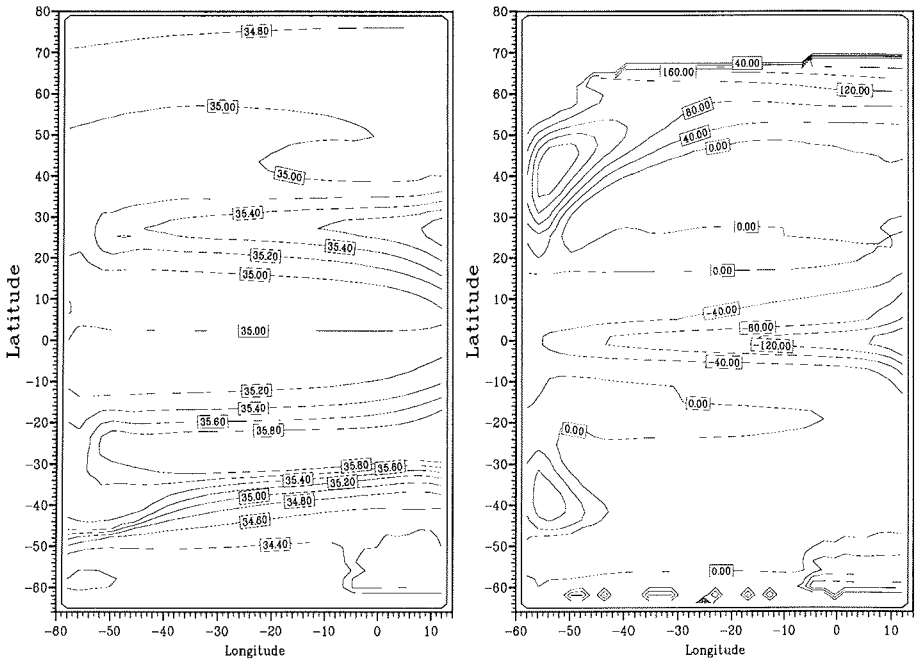

Figure 6.2: Left: Sea surface salinity field at the end of the spin up. Contour interval is 0.2 psu. Right: Heat flux out of the ocean upper boundary at the end of the spin up. The contour interval is $40\,Wm^{-2}$.

$$ST_O(\phi) = \frac{1}{\cos(\phi)} \int_{-90^0}^{\phi} a\cos(\phi') \frac{S_0}{\rho_w} (P-E)(\phi')\, d\phi' \quad , \tag{6.2}$$

where ρ_w and S_0 are the density of fresh water and reference salinity, respectively. The spin up process has been applied such that equations (6.1, 6.2) are fulfilled with less than 0.1% error. The heat flux out of the ocean at the end of the spin up is shown in figure 6.2 (right). The poleward western boundary currents near 40^0 loose much of the heat that the ocean absorbed in equatorial regions. Furthermore, in the deep water formation area between $60^0 - 70^0$ N, the ocean looses part of its potential energy by the surface heat flux.

Because the atmospheric model is zonally averaged the sea surface salinities under climatological $P - E$ have less meridional salinity difference than under the spin up procedure (2.2) using Atlantic salinity data of Levitus (1982). Figure 6.2 (left) shows the sea surface salinity field at the end of the spin up. The meridional gradients at the northern hemisphere are too low whereas on the southern hemisphere the salinity difference of up to 1.5 psu seems to be realistic. This field is strongly determined by the circulation and the fresh water fluxes used.

The stream function of the zonally integrated mass transport is a useful diagnostic

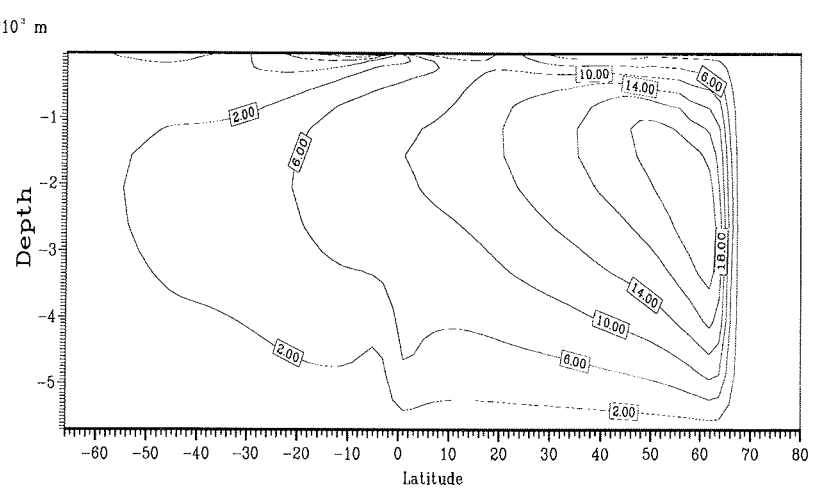

Figure 6.3: Stream function for the zonally integrated transport at the end of the spin up in Sv ($10^6 \frac{m^3}{s}$).

quantity for the thermohaline circulation:

$$\Phi(y,z) = \int_z^0 dz \int dx \; v(x,y,z) \quad . \tag{6.3}$$

The zonally integrated mass transport at the end of the spin up (figure 6.3) shows deep sinking between 60^0 N and 70^0 N and upwelling elsewhere. The circulation is a combination of wind driven Ekman transport in the upper layers with the thermohaline driven transport. North of the deep sinking area (70^0 N) sea ice is present. The thermodynamic sea ice model used will be explored in chapter 10. Sea ice isolates the oceanic mixed layer from the atmosphere since the heat flux is strongly reduced (see figure 6.2 right). In chapter 10, the feedback mechanisms due to sea ice are discussed. Here, we want to isolate the atmospheric-oceanic interactions. Therefore, a positive salinity anomaly at the southern boundary is induced instead of a negative anomaly in the deep water formation area. The perturbation in the south might seem artificial because the ACC is not represented in the model ocean, but this scenario may be interpreted as a "kick on" of the conveyor belt in the North Atlantic.

A fresh water deficit of 0.026 Sv is added at the southern boundary permanently. To close the water balance the fresh water of 0.026 Sv is distributed over the southern hemisphere. In the spin up steady state, sea ice was present at the southern boundary which can be seen from the heat flux out of the ocean in figure 6.2 (right). However, due to the positive salt flux anomaly this sea ice vanishes in all four following experiments. This sea ice effects slightly affect the radiation balance and have no influence on the results and subsequent conclusions.

The spin up steady state is integrated further for a few hundred years of integration in the coupled mode without any perturbation. No significant change of the state is

6.2 Experiments and Discussion

Some results of the four experiments are documented in table 6.2. Note, that the experiments MBC, SM and cHF are close to equilibrium according to criterium (6.1, 6.2).

Under mixed boundary conditions (MBC), the THC reinforces itself through advection of salt and a southern sinking state evolves (figure 6.4). The oceanic heat transport at 50^0 S is reduced by about $0.461\,PW$ (table 6.2). As in the SST-experiment in section 4.1 the anomalous heat flux $\delta F_{oa}(55^0 S)$ at the ocean-atmosphere interface significantly changes as a result of the fixed atmospheric temperature.

The high sensitivity of this system is in agreement with Bryan (1986) who gained qualitatively the same result. In his flat-bottom single basin extending from pole to pole, he obtained three qualitatively different stable steady states: Deep water formation in the north, in the south, and both in the north and south. The southern sinking case is similar to that of figure 6.4 where only 6.7 Sv as the maximal meridional volume transport is build in the northern hemisphere instead of 25.5 Sv in the reference case.

The development of the southern sinking state (figure 6.4) is related to the deep water formation process. Lenderink and Haarsma (1994) using mixed boundary conditions found that large areas of the ocean are in a potentially convective region in which convection is possible but not occuring. They observed a "domino" effect: Triggering or suppressing of convection in a small area results in a change of convective states in a much larger region. This effect may be responsible for the development of the completely different circulation (figure 6.4).

The circulation with mixed boundary conditions is very sensitive to the perturbation because the positive feedback of salt advection is included, whereas the negative feedback of temperature advection is underestimated through the strong relaxation to a fixed atmospheric temperature T_A^*. It is useful to understand the behaviour of a model using mixed boundary conditions in terms of the coupled system. In terms of the EBM, both long and short wave radiation are constant due to fixed atmospheric temperature. Because of the unchanged radiation budget, the anomalous oceanic heat transport (figure 6.6 a) is balanced in equilibrium by an anomalous atmospheric heat transport necessary to fix the atmospheric temperature. Mixed boundary conditions therefore imply an atmospheric model with strong anomalous atmospheric heat transport maintaining the atmospheric temperature T_A^*.

The system with Schopf's model as a thermal boundary condition (SM) shows an almost constant oceanic heat transport F_O (table 6.2). The stream function of the zonally integrated mass transport (figure 6.5) does not differ very much from the reference case. How can this very stable behavior be understood ?
Again, the total heat transport (ocean+atmosphere) in equilibrium remains constant because of the radiation budget. Therefore, the oceanic heat transport (figure 6.6 b) cannot change much since the atmospheric transport is fixed. This experiment demonstrates that including the atmospheric heat transport into the boundary conditions is necessary for the system to enable it to develop freely into another state of the circulation. The system with Schopf's model as a thermal boundary condi-

Table 6.2: Results for the final states of the experiments with different atmospheric models (as in table 6.1). $\Phi_{max}(SH)$ and $(WT_O)_{max}(SH)$ stand for the the maximal meridional overturning and northward oceanic heat transport on the southern hemisphere. The values of anomalous temperatures, salinity, density and heat flux $(T_O, T_A, S, \rho_O, F_{oa})$ at 55^0S are zonally and meridional averaged between 50^0 and 60^0 S latitude. Note that the system with Schopf's model (SM) as a thermal boundary condition is the most stable circulation whereas the system with mixed boundary conditions (MBC) is the most unstable one. The results of the two experiments with coupled heat flux (cH) and coupled both heat and fresh water flux (cHF) are nearly identical.

	units	MBC	SM	cH	cHF
$\Phi_{max}(SH)$	Sv	-32.1	-4.7	-21.1	-21.3
$(WT_O)_{max}(SH)$	PW	-0.786	-0.209	-0.441	-0.417
$\delta T_O(55^0S)$	K	1.03	0.96	2.04	2.01
$\delta S(55^0S)$	psu	0.62	0.41	0.67	0.67
$\delta \rho_O(55^0S)$	$kg\,m^{-3}$	0.41	0.25	0.36	0.36
$\delta T_A(55^0S)$	K	0	0.33	1.69	1.68
$\delta F_{oa}(55^0S)$	Wm^{-2}	43.76	0.98	14.01	10.87
$\delta F_s(50^0S)$	PW	-	0.0	0.234	0.238
$\delta F_l(50^0S)$	PW	-	0.0	0.013	0.015
$\delta F_O(50^0S)$	PW	-0.461	-0.068	-0.258	-0.242

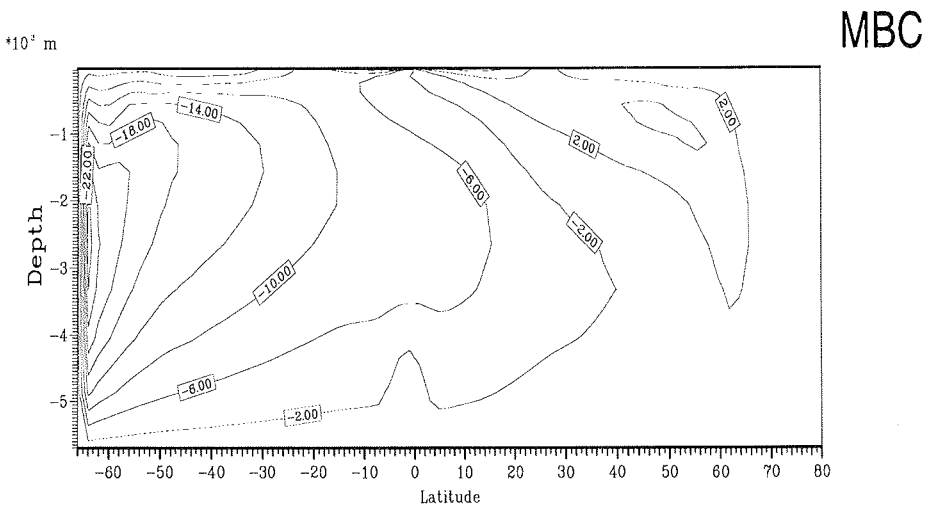

Figure 6.4: Stream function of the zonally integrated transport for the experiment with mixed boundary conditions (MBC) after 1906 years of integration. The maximal overturning rate and maximal southward heat transport on the southern hemisphere are -32.1 Sv and 0.79 PW , respectively.

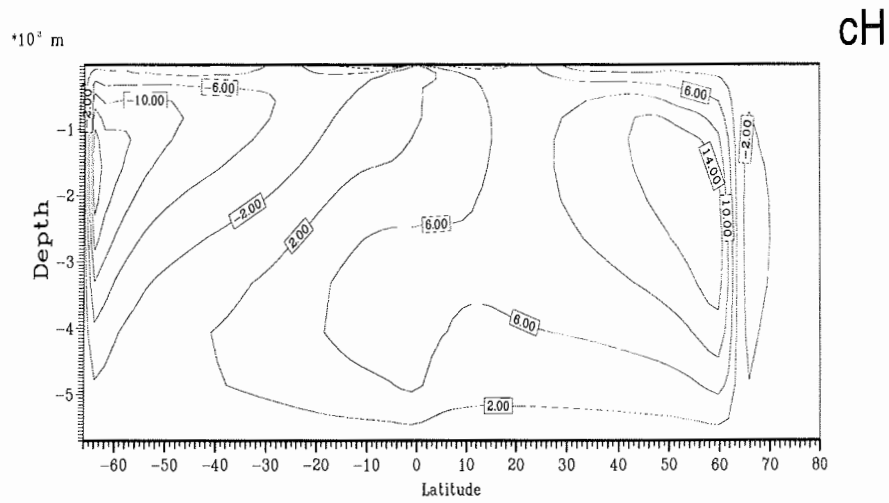

Figure 6.7: Stream function for the zonally integrated transport for the coupled experiment where the ocean surface receives a fixed fresh water flux (cH), 805 years after the reference case. The maximal overturning rate and maximal southward heat transport on the southern hemisphere are -21.1 Sv and 0.44 PW , respectively.

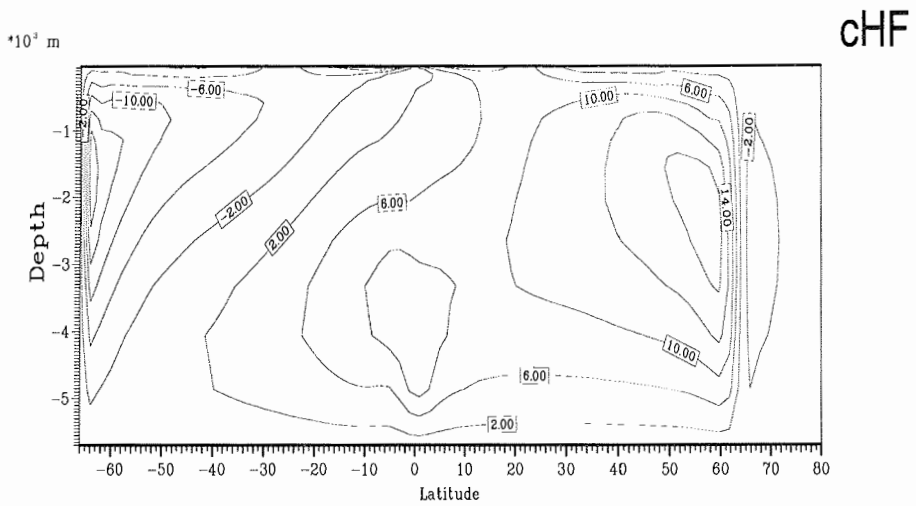

Figure 6.8: Stream function for the zonally integrated transport for the fully coupled energy balance model (cHF) close to equilibrium. Compared to figure 6.7 the overturning rate is about the same. The maximal overturning rate and maximal southward heat transport on the southern hemisphere are -21.3 Sv and 0.42 PW , respectively.

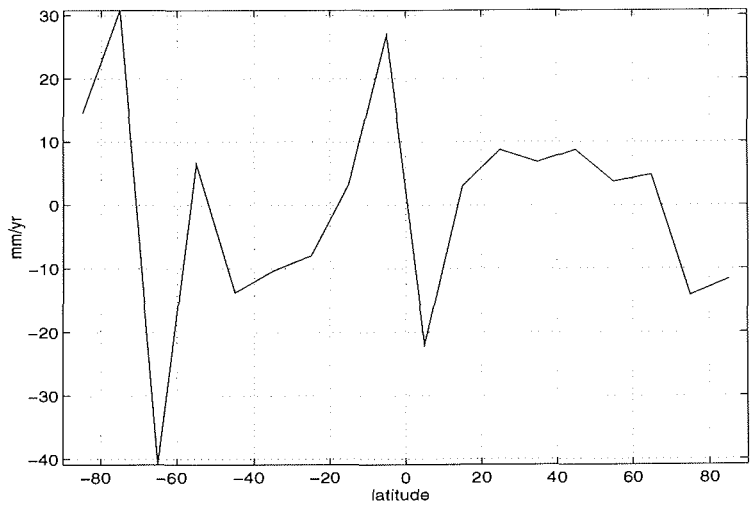

Figure 6.9: Change of fresh water flux for the ocean surface in the fully coupled system (cHF). Note that the anomalous fresh water flux is relatively small and of minor importance for the stability of the THC.

combined with a local warming (ca. 2^0 K) such that the local density change lies between the experiments MBC and SM.

The new boundary condition cHF affects the local processes as vertical mixing. These local processes may trigger a large-scale oceanic response. Diagram 2.1 shows this behaviour in a schematic way which was qualitative found here. The sensitivity of the coupled system (cH and cHF) lies between the systems using boundary conditions MBC and SM (figures 6.4, 6.5, 6.7, 6.8). The reason is that the stabilizing effect of oceanic large-scale heat advection is included in SM, cH and cHF, whereas the destabilizing effect of atmospheric heat transport is included in cH and cHF.

The stabilization of the THC in the coupled mode compared to mixed boundary conditions is in agreement with findings of Rahmstorf and Willebrand (1995). Their atmospheric model consists of the scale dependent restoring (3.36) which is similar to the case cH where the fresh water flux for the ocean surface is held fixed. They added a fresh water pulse into the northern North Atlantic which resulted in a shallower NADW formation connected with a cooling of 3 K north of 56^0 N. This cooling can only be explained by the diffusive term in (3.36) (Rahmstorf, 1994) which corresponds to the atmospheric heat transport.

The stabilizing effect of their boundary condition is based on the interaction between oceanic convection and diffusion in the atmospheric model (Rahmstorf, 1995 a). Indeed, the local scale effect of vertical mixing in the ocean depends on the boundary conditions used. Applying the conceptual model with mixed boundary conditions of Lenderink and Haarsma (1994) to a new boundary condition with weaker coupling (e.g. the EBM or formulation 3.36) provides much smaller areas of potential con-

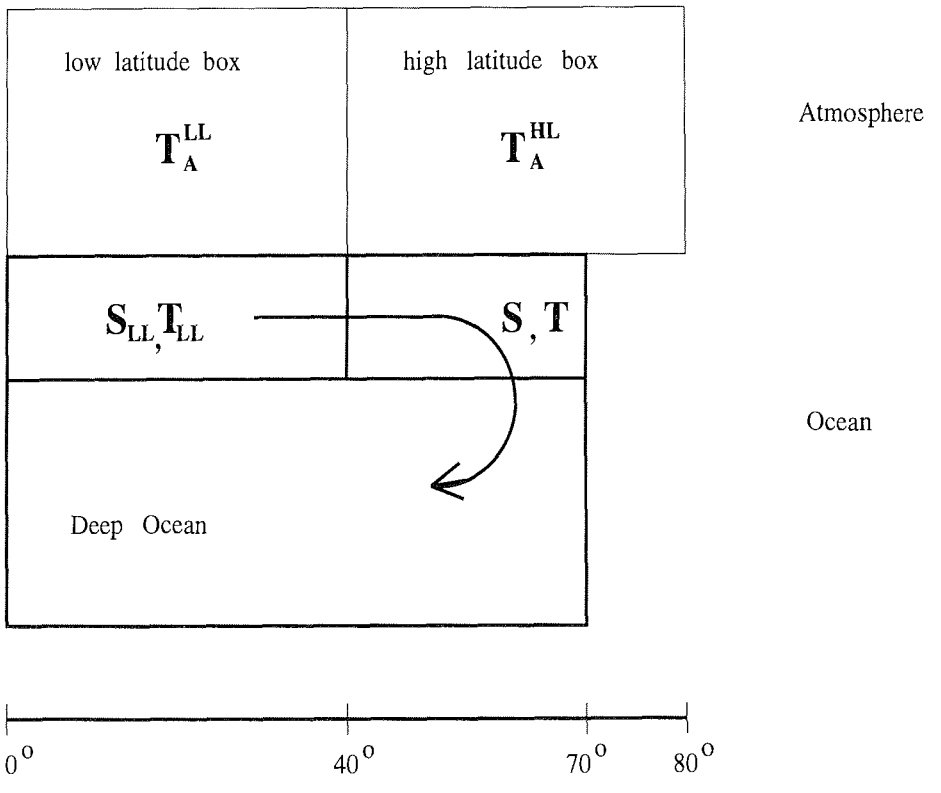

Figure 7.1: Schematic representation of the model configuration.

7.1.1 Ocean model

In the North Atlantic, both surface temperature and salinity decrease with increasing latitudes. We denote $\Delta T = T - T_{LL} < 0$ and $\Delta S = S - S_{LL} < 0$ as the differences in oceanic temperature and salinity between the high latitude and the low latitude boxes. The heat and salt balances are parameterized similar to Stommel's box model (1961, 1993). The advective transport of heat and salt for the high latitude box is calculated with an upstream scheme:

$$v \cdot A_1 \cdot \begin{cases} T_{LL} \\ S_{LL} \end{cases} - w \cdot A_2 \cdot \begin{cases} T \\ S \end{cases} \quad , \tag{7.1}$$

where v, w denote the meridional and vertical velocities and A_1, A_2 the interfaces between the high and low latitude and between the high and deep ocean boxes. The velocities v and w are expressed by the meridional mass transport Φ per areas A_1 and A_2, respectively. The non-linear equations for temperature T and salinity S for the high latitude box are

$$\frac{d}{dt}T = -\frac{\Phi}{V}\Delta T - \frac{F_{oa}}{\rho_0 c_p \Delta z} \tag{7.2}$$

$$\frac{d}{dt}S = -\frac{\Phi}{V}\Delta S - \frac{S_0}{\Delta z}(P-E) \quad , \tag{7.3}$$

where V is the volume of that box, $(P-E)$ denotes precipitation minus evaporation, F_{oa} is the heat flux at the ocean-atmosphere interface, and S_0 is a reference salinity of 35 psu. The heat capacity of the ocean layer that interacts with the atmosphere is $\rho_0 c_p \Delta z$ with $\Delta z = 100$ m, the thickness of the upper ocean boxes. The overturning rate Φ is assumed to be proportional to the meridional density difference:

$$\Phi = -c\,(\alpha \Delta T - \beta \Delta S) \quad , \tag{7.4}$$

where $\alpha = 0.15\,K^{-1}$ and $\beta = 0.8\,\mathrm{psu}^{-1}$ are the thermal and haline expansion coefficients, respectively, and $c = 17 \cdot 10^6\,m^3\,s^{-1}$ is a tunable parameter that is used to reproduce the present meridional overturning in the Atlantic. The overturning rate Φ must be positive, otherwise (7.2, 7.3) do not apply. This is no restriction as long as only today's circulation with cold water sinking at high latitudes is considered. All water transported poleward will be brought to the deep ocean at high latitudes, so vertical sinking is implicitly included in the model. Convective mixing with the deep ocean box is not considered.

Restoring the salinity to a climatological value S^*, the expression $\frac{S_0}{\Delta z}(P-E)$ in equation (7.3) must be substituted by $\frac{1}{\tau}(S - S^*)$ with an arbitrary time constant τ (often chosen to be about one month).

The heat flux between the ocean and atmosphere is calculated by a linearized bulk formula:

$$F_{oa} = Q_1 + Q_2(T - T_A) \quad , \tag{7.5}$$

with $Q_1 = -50\,Wm^{-2}$ and $Q_2 = 38\,Wm^{-2}K^{-1}$ for the high latitude box (Oort and Peixoto, 1983, Oberhuber, 1988).

Fresh water exchanges of the North Atlantic basin with other basins are neglected. This has been estimated for the North Atlantic (north of 24^0) as a volume loss of $0.03 \cdot 10^6\, m^3 s^{-1}$ with an atmosphere general circulation model (Zaucker and Broecker, 1992). There is a great uncertainty in these estimates. However, the climate system can be very sensitive to the zonal transport of water vapour, which has been shown by Birchfield (1989) and Stocker et al. (1992).

Coupled system

In analyzing the stability of the coupled system subject to salinity perturbations at high latitudes, a time scale separation is assumed. Local processes at high latitudes associated with changed sinking rates act on a much shorter time scale than the large-scale advection affecting the low latitude temperature and salinity. Therefore, as a first order approximation, salinities and temperatures at low latitudes and for the deep ocean are held constant. This assumption is appropriate as long as the volumes of the surface layer boxes are smaller than the deep ocean box and other possible equilibria of (7.2, 7.3) are not considered.

Assuming constant oceanic temperature at low latitudes, changes of the low latitude atmospheric temperature can be expressed by the high latitude atmospheric temperature using the energy balance (7.6):

$$\delta T_a^{LL} = \frac{K}{K + B + Q_2^{LL}} \quad \delta T_a^{HL} = \eta \quad \delta T_a^{HL} \quad , \tag{7.15}$$

where Q_2^{LL} is the heat flux rate at low latitudes, chosen as $50\, W m^{-2} K^{-1}$ (Oberhuber, 1988). We define a transport parameter K for the atmospheric heat transport as:

$$K = \frac{1}{L_y} \cdot \left(r \cdot \frac{K_s^{(1)} + K_{l0}^{(1)}}{L_y} \pm \frac{K_{l1}}{2} \right) \quad . \tag{7.16}$$

The term $\pm K_{l1}/2$ results from the temperature dependence of the latent heat transport in (7.12). The negative sign (reduced transport) applies for negative temperature anomalies δT_a^{HL}. The transport parameter K and the change in high latitude atmospheric temperature determine the anomalous atmospheric heat transport.

For the change in oceanic surface fresh water flux, the catchment area of the high latitude oceanic box must be take into account. At high latitudes with our chosen model geometry, the area of the atmospheric box is 1.9 times larger than the oceanic box. With (7.14) and (7.15) the change in surface fresh water flux is

$$\delta(P-E) = -1.9 \, \frac{r\, K_{l0}^{(1)}\, (1-\eta)/L_y \;\pm\; K_{l1}\, (1+\eta)/2}{L_y\, L_v \rho_w} \quad \delta T_A^{HL} \tag{7.17}$$

$$= -K_2 \quad \delta T_A^{HL} \quad , \tag{7.18}$$

where ρ_w is the density of fresh water and K_2 is a sensitivity coefficient of the hydrological cycle.

For simplicity we consider from now on only negative temperature anomalies, and therefore, only the minus signs in equations (7.16, 7.18) are used. For this case and for $r = 1$ the parameters K, K_2 and η are: $K = 3.2\ Wm^{-2}K^{-1}$, $K_2 = 12\ mm\,yr^{-1}\,K^{-1}$ and $\eta = 0.06$ using the estimates for $K_s^{(1)}, K_{l0}^{(1)}$ and K_{l1} specified above. The small value of η means that the low latitude response is only a small fraction of the atmospheric anomaly at high latitudes.

Balance of the coupled system

Choosing a basic state $(\Delta T^0, \Delta S^0) = (-13.5\ \text{K}, -1.5\ \text{psu})$, the equilibrium transport Φ^0 is $14 \cdot 10^6 m^3 s^{-1}$ and the equilibrium fresh water flux for the high latitude oceanic box is,

$$(P-E)^0 = -\frac{\Delta z}{S_0}\frac{\Phi^0}{V}\Delta S^0 = 1.25\ m\,yr^{-1} \tag{7.19}$$

which corresponds to a fresh water flux of $0.65\ m\,yr^{-1}$ for the high latitude atmospheric box. Both, stream function and fresh water flux, are typical for the present climate (Dickson and Brown, 1994; Oort and Peixoto, 1983).

Subtracting the basic state from (7.2) and (7.3) yields a set of non-linear differential equations for the perturbations $\Delta T' = \Delta T - \Delta T^0$ and $\Delta S' = \Delta S - \Delta S^0$:

$$\frac{d}{dt}\Delta T' = -\frac{\Phi^0}{V}\Delta T' - \frac{\Phi'}{V}\Delta T' - \frac{\Phi'}{V}\Delta T^0 - \frac{F'_{oa}}{\rho_0 c_p \Delta z} \tag{7.20}$$

$$\frac{d}{dt}\Delta S' = -\frac{\Phi^0}{V}\Delta S' - \frac{\Phi'}{V}\Delta S' - \frac{\Phi'}{V}\Delta S^0 + \frac{S_0}{\Delta z}K_2\ \delta T_A^{HL} \tag{7.21}$$

The deviation from the equilibrium atmosphere-ocean heat flux, F'_{oa}, and fresh water flux, $K_2\,\delta T_A^{HL}$, depend on the formulation of the atmosphere model. Making the substitution

$$\epsilon = \frac{\delta T_A^{HL}}{\Delta T'} \tag{7.22}$$

F'_{oa} can be written as

$$F'_{oa} = (1-\epsilon)\ Q_2\,\Delta T' \quad . \tag{7.23}$$

The surface fresh water flux term in (7.21) becomes

$$\frac{S_0}{\Delta z}K_2\ \delta T_A^{HL} = \frac{S_0}{\Delta z}K_2\ \epsilon\ \Delta T' \quad .$$

In the case of a restoring boundary condition this term has to be substituted by $-\frac{1}{\tau}\Delta S'$, which effectively removes sea surface salinity anomalies.

Different representations of the atmospheric heat transport are now reduced to different values of ϵ. For a fixed atmospheric temperature, as with mixed boundary

$$\epsilon > \left[-\frac{S_0 K_2}{\Delta z}\frac{c\beta}{V}\Delta T^0 + \frac{Q_2}{\rho_0 c_p \Delta z}\left(\frac{\Phi^0}{V} + \frac{c\beta}{V}\Delta S^0\right) \right]^{-1} \left\{ \frac{Q_2}{\rho_0 c_p \Delta z}\left(\frac{\Phi^0}{V} + \frac{c\beta}{V}\Delta S^0\right) + \frac{c^2\alpha\beta}{V^2}\Delta S^0 \Delta T^0 - \left(\frac{\Phi^0}{V} + \frac{c\beta}{V}\Delta S^0\right)\left(-\frac{\Phi^0}{V} + \frac{c\alpha}{V}\Delta T^0\right) \right\} . \quad (7.28)$$

The analysis is restricted to a range of basic states where the bracket [...] is negative. Positive values correspond to basic states that are not realized in the present climate, viz a reversed thermohaline cell or a small ratio of meridional salinity gradient to meridional temperature gradient. For mixed boundary conditions (fixed atmospheric temperature and fresh water flux) the range of basic states considered is characterized by

$$0.5 < \frac{\beta\Delta S^0}{\alpha\Delta T^0} < 1 . \quad (7.29)$$

For this range the stability condition (7.28) always fails for mixed boundary conditions. A freshwater perturbation at high latitudes changes the density and reduces the northward salt transport, which amplifies the decrease in density and leads to a "polar halocline catastrophe". The finding of an unstable THC under mixed boundary conditions with respect to infinitesimal changes in high latitude salinity is consistent with earlier results from simplified models of Marotzke et al. (1988) and Marotzke (1990) and a three dimensional model of Weaver and Sarachik (1991). In other models using mixed boundary conditions (e.g. Bryan, 1986) finite amplitude perturbations may be necessary to initiate a transition for which the ocean becomes unstable. The sensitivity of the THC under mixed boundary conditions is influeneced by the meridional salinity difference ΔS^0 resulting e.g. from the strength of the fresh water flux forcing (Weaver et al., 1991). This finding is consistent with (7.29).

However, in more complex models finite amplitude perturbations may be necessary to initiate a transition for which the ocean becomes unstable (e.g. Bryan, 1986). All ocean models under mixed boundary conditions show a very high sensitivity against sea surface salinity perturbations at high latitudes.

Since the real climate system is less sensitive to these perturbations, there must be at least one neglected negative feedback to stabilize the climate system. When the meridional mass transport is reduced due to a salinity anomaly at high latitudes, the atmosphere will be cooled by a reduced heat flux from the ocean. Deep water formation can still take place at a reduced rate with fresher but colder water. In our coupled system with the above-estimated values of K and K_2, the right hand side of (7.28) is 0.57 which is less than the value for ϵ estimated by (7.25). Therefore, this system is stable with respect to infinitesimal perturbations in high latitude salinity. However, with another choice of the transport parameters K and K_2 the system can be closer to the bifurcation point at which the system becomes unstable.

To show the effect of different transport parameters, the stability condition (7.28) is calculated and plotted in the parameter space (K_2, K) in figure 7.2 (solid line). Increasing the meridional atmospheric transports of heat and moisture (increasing

K_2 and K) destabilizes the system. Enhanced eddy activity brings more warm and humid air to regions where deep water formation takes place and reduces the density of the surface water. Note that a higher power law for the eddy heat transports destabilizes the system. With our choice of parameters the system is linearly unstable above $r = 3.3$ (figure 7.2). The stability appears to be sensitive to both heat and fresh water flux changes through eddy activity. Changes of the fresh water flux act as a strong destabilizing feedback. For a negative temperature anomaly considered, the temperature dependent part of δF_l in (7.12) reduces the latent heat transport and the destabilizing effect of the atmospheric heat transport and fresh water flux. However, the effect of the hydrological cycle is a great uncertainty and must be studied quantitatively by complex climate models.

According to condition (7.28), the stability of the coupled system (7.20,7.21) depends on the basic state $(\Delta T^0, \Delta S^0)$. The sensitivity with respect to the basic state is analyzed, fixing the transport coefficients (K_2, K) at our previous estimates. The present circulation is characterized by a temperature-controlled deep water formation with a strong overturning stream function Φ^0. The corresponding basic state $(\Delta T^0, \Delta S^0) = (-13.5\text{ K}, -1.5\text{ psu})$ with $c = 17 \cdot 10^6 m^3 s^{-1}$ is stable for high latitude salinity perturbations (figure 7.3). Furthermore, increasing the meridional overturning parameter c stabilizes the system by shifting the line of critical stability upwards in figure 7.3 (dashed line for an increase in c of 20%). Figure 7.3 indicates that a different basic state with either a smaller meridional temperature gradient $|\Delta T^0|$ or a larger salinity gradient $|\Delta S^0|$ would be linearly unstable. Such a different basic state could for instance result from different greenhouse gas concentrations in the atmosphere which, according to coupled GCM results (Manabe and Stouffer, 1993), tend to produce a smaller temperature difference and a larger salinity contrast than presently observed. This climate state is connected with a decreased sensible heat transport and an increased latent heat transport, partly compensating each other (see section 4.2).

However, we must take into account that in a warmer than today's climate, e.g. the Eemian interglacial or a climate with higher greenhouse gas concentrations, the temperature dependence of latent heat transport would be larger (to be represented by a larger coefficient K_{l1} in our model). For negative temperature anomalies in such a warmer climate the sensitivity coefficient of the hydrological cycle K_2 in (7.18) would be reduced which again stabilizes slightly the system.

Our stability analysis shows that the less the heat flux is changed the more stable is the system, corresponding to high values of ϵ. Because the anomalous heat flux F'_{oa} in (7.23) is proportional to the heat flux rate Q_2, the line of critical stability in figure 7.2 (the dashed and solid lines) shifts downward as the heat flux rate Q_2 is increased. However, in (7.23) changes of Q_2, denoted by δQ_2, are neglected which would give an additional term $\delta Q_2 \cdot (T - T_A^{HL})$ to the anomalous heat flux. Any physical process associated with high latitude salinity perturbations (e.g. enhanced surface wind speed) which increases the heat flux rate Q_2 would reduce the anomalous heat flux $|F'_{oa}|$ and with that the sensitivity of the system. This finding is in agreement with that of section 4.1 where a long lived SST anomaly was imposed to study the behavior of the atmospheric model. These experiment show that the enhanced wind speed decreases the response of the heat and fresh water fluxes. On the other hand, the latent heat flux at the ocean-atmosphere interface (3.27) is re-

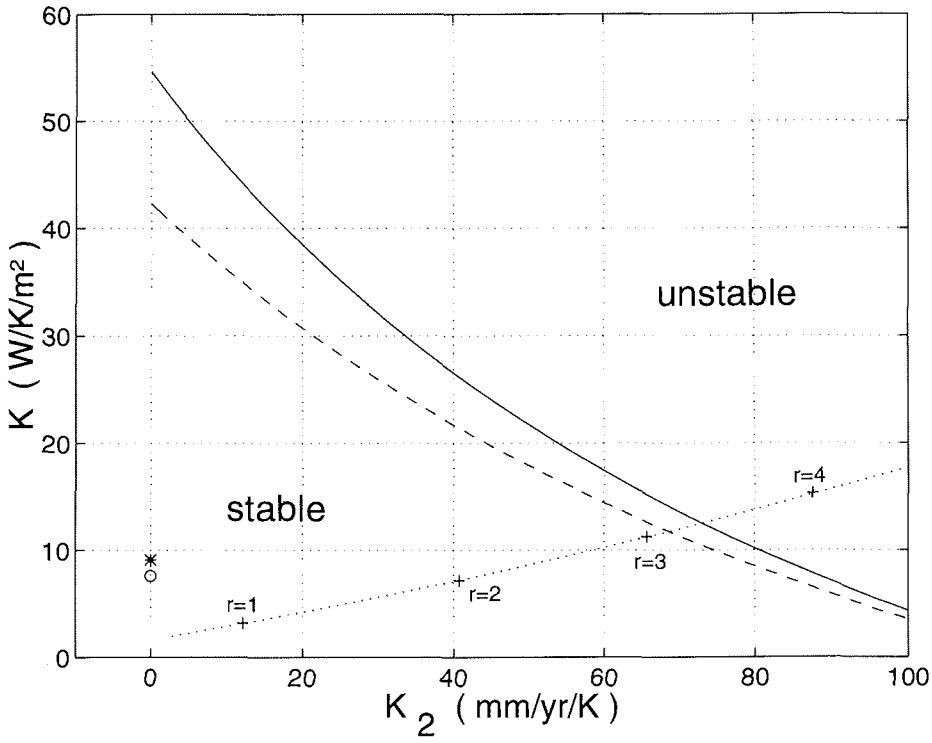

Figure 7.2: Stability diagram in the parameter space for the eddy coefficient of heat transport K and the sensitivity coefficient of the hydrological cycle K_2, which is defined by: $\delta(P-E) = -K_2 \quad \delta T_A^{HL}$. The coupled system is linearly stable below the curve and unstable above. The solid line and the pair of coefficients, marked by $(+)$ lying on the dotted curve, correspond to our coupled system for different power laws with exponent r. With the estimated parameters (K_2, K) our coupled system is stable with respect to small perturbations in high latitude salinity until $r \leq 3.3$. The dashed line corresponds to the parameters $(Q_2, B) = (46\frac{W}{Km^2}, 3\frac{W}{Km^2})$, which may be compared with the values of Stocker et al. (1992), marked by $(*)$, and Rahmstorf and Willebrand (1995), marked by (o). Higher values of Q_2 have a destabilizing effect for the system since the coupling between ocean and atmosphere is stronger. Note that the atmospheric models of Stocker et al. (1992), Rahmstorf and Willebrand (1994) and Zhang et al. (1994) are on the $K = 0$ axis.

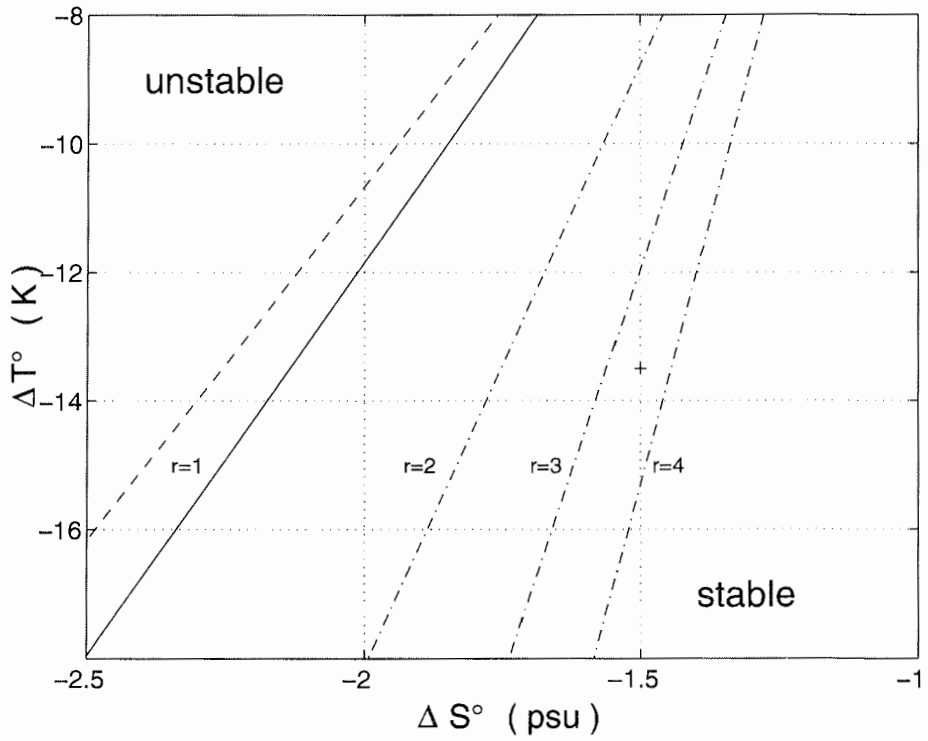

Figure 7.3: Stability diagram in the parameter space $(\Delta T^0, \Delta S^0)$ with fixed transport parameters (K_2, K). The coupled system is linearly stable below the curve and unstable above. The dashed and solid lines correspond to a linear diffusion $(r = 1)$ for the atmospheric transports while the dashed dotted lines correspond to higher power laws. A strong thermally dominated deep water formation and small salinity differences ΔS^0 favor the stability of the THC. An enhanced overturning rate (by increasing the parameter c by 20% ; dashed line) shifts the line of critical stability upwards.

Table 7.1: Critical salinity perturbation for different values of the parameter r. The parameter n is defined by: $\delta S_{crit} \approx n \cdot \delta S_{GSA} = n \cdot 0.048$ psu.

r	δS_{crit} psu	n
1	0.63	13
2	0.27	5
3	0.05	1

duced by a decreased temperature which will destabilize the coupled system.

The remaining question for our coupled box model is how large perturbations might cause a "polar halocline catastrophe". For (7.20,7.21) there is no easy Lyapunov function (as in Cessi and Young, 1992) to estimate analytically the basin of attraction and the parameter dependency of that region. This is unfortunate because the linear part of the dynamics (7.20, 7.21) has a non-normal matrix, so that the condition (7.28) might be valid only in a very small neighborhood of the stable solution (Trefethen et al., 1993). Therefore, it is necessary to simulate the stability behavior for finite perturbations numerically.

Table 7.1 shows the critical salinity perturbations for $r = 1, 2, 3$. Larger perturbations will lead to a a different state of the non-linear system (7.20,7.21) where the meridional mass transport vanishes ("polar halocline catastrophe").

It is useful to compare the critical perturbation with the freshening of the Great Salinity Anomaly (1968-1982) which was characterized by a salt deficit in the upper few hundred meters in the North Atlantic. Rough estimates of this salt deficit have been given by Dickson et al. (1988). The salt deficit is amounted to be about $7.2 \cdot 10^{13} kg$, integrated over the period where the anomaly passages the Labrador Sea (mid-1971 to late 1973). In the polar box that deficit corresponds to a freshening of $\delta S_{GSA} = 0.048$ psu. This value depends on the volume of the high latitude box. Stability condition (7.28) is independent on Δz, but the response time varies with the depth of the mixed layer.

Figures 7.4 and 7.5 show time series of salinity and temperature for a perturbation of δS_{GSA} for the linear diffusion law ($r = 1$). The initial increase of the salinity perturbation, as seen in figure 7.4, is due to the non-orthogonal stable manifolds. The relaxation times are given first by the (uncritical) eigenvalue with smaller real part and afterwards by the other, critical eigenvalue.

The coupled system with the above-estimated parameters remains stable for a salinity perturbation of $\delta S \leq 13 \cdot \delta S_{GSA}$ for the linear diffusion law, $\delta S \leq 5 \cdot \delta S_{GSA}$ for the quadratic power law and $\delta S \leq 1 \cdot \delta S_{GSA}$ for $r = 3$. Time series for an initial salinity perturbation of $5 \cdot \delta S_{GSA}$ for the quadratic power law are shown in figures 7.6, 7.7 and 7.8. According to the linear stability analysis (figure 7.3), the critical salinity change $(\Delta S^0)_{crit}$ of the basic state with an unchanged ΔT^0 is about -0.25 psu for $r = 2$. This shows that the non-linear advection terms $-\frac{\Phi}{V}\Delta T$ and $-\frac{\Phi}{V}\Delta S$ modifiy the critical perturbation only slightly. The non-linear oceanic transport

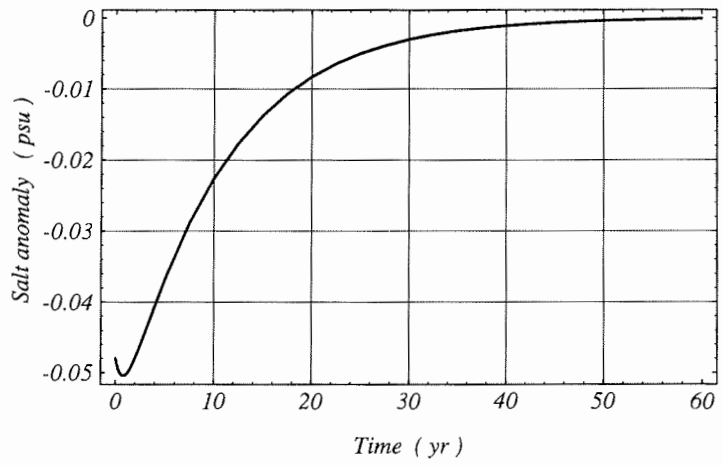

Figure 7.4: Time series of salinity anomaly in the high latitude box. With parameters $(K_2, K) = (12\frac{mm}{yr\,K}, 3.2\frac{W}{m^2K})$ for the meridional atmospheric transports of heat and moisture and $r = 1$, the system recovers from a perturbation in sea surface salinity of $\delta S_{GSA} = 0.048$ psu .

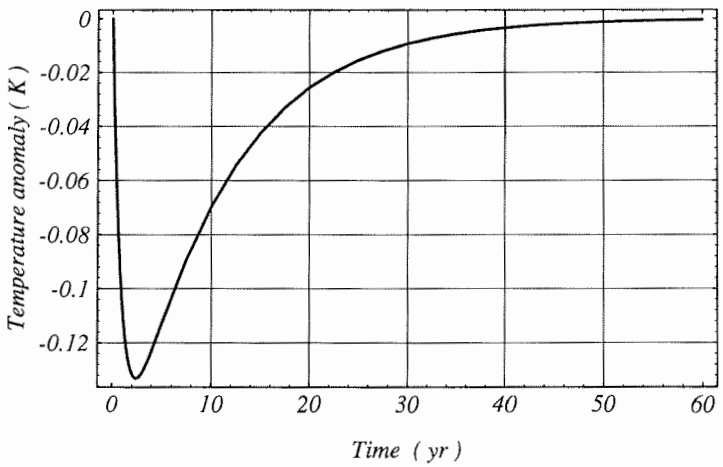

Figure 7.5: Time series of sea surface temperature anomaly in the high latitude box perturbed with $\delta S_{GSA} = 0.048$ psu at $t = 0$ for the same experiment as in figure 7.4.

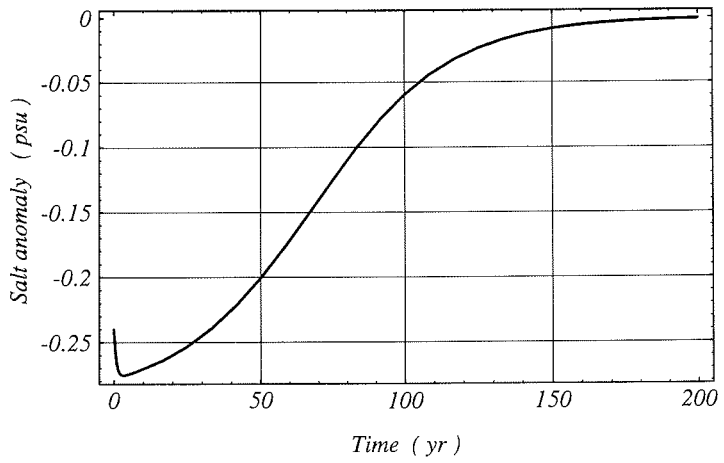

Figure 7.6: Time series of surface salinity anomaly in the high latitude box after a perturbation of $5 \times \delta S_{GSA}$ with a quadratic power law for the atmospheric transports.

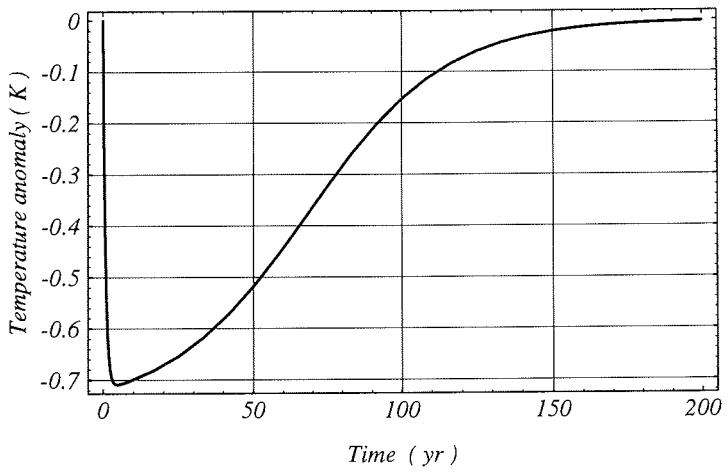

Figure 7.7: Time series of sea surface temperature anomaly in the high latitude box after a perturbation of $5 \times \delta S_{GSA}$ with a quadratic power law for the atmospheric transports.

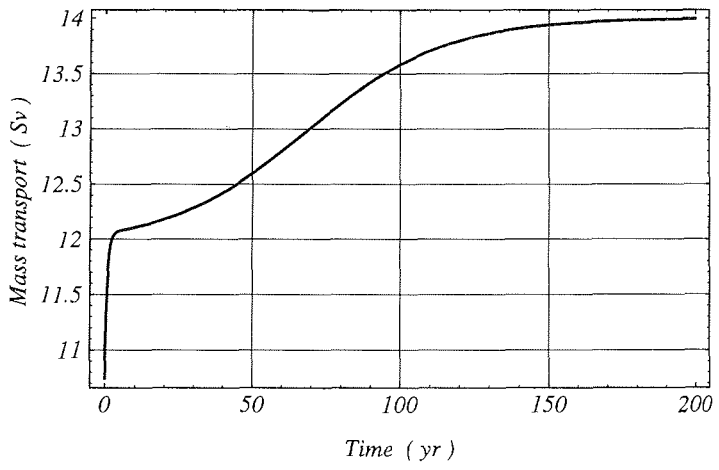

Figure 7.8: Time series of the meridional mass transport Φ (in Sv = $10^6 m^6 s^{-1}$) in the ocean according to (7.20, 7.21) with a quadratic power law for the atmospheric transports. The system is initialized with a surface salinity anomaly of $5 \times \delta S_{GSA}$. The system recovers from this perturbation and reaches the basic state with 14 Sv transport after 200 years.

terms of the system have a small stabilizing effect on the THC.

7.3 Discussion of sensitivity studies

It is useful to compare different sensitivity studies in terms of the transport coefficients and heat flux rates of our box model. All experiments listed in table 7.2 consider a thermally-dominated deep water formation as the basic state. The values of ϵ and K_2 roughly indicate the stability of the THC due to different boundary conditions.

Fixing the atmospheric temperature under mixed boundary conditions could be interpreted formally as an atmosphere with a poleward heat transport being so effective that the atmosphere temperature remains unchanged. For mixed boundary conditions, the heat flux rates Q_2 and Q_2' in (7.27) are used to calculate an equivalent coefficient $(BK)_{equiv}$ that can be compared with $B + K(1 - \eta)$ of our model:

$$(BK)_{equiv} = \frac{Q_2\, Q_2'}{Q_2 - Q_2'} \quad . \tag{7.30}$$

Table 7.2: Comparison of different experiments in the literature. The present study is denoted "Box". All other values are estimated from the information given in the respective papers. For Rahmstorf and Willebrand (1995, RW) the transport coefficient K is recalculated for the North Atlantic by assuming zonal homogeneity. The resulting value is an upper limit of an effective K. Boundary conditions (BC) are abbreviated as EBM for energy balance model, SM for Schopf's model and (m)MBC for (modified) mixed boundary conditions. For the boundary conditions EBM and SM the parameter ϵ is calculated from (7.24) whereas for mixed boundary conditions ϵ_{equiv} and $(BK)_{equiv}$ are calculated according to (7.27,7.30). The values of ϵ and K_2 indicate roughly the sensitivity of the THC due to the boundary conditions.

Lit.	BC	Φ_0 Sv	Q_2 $\frac{W}{m^2K}$	B $\frac{W}{m^2K}$	K $\frac{W}{m^2K}$	K_2 $\frac{mm}{yrK}$	$Q_2(1-\epsilon)$ $\frac{W}{m^2K}$	ϵ
Box($r=1$)	EBM	14	38	2	3.2	12	4.6	0.88
Box($r=2$)	EBM	14	38	2	7.2	40	6.8	0.82
SWM [137]	EBM	14	48.6	4.1	9.1	0	9.5	0.80
RW [118]	EBM	13	46	3	7.6	0	8.7	0.81
NSM [101]	EBM	7 – 10	100	1.7	ca.$Q_2/2$	70	ca.$Q_2/2$	0.5
ZGL [162]	SM	13	45	2.4	0	0	2.3	0.95
					$(BK)_{equiv}$	K_2	Q_2'	ϵ_{equiv}
ZGL [162]	mMBC	13	45	–	7.9, 5.1	0	6.8, 4.5	0.85, 0.9
MM [98]	mMBC	17	40	–	168, 54, 0	0	27, 16, 0.4	0.3, 0.6, 1
PK [113]	mMBC	22	61	–	284, 120, 0	0	41, 30, 0	0.3, 0.5, 1
B [14]	MBC	20	97	–	∞	0	97	0

The transport quantity $(BK)_{equiv}$ in equation (7.30) is infinite under mixed boundary conditions with $Q_2 = Q_2'$. In terms of our model that system belongs to the unstable region at the $K_2 = 0$ axis in figure 7.2.

Mixed boundary conditions result in very unstable systems, as can be seen from the large transport coefficients $(BK)_{equiv}$ and corresponding small values of ϵ_{equiv} (Bryan, 1986). Zhang et al. (1993), Mikolajewicz and Maier-Reimer (1994) and Power and Kleeman (1994) consider a range of different time scales (7.26) and get a more stable system the longer the time scale. By increasing the time scales they mimic a non-zero K corresponding to $(BK)_{equiv}$. In table 7.2, this kind of boundary condition are denoted by modified mixed boundary condition (mMBC).

An atmosphere without anomalous meridional heat transport, which corresponds to the case $\epsilon = \epsilon_{max} = \frac{Q_2}{Q_2+B}$ and $(K_2, K) = (0, 0)$, is Schopf's model (1983) which was used by Zhang et al. (1993) as the thermal boundary condition for their ocean model. Neglecting the destabilizing effect of the meridional heat transport, their resulting system was artificially stable with respect to perturbations in high latitude surface salinity.

Several investigations have included atmospheric transports with an EBM in a coupled ocean-atmosphere system. Transport coefficients (K_2, K) for some studies are recalculated for the North Atlantic domain (table 7.2). Stocker et al. (1992) coupled a zonally averaged EBM to an zonally integrated ocean model. They found that the steady state depends on the assumptions about the zonal redistribution of precipitation. For the case of constant fresh water flux -otherwise K_2 could be negative- the resulting parameters yield a system that is very well in the stable region of figure 7.2. This is partly a consequence of neglecting meridional transport of water vapour. Rahmstorf (1994) and Rahmstorf and Willebrand (1995) also neglect changes in the fresh water flux. Thus, their model also corresponds to points at the $K_2 = 0$ axis in figure 7.2. The critical stability for their model parameters, calculated with (7.28), corresponds roughly to the dashed line in figure 7.2. The lower critical stability compared to our model is due to a larger heat flux rate. We find that for the EBMs of table 7.2, values for ϵ are all similar, except for Nakamura et al. (1994) who admittedly overestimate the atmospheric heat transport due to their tuning. They consider a large catchment area for the fresh water flux and find that the moisture feedback plays the important role in destabilizing the THC.

Comparing box models like that of Nakamura et al. (1994) and the model presented in this chapter with the coupled EBM-OGCM results of chapter 6, it seems that box models are more sensitive to perturbations in surface fresh water flux at high latitudes than are GCMs. The cause of the higher sensitivity likely lies in the coarse resolution of the box models and their simplified physics. The ocean circulation can easily be influenced by changes in the thermohaline surface conditions in deep water formation areas, whereas changes in other areas have little effect on the large-scale transports. Box models do not recognize the spatial structure imposed by rather localized sinking regions in the ocean.

7.4 Comment on "flux corrections"

The results of the analytical box model may be helpful in interpreting "flux corrections" which is a common technique to circumvent difficulties with incompatible surface fluxes of oceanic and atmospheric circulation models. Flux corrections are applied to the ocean-atmosphere interface to correct erroneous representations of model physics and to prevent coupled GCMs from drifting (Sausen et al., 1988).

Locally, the artificial additional surface fluxes can have very large absolute values, e.g. in the GFDL coupled model (Manabe and Stouffer, 1988) up to $5\,m\,yr^{-1}$(!) in regions of deep water formation (figure A1 therein). The question is whether and how this procedure affects the sensitivity of the coupled system. This is a difficult question because the specific behavior of the model components and regional effects might affect the sensitivity. However, the following ideas might explore the effect of flux correction in terms of the simple model which can be helpful in understanding the sensitivity of complex climate models.

The artificial sources at the surface are denoted by

$$\widetilde{F_{oa}} \quad \text{and} \quad \widetilde{(P-E)} \quad .$$

These sources correspond to a northward heat and fresh water transport (see (6.1), 6.2)). The fixed climate component associated with the flux correction and artificial northward heat WT_{Ghost} and fresh water FT_{Ghost} transport may be named "ghost".

$$WT_{Ghost}(\phi) = \frac{1}{\cos(\phi)} \int_{-90^0}^{\phi} a\cos(\phi')\,\widetilde{F_{oa}}(\phi')\,d\phi' \tag{7.31}$$

$$FT_{Ghost}(\phi) = \frac{1}{\cos(\phi)} \int_{-90^0}^{\phi} a\cos(\phi')\,\widetilde{(P-E)}(\phi')\,d\phi' \quad . \tag{7.32}$$

Therefore, the coupled atmosphere-ocean-ghost system fulfills the requirement that in equilibrium the radiation on top of the atmosphere is identical to the the sum of heat transport divergences of the climate components (atmosphere, ocean and ghost). Nakamura et al. (1994) and in a subsequent paper Marotzke and Stone (1995) analyze the stability of THC in a box model similar that the present one. Their heat and fresh water flux is calculated directly by the divergence of latent and sensible heat transport. Therefore, they cannot separate between the effect of surface fluxes and atmospheric transport. They argued that the additional surface flux corresponds to over- or underestimated atmospheric heat and fresh water transport. However, these additional transports WT_{Ghost} and FT_{Ghost} are fixed as a third fixed climate component which do not enter along with the atmospheric transport of heat and moisture into the stability of the THC.

The basic state $\Delta T^0, \Delta S^0$ and Φ^0 and the atmospheric transport properties are not affected by the flux correction because both atmosphere and ocean reproduce today's climate. As long as the model is considered linear, as in the present box model, the sensitivity is not influenced because only the anomalies are handed over to the other climate component. However, large flux corrections leave the linear range of the model. This can be seen by the quantities K, K_2, Q_2 of the box model which include a non-linear dependence on temperature due to the saturation mixing ratio. Therefore, ϵ, Q_2, K_2 may be strongly affected by the flux correction procedure changing the stability behaviour. For example, from underestimating Q_2 it follows that ϵ is too small and that the sensitivity of the system is underestimated by flux correction. If ϵ has a small value the anomalous $P-E$ is underestimated, too:

$$(P-E)' = K_2\,\delta T_A = K_2\,\epsilon\,\Delta T' \quad . \tag{7.33}$$

If the absolute values of the additional (artificial) surface fluxes $|\widetilde{F_{oa}}|$ or $\widetilde{(P-E)}$ are large, the relative change of the surface fluxes are small. Therefore, such coupled atmosphere-ocean-ghost models are probably less sensitive than the ocean-atmosphere system because the ocean and atmosphere model components would be partly decoupled. Variations predicted from the model components may be then neglectable compared to the absolute values of the additional (artificial) surface fluxes.

Chapter 8

Climate studies in a simple coupled model

A simple coupled model is used to investigate the sensitivity of the system with respect to radiative forcing and stochastic weather perturbations. Additional radiative forcing may come from increased tracer gas concentrations in the atmosphere whereas the atmospheric weather fluctuations may reflect unresolved effects of the EBM modeled as white noise.

The geometry of the coupled model represents the North Atlantic and is the same as in section 7.1 (figure 7.1). Here, the non-linear atmospheric equations are solved forward in time where the EBM described in chapter 3 is used. A time dependent response to a CO_2 forcing is studied in this simple coupled model which may be helpful to understand scenarios in complex climate models.

Furthermore, the variability in the box model perturbed by weather fluctuations will be examined. The power spectra for different transport parameterizations in the ocean are compared.

The heat and salt balances are solved for all three boxes in the ocean. The temperature and salinity equations for the low latitude box and the deep ocean are analogous to the balance of the high latitude box (7.2, 7.3) in the analytical model. As in chapter 7 the ocean model has no local mixing and therefore, temperatures and salinities are purely determined by advection and the surface fluxes. To maintain continuity, the overturning rate Φ must be identical for all three interfaces between the oceanic boxes. Gravitational instabilities are not visible in the ocean model in spite of neglecting convective mixing. The formulation of the atmospheric model is identical to that given in section 3.1 including the diffusive parameterizations (3.18) and (3.20) for the sensible and latent eddy heat transport. Because of the model geometry of the Atlantic basin (section 7.1) other transport mechanisms apart from the transients at 40^0 N are small and are not considered.

As in the analysis given in section 7.1.1, the model is tuned to reproduce present

Table 8.1: Variables and parameters of the box model in equilibrium. In the tuning procedure ($1 \times CO_2$), temperature and salinities are prescribed. The superscripts D, HL, LL denote the deep, high latitude and low latitude boxes of the model, respectively. The heat transport (sensible atmospheric, latent atmospheric and oceanic) at 40^0 N are denoted by F_s, F_l and F_o.

Variable	Units	$1 \times CO_2$	$2 \times CO_2$	$4 \times CO_2$
Φ	$10^6\, m^3 s^{-1}$	10.0	9.64	9.29
$T_o^{HL} = T_o^D$	°C	7.0	9.25	11.13
T_o^{LL}	°C	21.0	22.93	24.49
$S^{HL} = S^D$	psu	34.5	34.49	34.49
S^{LL}	psu	35.5	35.61	35.69
T_A^{HL}	°C	5.0	7.24	9.20
T_A^{LL}	°C	19.5	21.4	22.93
$(P-E)^{HL}$	$mm\, yr^{-1}$	357	382	385
$(P-E)^{LL}$	$mm\, yr^{-1}$	−165	−176	−178
F_{oa}^{HL}	Wm^{-2}	−39.8	−37.5	−35.3
F_{oa}^{HL}	Wm^{-2}	18.4	17.3	17.6
F_s	PW	0.689	0.653	0.612
F_l	PW	0.714	0.764	0.770
F_o	PW	0.603	0.568	0.568
Parameter	units	$1 \times CO_2$		
A	Wm^{-2}	208.0		
B	$Wm^{-2}K^{-1}$	2.2		
Q_{sol}^{HL}	Wm^{-2}	250		
Q_{sol}^{LL}	Wm^{-2}	400		
Q_1^{HL}	Wm^{-2}	−30.2		
Q_2^{HL}	$Wm^{-2}K^{-1}$	35.0		
Q_1^{LL}	Wm^{-2}	−78.4		
Q_2^{LL}	$Wm^{-2}K^{-1}$	40.0		

values. In the tuning procedure, salinities and oceanic temperatures are set. The resulting fresh water flux is calculated from the oceanic salt transport in equilibrium (7.19). The parameters used here are listed in table 8.1 (under $1 \times CO_2$). A slightly different parameterization of the poleward transport is adopted which is based on scaling arguments in the following section.

8.1 Scaling for meridional overturning

For the balance, it is assumed that the non-dimensional Rossby number (ratio of typical nonlinear acceleration terms to Coriolis forces), Ekman number (ratio of

strength of viscous to Coriolis forces) and the non-dimensional frequency, which measures temporal acceleration against Coriolis force are small compared to unity. Then equations (5.1, 5.2) reduce to the geostrophic balances and the thermal wind balance:

$$f\,\mathbf{v}_z = -\frac{g}{\rho_0}\,\mathbf{k}\times\nabla\rho \qquad , \tag{8.1}$$

where ρ_0 is the reference density. With (8.1) the horizontal velocity scales as

$$V \sim d\frac{g}{\rho_0}\frac{\Delta\rho}{fL} \qquad , \tag{8.2}$$

where d and L are the vertical and horizontal length scales, respectively. From the zonally integrated continuity equation (5.4) it follows

$$\frac{V}{L} \sim \frac{W}{d} \qquad . \tag{8.3}$$

Furthermore, a vertical advective-diffusive density balance (Welander, 1986; Bryan, 1987) is assumed:

$$w\,\rho_z \;=\; A_{HV}\;\rho_{zz} \qquad \text{which yields} \qquad W \sim A_{HV}\frac{1}{d} \qquad . \tag{8.4}$$

With the scaling laws (8.2, 8.3, 8.4) the overturning stream function Φ defined by (6.3) scales as:

$$\Phi \;\sim\; d\,L\,V \;\sim\; \left(A_{HV}^2\,\frac{L^4\,g}{f\,\rho_0}\,\Delta\rho\right)^{1/3} \qquad . \tag{8.5}$$

Therefore, the overturning Φ scales with a 2/3 power with the vertical tracer diffusivity and a 1/3 power with meridional density difference (Bryan, 1987; Winton, 1994). In the ocean box model the northward heat and salt transport are parameterized with a 1/3 power law with meridional density difference. How the overturning parameterization affects the variability of the coupled model will be analyzed in section 8.3.

8.2 Sensitivity to changes of the atmospheric CO_2-concentration

In contrast to section 4.2, the time dependent response to a CO_2 forcing is now studied in a simple coupled model. Empirically, the change of surface temperature to CO_2 concentrations is approximately proportional to the logarithm of the relative change in CO_2 concentration (Schneider, 1972). The saturation of the main CO_2 absorbtion band at $15\mu m$ is responsible for the logarithmic law (Augustsson and Ramanathan, 1977). The change ($15\mu m$) in downward long wave radiation

originates mostly from the lower troposphere and is much larger at high latitudes than at low latitudes. In the $9.6\mu m\, O_3$ band, the change is small. The change of the radiation heat balance is modeled as

$$\Delta Q_R = \frac{4\ Wm^{-2}}{ln\,2}\ ln\frac{[CO_2]}{[CO_2]_{ref}} \quad , \tag{8.6}$$

and is added to the heat balance (3.11). The acronyms $[CO_2]$ and $[CO_2]_{ref}$ denote the actual CO_2 concentration and a reference concentration, respectively. Relation (8.6) changes somewhat for large increase of the CO_2 concentration where other bands become more important (Cess et al., 1980). However, even highly complex coupled GCM-CO_2 studies (e.g. Cubasch et al., 1995) use similar forcing terms as in equation (8.6). It can be shown with the radiative sheme of Schmetz (1984) that about a quarter of the change in radiation ΔQ_R will reach the ocean surface (Q_1-change).

The CO_2 concentration is assumed to double in one hundred years with an exponential increase (figure 8.1). When using the relation (8.6), the reference concentration of 350 ppmv does not enter the calculation. The increase of the high latitude oceanic and atmospheric temperature is synchronous and almost linear (figure 8.1 middle). As a result, the surface heat flux at the atmosphere-ocean interface remains almost constant which is in agreement with coupled GCM results of Manabe and Bryan (1985, figure 17 therein). The synchronous increase and almost unchanged heat flux is also found for low latitudes (not shown).

The simple coupled model qualitatively reproduces the main features of CO_2 studies with complex coupled models, viz polar amplification of surface temperature, intensification of the hydrological cycle, weakend thermohaline circulation and the synchronous response of high latitude surface water and deep water.

In the experiment, the overturning Φ reduces from 10 Sv to about 9.5 Sv in 200 years (figure 8.1 down) and the oceanic heat transport decreases by about 10%. As we have seen in section 4.2, changes of latent and sensible heat transports are competing effects in the atmosphere. A reduced sensible heat transport (figure 8.2) due to a reduction of the meridional temperature gradient is partly balanced by an enhanced latent heat transport which is due to higher temperatures and more moist air in the atmosphere. When the temperature dependent term $\partial q_s/\partial T_A$ in the latent heat transport is fixed, CO_2 scenarios cannot be described correctly.

The equilibria with changed CO_2-concentrations of table 8.1 differ up to 50% from the transient run (figures 8.1, 8.2, 8.3). The equilibrium time of the system is governed by the ocean ($3000 - 5000$ yrs). The qualitative difference in the response for transient and equilibrium scenarios has also been found in coupled GCMs (e.g. Washington and Meehl, 1989). This difference demonstrates that the rate of increase of trace gas concentrations in the atmosphere is important. When dealing with transient phenomena, the total heat transport is, according to figure 8.2, not fixed. Therefore, the method of Tang and Weaver (1995) to fix the total (atmospheric+oceanic) heat transport may be questioned.

Enhanced transport of moist air to high latitudes. influences the fresh water flux $P - E$ (figure 8.3) and thus the THC. However, in the first 20 years of the transient run a decrease in $P - E$ is observed. A reduction in the atmospheric temperature

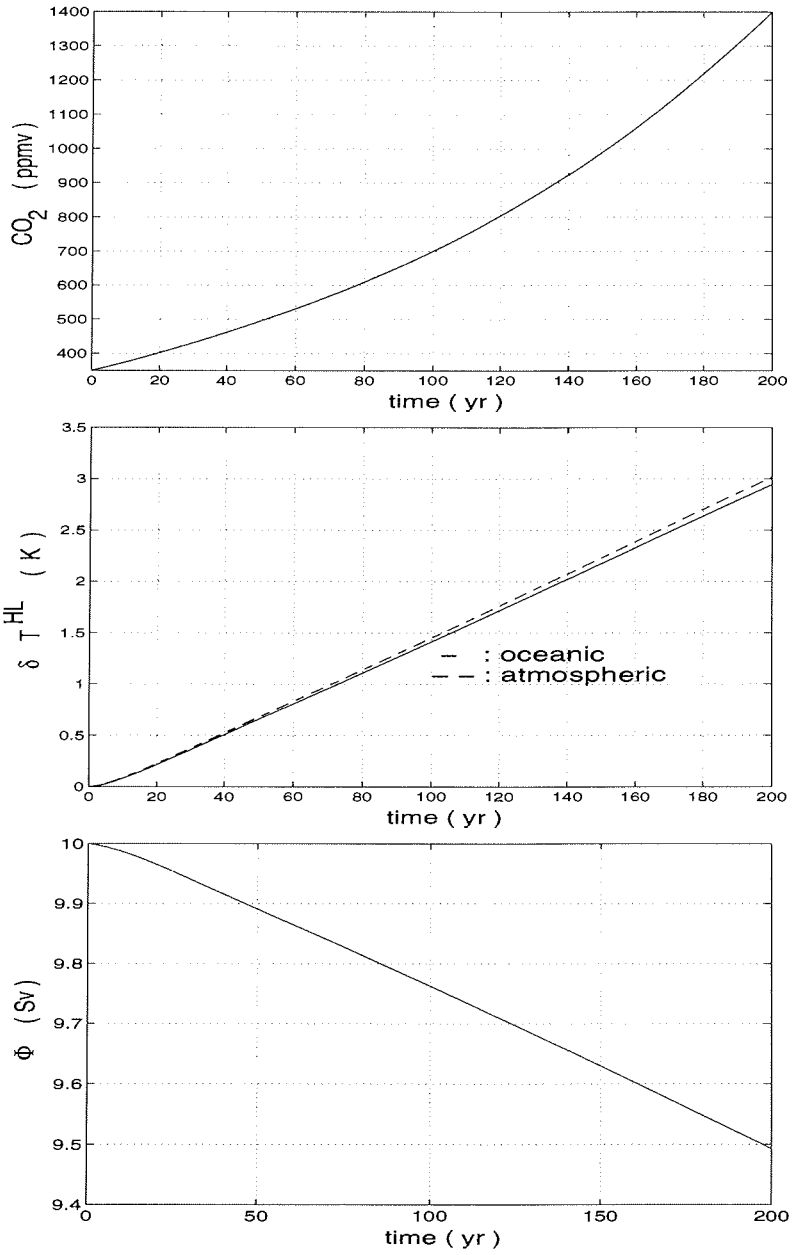

Figure 8.1: Scenario of an increased CO_2 content in the atmosphere. An exponential increase with a doubling of CO_2 in one hundred years is assumed. The high latitude temperatures T^{HL} in the ocean and atmosphere increase whereas the meridional overturning Φ decreases due to increasing CO_2.

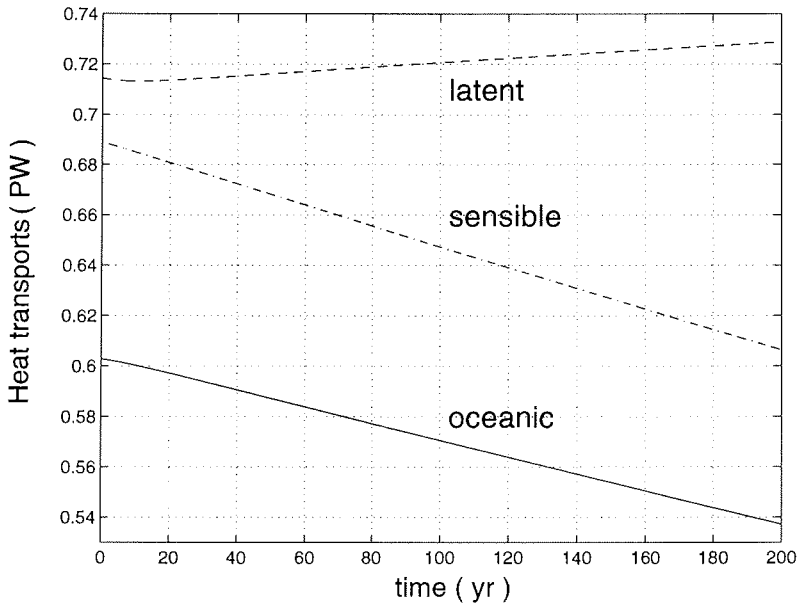

Figure 8.2: Northward heat transport for the CO_2 scenario given above. The latent heat is increasing because of increasing temperature in the saturation mixing ratio of water vapor. In contrast, the sensible heat transport decreases because of reduced temperature gradient. The oceanic heat transport is reduced due to a slowed THC.

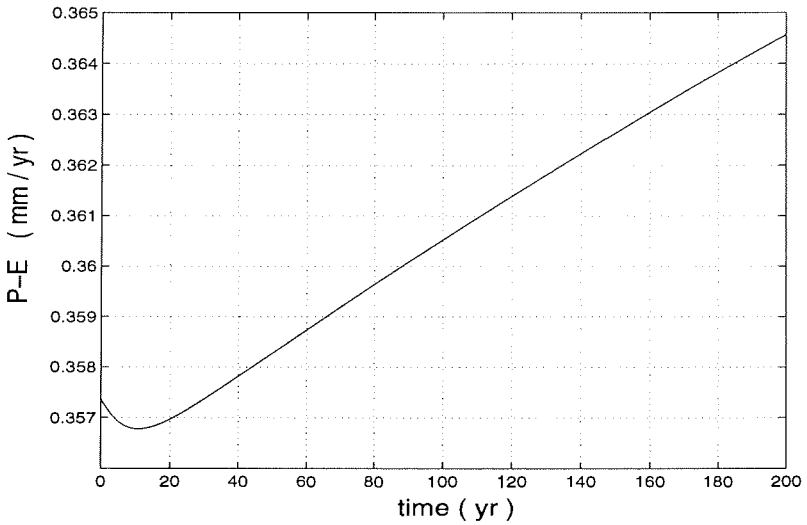

Figure 8.3: Fresh water flux at high latitudes for the above increase of CO_2 content in the atmosphere. Note the small absolute changes.

gradient is only partly balanced by increased temperature at 55^0 N. The author is not sure whether this model behavior might be seen in more complex models. Comparing table 8.1 and figure 8.3, the anomalous fresh water flux is much less after 200 years than in equilibrium run for quadrupled CO_2 concentration. The high latitude salinity (change of -0.006 psu after 200 yrs) is reduced by both increased $P - E$ and reduced oceanic transport. When CO_2 is increased, the sinking at high latitudes is weakend which is associated with a warmer and fresher upper ocean.

On the other hand, a reduced THC (figure 8.1 bottom) due to more CO_2 brings less warm water to high latitudes and therefore reduces the warming at these latitudes (e.g. over Europe). In this simple model, the stabilizing feedback of the THC is induced by the reduced oceanic heat transport in the more humid climate. However, the sensitivity of the circulation to changes in the surface water and atmospheric tracer gas concentrations remains an open question in complex climate and complex climate models.

8.3 Variability in a stochastic box model

The time scales for atmosphere and ocean are very different. The atmospheric weather perturbations have time scales of several days whereas the typical scale of the ocean is much larger. Hasselmann (1976) suggested considering the climatic weather fluctuations as an additive white noise (uncorrelated in time). The fluctuations would then be integrated by the slower parts of the climate system (e.g. the oceans). Here, fluctuations in the atmospheric sensible and latent heat transport are modeled as a stochastic process. The variation of atmospheric heat transport can vary by up to 100% of its mean value, which may influence the strength and statistics of the THC.

The stochastic EBM approach is similar to previous studies of Lemke (1977), Arskiy et al. (1989) and Kim and North (1991) with additive fluctuating variations in the atmosphere. None of the prvious studies coupled the EBM to an active THC. The numerical box model described above is used to analyze oceanic variability induced by these weather fluctuations.

The stability of stochastic differential equations (SDE) can be analyzed by Lyapunov-exponents or by construction of a Lyapunov-function (Lohmann, 1992). If the forcing is strong enough, the model-climate can switch between the basic states of the associated deterministic system. Such a mechanism was suggested by Matteucci (1989) who introduced a new time constant corresponding to the exit time between equilibria. However, other basic states of the coupled box model, associated with upwelling at high latitudes or an earth with large areas covered with ice, are not considered here.

On decadal time scale, climate variability of coupled ocean-atmosphere GCMs (e.g. Delworth et al., 1993) suggests that the model variability is associated with variations about one stable climate state rather than variations resulting from transitions between several basic states (Griffies and Tziperman, 1995). Therefore, to study

variability of the ocean on a time scale of years, the box model is placed in the linear stable state which is - in the language of section 7.2 - thermally dominated. We will see that under a moderate amount of stochastic forcing (20% of the mean values), the coupled model integrates the $\delta-$correlated noise of sensible and latent heat transport, thereby affecting the oceanic variability.

The SDE, linearized about the deterministic stable equilibrium, is called "Ornstein-Uhlenbeck process" (e.g. Rieckers and Stumpf, 1977). The power spectrum (variance cross spectrum) is a useful tool to analyze variability of SDEs. The power spectrum $S(\omega)$ for the Ornstein-Uhlenbeck process is given by

$$S(\omega) = \frac{c}{\lambda^2 + \omega^2} \quad , \tag{8.7}$$

where λ is the Eigenvalue with the greatest real part of the negative definite matrix of the linearized system and constant c is determined by the strength of the stochastic perturbation. This function is calculated for different experiments with different power laws for the meridional mass transport:

$$\Phi \sim \Delta\rho^{\kappa} \qquad \text{with} \qquad \kappa = 1/3 \ , 1 \ , \text{ and } 2 \ . \tag{8.8}$$

The case $\kappa = 1$ was suggested by Stommel (1961) whereas the case $\kappa = 2$ was derived from vorticity equations (Maas, 1994). Figure 8.4 shows that for all power laws considered the power spectra $S(\omega, \lambda)$ fit quite well with (8.7) obtained from the linear SDE. The experiments show that the higher the power, the more the low frequency variability is pronounced. This is because the ocean is more sensitive to changes for higher power laws. In other words, the real part of the eigenvalue λ, which is negative for all the three cases, is closer to zero the higher the power κ is. The peaks at $7,2$ and 0.9 years are numerical artefacts of the random generator.

The variability on a decadal time scale is stressed whereas higher frequencies show a linear decrease in amplitude (figure 8.4). The power spectra for the three different parameterizations of oceanic heat and salt transport can be explained by the linearized SDE with red noise (8.7). How is the oceanic variability induced ?
For the power law $\kappa = 1/3$, fresh water fluctuations for the ocean surface due to fluctuations in latent heat transport are set to zero. Comparing the variability of the two cases (the solid and the dotted lines in figure 8.4) shows that the influence of fresh water flux on oceanic variability is small compared to the heat flux.

This coupled stochastic model suggests that long term variability may be induced by purely random weather events entering in the heat flux.

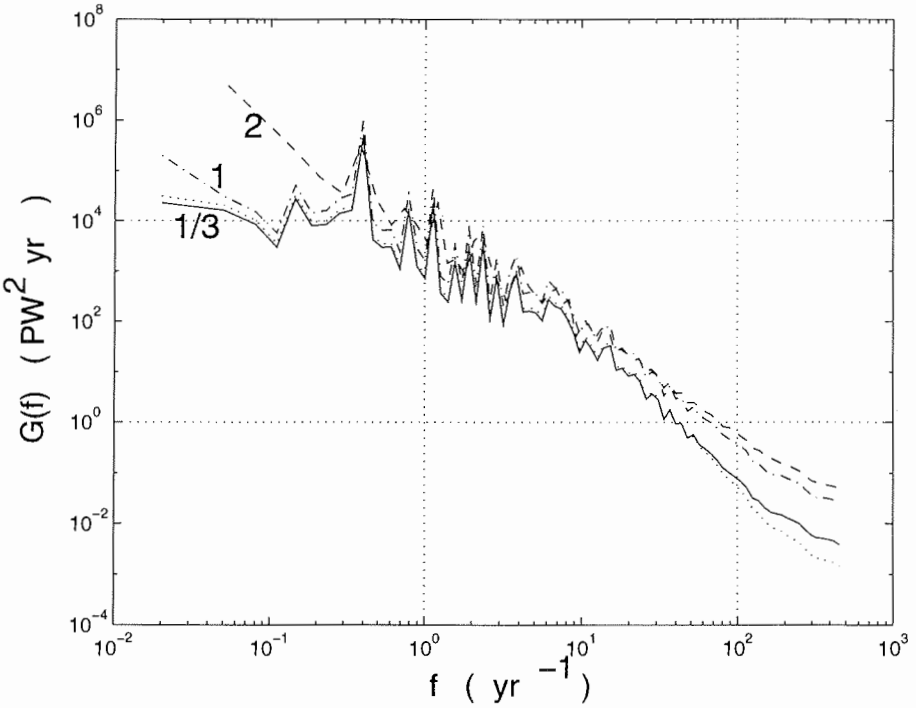

Figure 8.4: Power spectrum of the oceanic heat transport for different power laws for the meridional mass transport $\Phi \sim \Delta\rho^{\kappa}$. The power law $\kappa = 1/3$ obtained from scaling arguments (8.5) results in a flat low frequency behavior $(-)$. Higher power laws enhance the low frequency variability because the THC is more sensitive (dashed dotted lines for $\kappa = 1$ and dashed lines for $\kappa = 2$). If the ocean with $\kappa = 1/3$ receives stochastic forcing in heat flux only, the variability changes slightly $(\cdots)$ from the reference experiment $(-)$.

Chapter 9

Variability in coupled OGCM-EBM experiments

Recent analyses of climate records strongly indicate variability on the decadal to interdecadal time scale (Hibler and Johnsen, 1979; Dickson et al., 1988; Ghil and Vautrad, 1991; Deser and Blackmon, 1993; Kushnir, 1994; Reverdin et al., 1994). Several mechanisms for climate variations on decadal time scale have been suggested, both in highly complex coupled GCMs (Delworth et al., 1994; Latif and Barnett, 1994) and ocean only models (Wright and Stocker, 1991; Weaver et al., 1991; Weaver and Sarachik, 1991; Winton and Sarachik, 1993).

As we have seen in the previous chapters, the stability of the THC depends on the imposed boundary conditions, the basic state and the representation of the atmospheric transport. This is also valid for long-term variability. However, modelers are far from explaining climate variations. What they can do, is to analyze possible mechanisms of the complex climate system leading to variability. Here, one mechanisms for decadal variability is extracted which might be helpful in understanding natural variations induced by strong meridional gradients in salinity.

The spin up and the oscillating behavior of the coupled system is described in section 9.1. An explanation for the self-sustained oscillations of the system will be given in section 9.2. Subsequent experiments (section 9.3) will show that the ability of significant variability in the coupled system depends strongly on the basic state. The ocean in the oscillator regime is more sensitive to perturbations than other basic states. The results will be discussed in section 9.4.

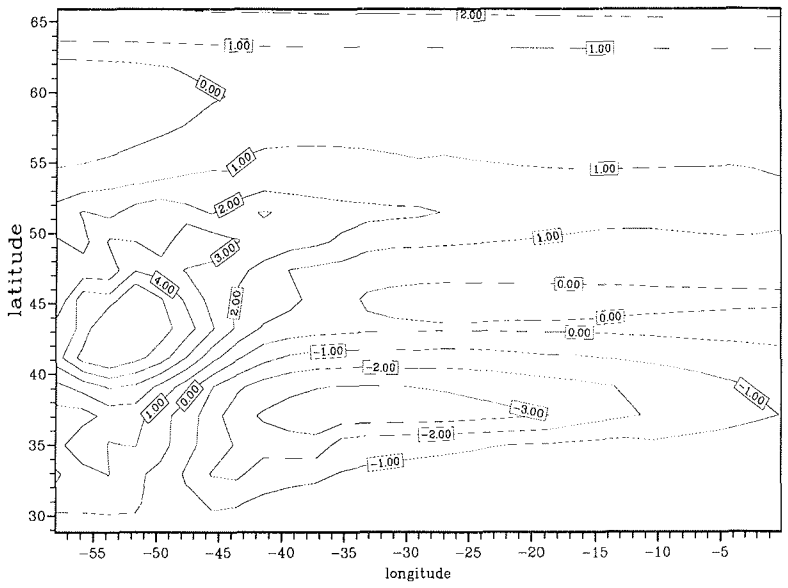

Figure 9.1: Fresh water flux obtained from the restoring boundary condition for salinity. The flux represents the mean Precipitation - Evaporation + Runoff for the coupled model. Units are $m\,yr^{-1}$ with contour interval $1\,m\,yr^{-1}$.

9.1 Spin up and oscillating regime

The ocean circulation model described in section 5 is coupled to the atmospheric EBM of chapter 3. The ocean model has a resolution of two degrees in the horizontal and 16 vertical levels. The geometry of the ocean model is a 64^0 wide sector with flat bottom topography (5700 m deep) ranging from the equator to 70^0 N. Different time steps for tracer (12 h) and velocity (1 h) are used.

The ocean model was spun up under restoring boundary conditions for salinity and for temperature using the heat flux formulation (section 3.4). Here, the temperatures of Oort (1983) were slightly increased (up to $+4K$) reflecting a warm Atlantic ocean. The fresh water flux is diagnosed and used as the mean fresh water flux in the atmospheric model. The northern part of the diagnosed fresh water flux field which represents precipitation - evaporation + runoff is shown in figure 9.1. Because zonal mean climatological salinities (Levitus, 1983) are used, large freshening areas occurs at the western boundary current to obtain relatively low salinities. This is a usual feature when diagnosing the fresh water flux from climatological salinities (see e.g. Weaver et al., 1993). At the northern boundary, the fresh water flux reaches about $2myr^{-1}$.

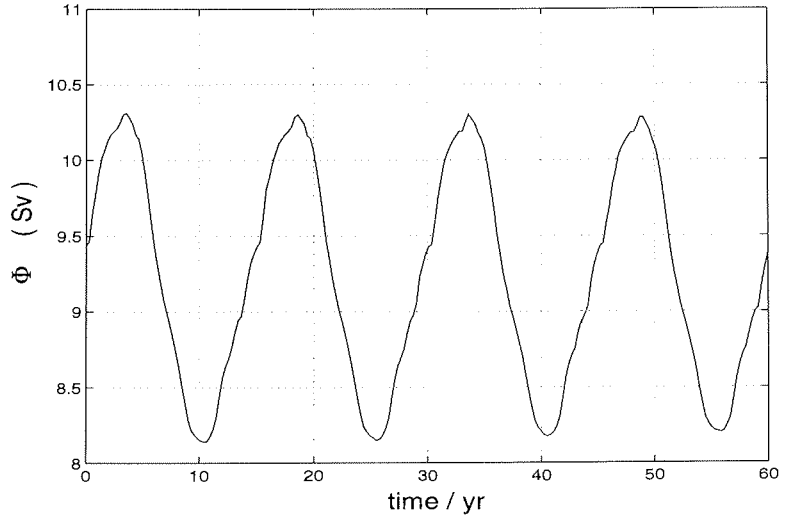

Figure 9.2: Time variation of the maximal zonally integrated mass transport in the northern hemisphere.

After switching to the coupled mode the system becomes unstable. The THC breaks down, but reestablishes with a weaker northward heat and salt transport than before. This causes fresher and colder water in high latitudes. The new climatic state is colder than before such that the new atmospheric temperature is close to the zonal mean values previously used (chapter 6). Matching with this, the sensible heat transport is enhanced whereas the latent heat transport is reduced.

Without any external perturbation, the system transits to an oscillating regime after a few hundred years. The variation of the zonally integrated mass transport is seen in figures 9.2, 9.3 and 9.4. During an oscillation period of 15 years the overturning rate varies between 10.3 Sv (figure 9.3) and 8.2 Sv (figure 9.4). Matching with the mass transport the heat flux changes much. The heat flux out of the ocean for times where the circulation is minimal and maximal is shown in figure 9.5. When the THC is in its minimum, a significant heat loss at high latitudes takes place only in the eastern part of the North Atlantic. The heat loss around 55^0 N coincides with the sinking region whereas in the north-western part of the ocean basin upwelling is observed. The heat loss westward of 30^0 E is less than $20\,Wm^{-2}$ between $50^0 - 60^0$ N (figure 9.5 left). This difference in the zonal direction is the reason for different pattern in the overturning stream function (figures 9.3, 9.4). In the situation for maximum mass transport, the heat loss (figure 9.5 right) is more zonally uniform than seen in figure 9.5 left.

We will see that the variation in sea surface salinity (SSS) is crucial for the variations in heat flux and overturning rate. Therefore, different variables are analyzed for the latitudinal strip $50^0 - 60^0$ N. Figure 9.6 shows that the variations of SST, SSS and heat flux are in phase. Warming coincides with salty water and a strong heat loss of the ocean surface. The variations in SSS and heat flux are enormous (0.25 psu and $10\,Wm^{-2}$ about the mean values).

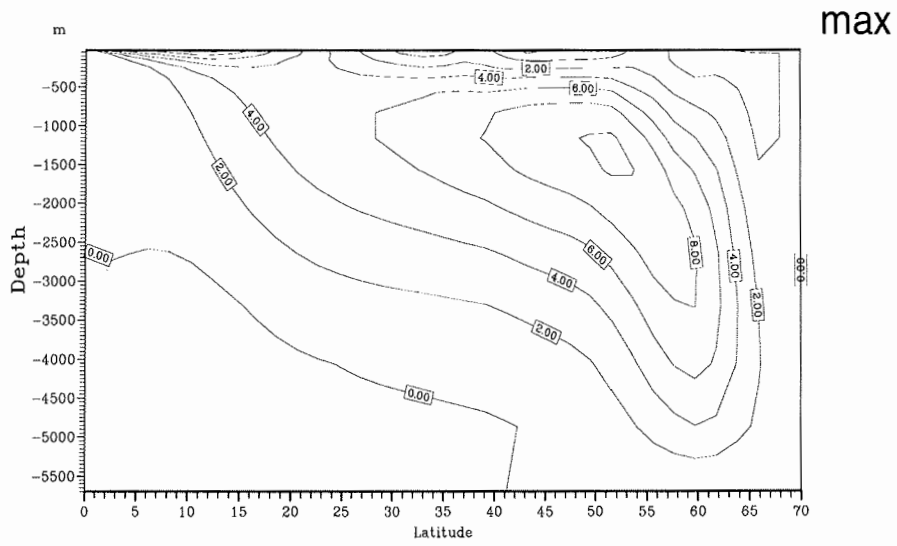

Figure 9.3: Stream function for the zonally integrated transport in Sv ($10^6 \frac{m^3}{s}$) when the THC is maximal. The maximal overturning rate is 10.3 Sv.

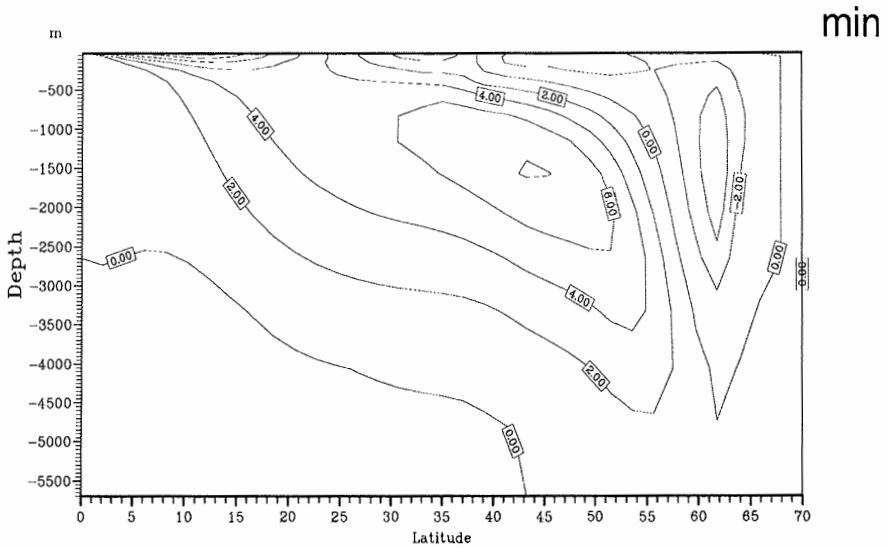

Figure 9.4: Stream function for the zonally integrated transport in Sv ($10^6 \frac{m^3}{s}$) when the THC in minimal. The overturning rate is 8.2 Sv.

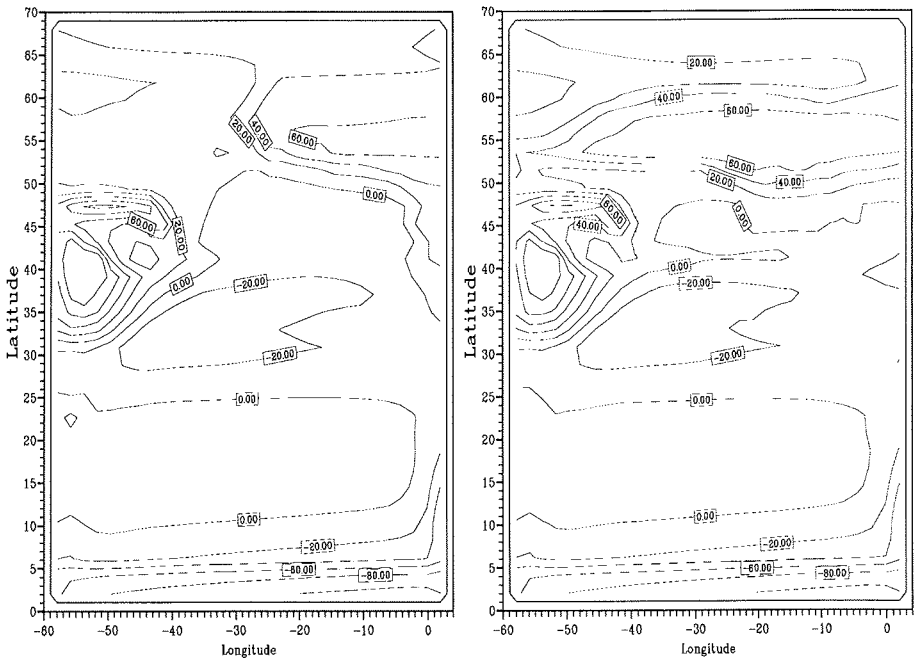

Figure 9.5: Snap shots of surface heat flux when the mass transport is minimal (left) and maximal (right). Positive values stand for heat loss from ocean to atmosphere. The contour interval is 40 $W\,m^{-2}$. The right snap shot corresponds to to year 11 and the left to the years 3.3 and 18.5 in figures 9.2, 9.6 and 9.7.

According to Reverdin et al. (1994) the amplitude of sea surface salinity modifications in the northern North Atlantic is typically of the order of 0.1 psu. However, larger signals are observed (up to 0.5 psu) in the Labrador Current and the Icelandic Sea. Furthermore, they claimed that larger amplitudes are expected where spatial gradients are large. Nevertheless, the model variations in salinity are too strong compared to observations.

The sea surface temperature (SST) is in phase with surface salinity partly compensating the decrease in density (about 50%). Furthermore, the atmospheric temperature is completely in phase with the SST varying between 7.7 and 8.2 ^{0}C at 55^0 N. The signal of cooling and warming is quite uniform in atmosphere such that the temperature gradient does not change very much.

The change in the atmospheric heat transport is in anti-phase to SST and is small (ca. 0.005 PW at 50^0 N) because of small anomalous temperature gradients. The latent heat transport is of minor importance because the temperature and temperature gradient effects balance for each other. Therefore, the anomalous fresh water flux is quite small (figure 9.7 b).

The oceanic heat transport is in phase with the mass and salt transport and has a variance of about 0.01 PW (figure 9.7 a). Variations of the momentum flux (figure 9.7 c) are less than 5% of the absolute value (see figure 9.7 c) and are of minor importance. This can be obtained by analyzing the vertical integrated stream function in the ocean model. The signal of salinity variation is also found in the second layer but with less amplitude. The deeper layers are only weakly influenced. In the next section, the dynamical behaviour of the oscillatory mode will be explored.

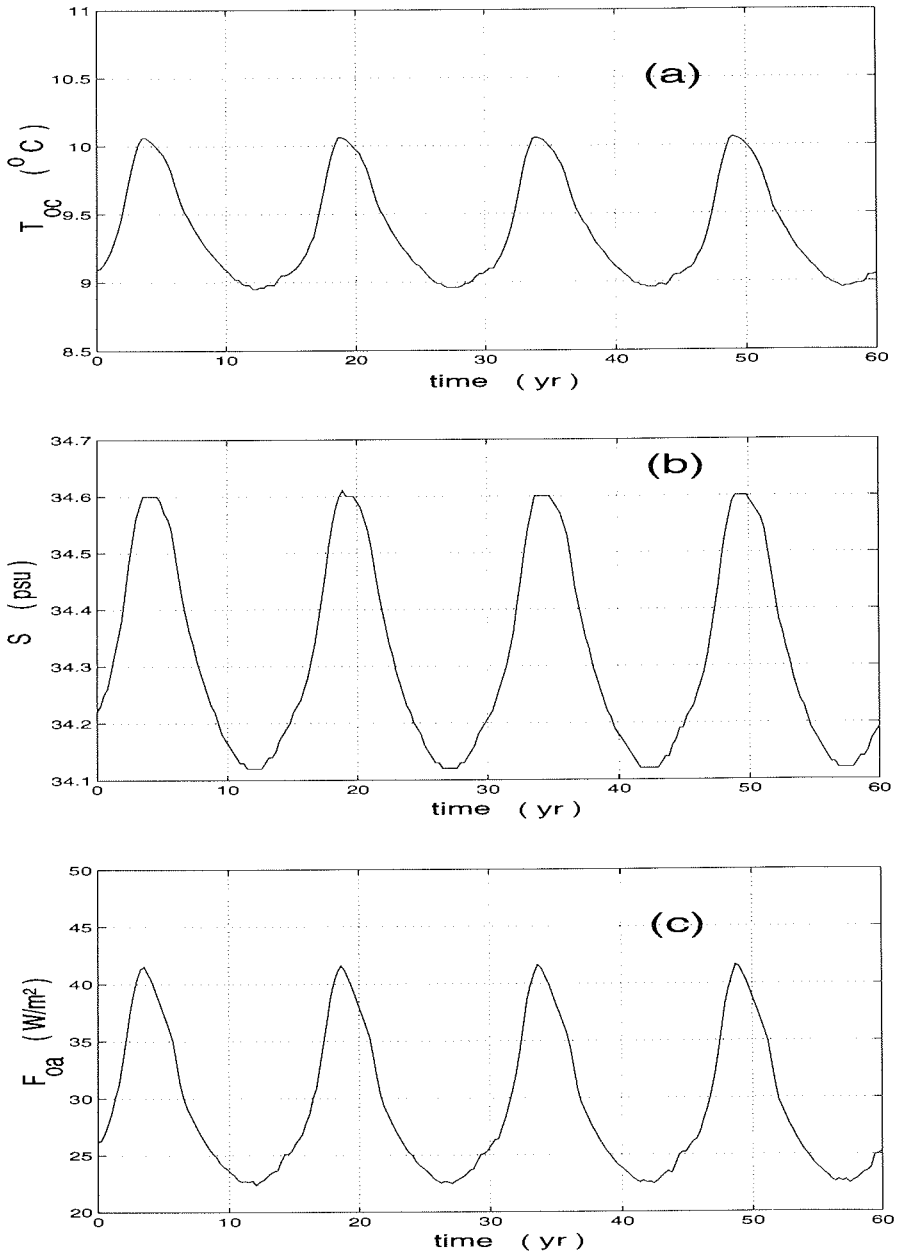

Figure 9.6: Variation of surface oceanic temperature, salinity and heat flux averaged between 50^0 and 60^0 N. The units are ^{0}C, psu and $W\,m^{-2}$, respectively.

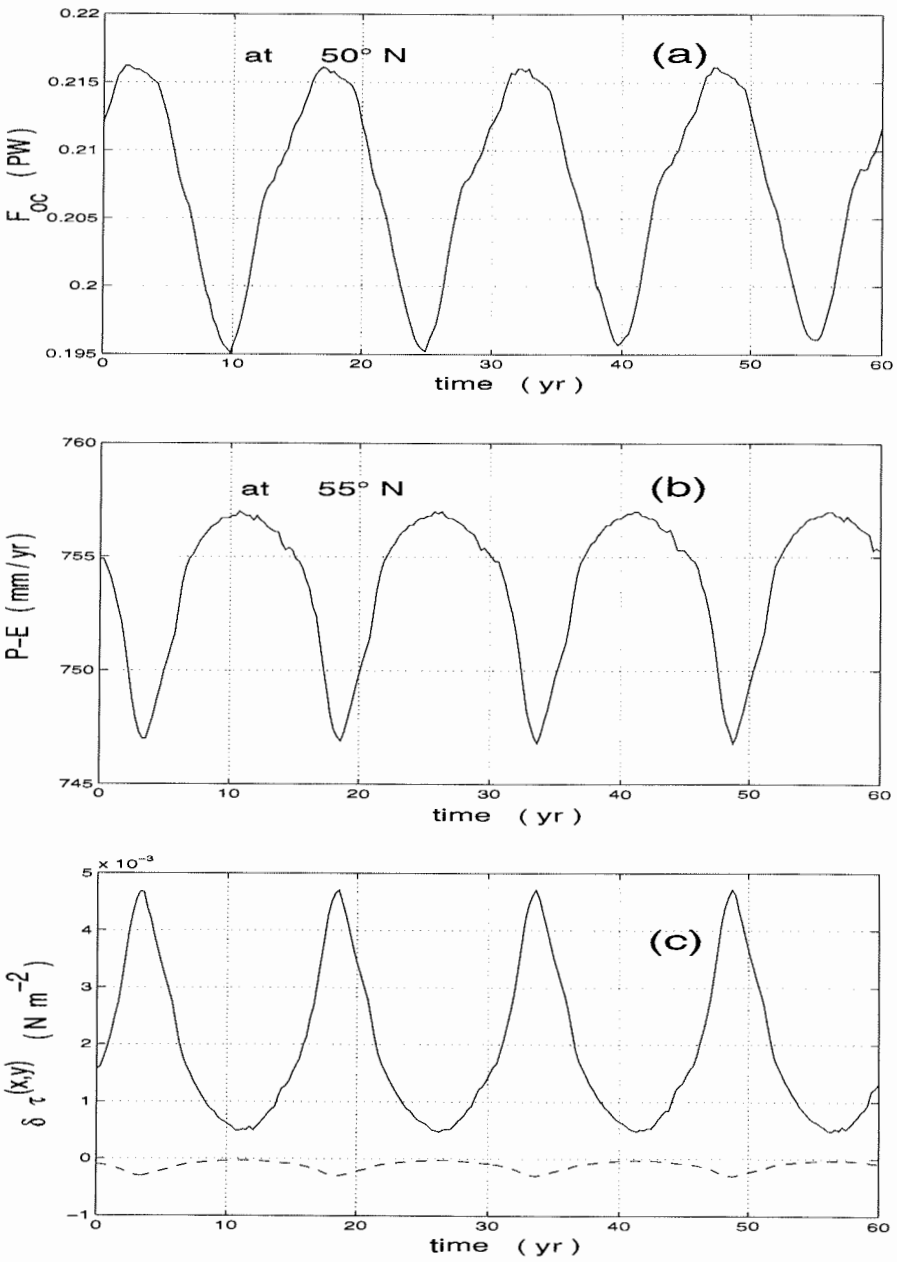

Figure 9.7: a: Variation of oceanic heat transport at 50^0 N. The variations of the fresh water flux and momentum flux at 55^0 N are shown in the pictures b and c. The zonal component of wind stress is drawn with solid line whereas the meridional component with dashed lines.

9.2 Dynamical behaviour of the self-sustained oscillations

The variations in the coupled system are self-sustained oscillations. It is therefore natural to ask what are the driving mechanisms behind this behaviour. As we have seen in the last section, the phenomenon seems to be not connected to an interaction of atmospheric and oceanic transport processes. Instead, the oscillations can be explained by a simple dynamical behaviour of the ocean.

To see this, the surface velocities are plotted over the sea surface salinity field in figure 9.8. Five different time slices show a movement of a fresh surface watercap towards the east. The salinity gradients in this oscillating regime are very strong. The horizontal distribution of high latitude salinity leads to horizontal density gradients influencing the motion which itself influences the density field. To be more more precise, the thermal wind relation (8.1) is used:

$$f\,\mathbf{v}_z = -\frac{g}{\rho_0}\,\mathbf{k}\times\nabla\rho \qquad , \tag{9.1}$$

where ρ_0 is the reference density. According to equation (9.1), the density gradients are orthogonal to the shear of the velocity. The velocities in the first layer are greater than in the layers underneath. The velocity variations can therefore be associated with its vertical shear. From this follows that the baroclinic velocity in the surface layer follows the isohalines. Temperature effects are in phase with SSS and modify the isopycnals slightly.

In picture 9.8 a, the circulation is in its maximum whereas between (c) and (d) in its minimum. The period of the oscillation is 15 years, the snap shots are taken every three years. Different stages of the circulation are considered:

- When the THC is maximal (picture a) the vertical shear of the velocity and the velocity is strong at the western part transporting water into the southeast.
- When the fresh water anomaly has moved further eastward, the fresh water covers large areas between 50^0 and 60^0 N reducing the outgoing heat flux. In this stage (c, d) , the oceanic heat transport is reduced. Furthermore, the velocity in the western part of the basin is reduced transporting water southeastward.
- The reduced velocity causes increased velocities at the western boundary between 45^0 and 55^0. The change is significant in the second layer (not shown) which causes enhanced salt transport forming a salt tongue at 53^0 N (pictures d and e).
- The salinity tongue advects further eastward and is partly diluted by the fresh water flux shown in figure 9.1. Large freshening areas between 40^0 and 50^0 N form strong density gradients which increase the velocity close to 52^0 N (picture a). The enhanced southeastward advection of fresh water from higher

latitudes reduces salinity at high latitutes and the transport of salty subsurface water.

The thermal wind relation (9.1) combined by the figure suggests that the phenomenon is an advective one. The typical advection velocity is given by $1\ cm\ s^{-1}$ for these latitudes ($40 - 60^0$ N) where the SSS variability is found. Strong salinity gradients in the northern North Atlantic are responsible for the self-sustained oscillations. Such gradients may result from an enhanced hydrological cycle in a warmer climate or from freshening areas due to melt water.

Figure 9.8: Sea surface salinity and surface velocities for five different times. Units are psu and $cm\ s^{-1}$. For the observed oscillation with period 15 years, the snap shots are taken every three years. The first picture (a) corresponds to the time where the mass transport is maximal whereas in the state between pictures (c) and (d) the mass transport is minimal. Strong variations in sea surface salinity are responsible for the variation of the strength of the THC seen in figure 9.2. The sea surface salinity gradients are orthogonal to the the velocity in the surface layer.

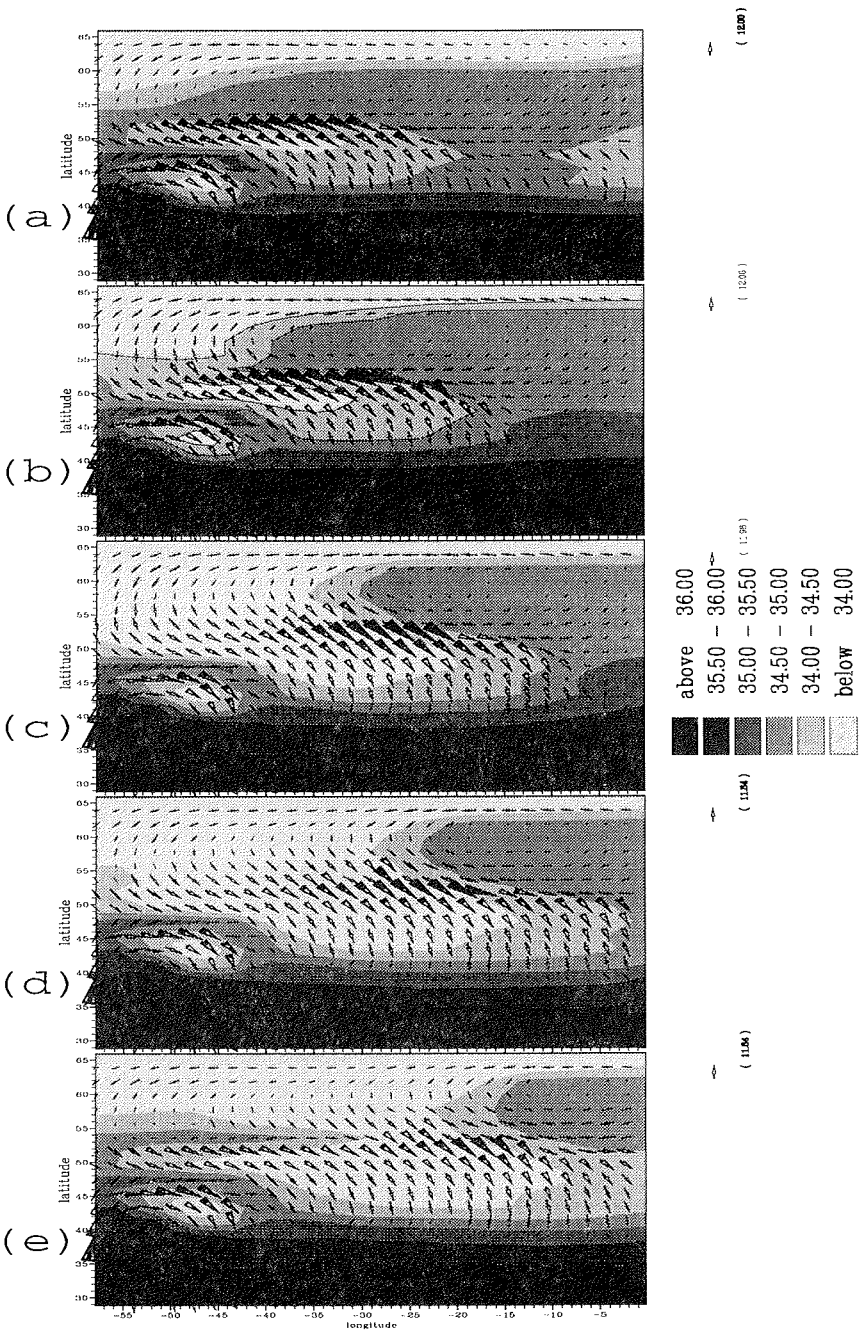
(a)
(b)
(c)
(d)
(e)
latitude
longitude
above 36.00
35.50 - 36.00
35.00 - 35.50
34.50 - 35.00
34.00 - 34.50
below 34.00

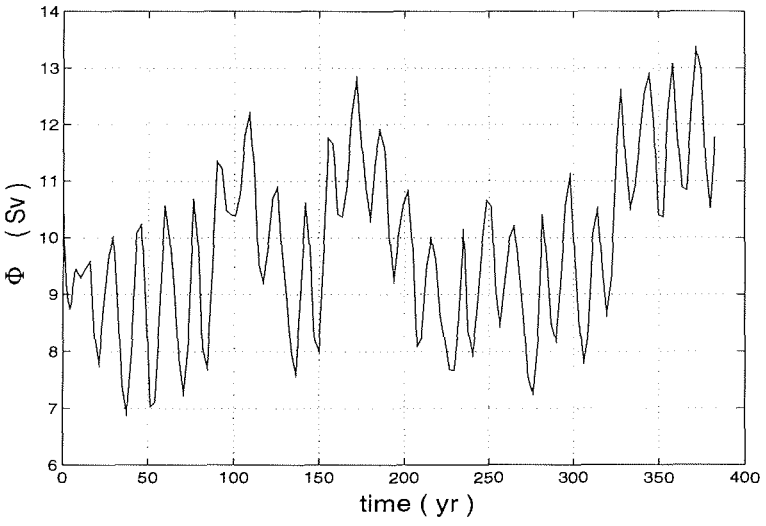

Figure 9.9: Variation of the maximal meridional mass transport after a perturbation in surface salinity.

9.3 Sensitivity

The oscillatory mode is driven by horizontal density gradients. It is therefore natural to ask how sensitive the circulation is to perturbations in density. A perturbation of -1 psu is induced in the area of $40^0 - 52^0$ N and $60^0 - 40^0$ east. This area is chosen because the sensitivity of the THC is greatest to perurbations in that area. The coupled system is integrated for 380 years (figure 9.9). The perturbation does not not destroy the 15 year cycle, but modulates the THC on time scales of a few hundred years. The timeseries of heat flux and temperature show the same modulation. Furthermore, the atmospheric variables show an additional high frequency behaviour which has not been analyzed in detail yet.

Three different basic states that differ in the fresh water flux (figure 9.10) are analyzed with respect to the sensitivity. The above experiment is denoted by (A) where the oscillatory regime is observed. In a second experiment, denoted by (B), the zonally averaged fresh water flux of Sellers (1969) is used. The third experiment (C) uses the fresh water flux which comes out if the zonal mean fresh water flux of Sellers (1969) is multiplied by 3. This might be interpreted as the enhanced hydrological cycle over the Atlantic compared to the zonal mean.

Experiments (B) and (C) are integrated to a steady state. In both experiments no transition to an oscillatory mode is observed. Therefore, it is concluded that different types of fresh water fluxes may be responsible for different modes of the circulation. In the steady state, the maximal overturning of (B) is 25.8 Sv whereas of (C) is 27.7 Sv. The perturbation modifies the maximal overturning stream function by less than 1 Sv for both cases. After a few decades the old basic states are

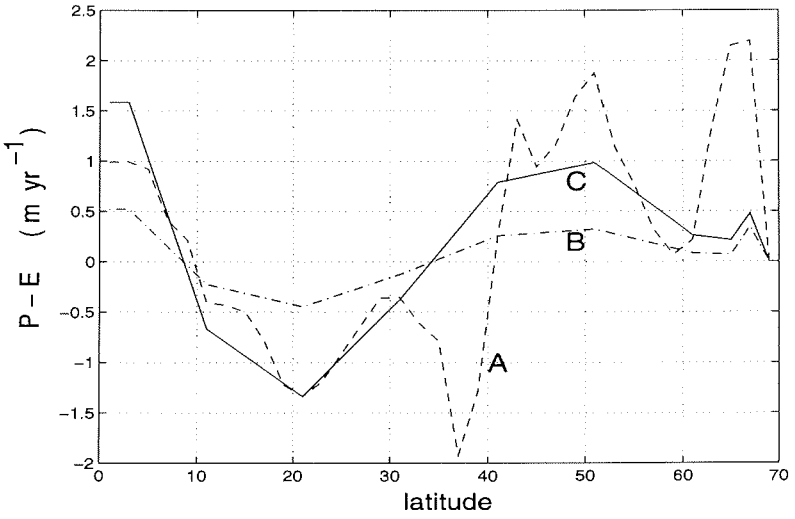

Figure 9.10: Initial fresh water flux for three different experiments: A: diagnosed from restoring. B: fresh water flux of Sellers (1969). C: 3× fresh water flux of Sellers.

reached (not shown). Therefore, the sensitivity of the circulation is strongly affected by the characteristics of the basic state. This is in agreement with the findings of the analytical model in chapter 7 that the stability of the circulation depends strongly on the basic state.

This also is consistent with findings of Weaver and Sarachick (1991), Weaver et al. (1991, 1993), and Winton and Sarachik (1993) who analyzed the variability of the THC using mixed boundary conditions with different (but constant) fresh water flux. They found that if the fresh water flux is sufficiently strong, self-sustained oscillations exists while otherwise no variability was found.

9.4 Discussion

The above experiment suggests that internal oceanic processes are mainly responsible for the variability observed in the model. The present climate is not well represented in oscillatory coupled mode because meridional temperature and salinity gradients are too strong. The phenomenon is interesting because the transport of salt is influenced by the density gradients resulting from saltinity. In this self-sustained oscillation horizontal salinity gradients affect the motion such that the gradients move with the horizontal motion. This advective mechanism may be observed in the real ocean if large freshening occurs.

It was furthermore shown that the potential of an ocean model showing oscillations depends on the basic state. Among other boundary fluxes, the basic state is deter-

mined by the fresh water flux which was varied here. The modulation due to the perturbation in salinity seems to be characteristic of the oscillatory mode.

The bifurcation to different modes of circulation depending on changed climatic conditions is an important issue. Mathematically, variations of the dynamical system can be caused by several topological structures in phase space. Physically, the system should have at least two negative feedback mechanisms to oscillate. Recently, Rahmstorf (1995 b) calculated different equilibria of the THC with respect to changed fresh water flux forcing. The thermal bandary condition was chosen as in equation (3.36). He found a transition from a stable model solution to a limit cycle if the surface fresh water is increased moderately south of Greenland. For stronger changes in fresh water flux, the THC spins down. This feature of the basic state is consistent with the above experiments.

Oscillations are found in more simplified models, too. The stochastic box model of the previous section suggests that oceanic variability might be induced by random fluctuations in the atmosphere. Other examples are that variations can be caused by by switching between states of Stommel's model (Tang and Weaver, 1995) or interaction between sea ice and ocean temperature (Moritz, 1979). Sea ice effects will be discussed in chapter 10.

Recent work suggests that a model driven by a constant heat flux can show interdecadal oscillations (Greatbatch and Zhang, 1994; Cai et al., 1995; Chen and Ghil, 1995). Several sources of feedback are neglected in models using constant fluxes at the upper boundary. Therefore, a constant heat flux is not a valid approach because it does not occur in coupled models or in nature. The above experiment and the results of the previous chapters have shown that the heat flux at the ocean-atmosphere interface strongly depends on the behaviour of the circulation itself.

In a coupled atmospheric-oceanic circulation model, Delworth et al. (1993) observe anomalies moving anti clockwise around the northwestern part of the Atlantic basin. Their coupled model shows irregular oscillations of the THC in the northern North Atlanic with a time scale of around 50 years. However, flux corrected models might not show the correct sensitivity (section 7.4) and could behave as decoupled model components if the flux correction is strong. Indeed, Delworth et al. (1993) speculate that the irregular oscillation in their model is triggered by nearly random surface buoyancy forcing of heat and water fluxes. In their analysis, the oscillations are primarily a result of oceanic processes.

These uncertainties indicate that further studies are needed to get more insight into the low frequency behaviour of the ocean. Models of different complexity may be useful to extract basic mechanisms. The next chapter shows that a climate component which was so far neglected influences strongly the sensitivity of the THC: Sea ice.

Chapter 10

Feedback mechanisms affecting the thermohaline circulation - Sea ice effects

The coupled 3-D ocean circulation - atmospheric energy balance model includes a thermodynamic sea ice model. The numerical experiments, presented here, indicate that sea ice considerably alters the sensitivity of the coupled system. The mechanisms that occur in this simplified model may also be seen in coupled circulation models including sea ice.

The sensitivity to a salinity perturbation at high latitudes is investigated for different types of boundary conditions to isolate relevant feedback processes. The experimental strategy is similar to that of chapter 6. The feedback mechanisms affecting the THC are explored by numerical experiments (sections 10.3, 10.5). The experiments show a large sensitivity to perturbations in sea surface salinity attributable to the interaction between sea ice and the thermohaline circulation.

The thermodynamic sea ice model is described in section 10.1. The initial state for subsequent experiments will be explored in section 10.2. In the coupled experiment, denoted by cHF in chapter 6, heat and fresh water flux are coupled in the atmosphere-ocean system. This system will be discussed in section 10.3. In the coupled system, the circulation does not collapse due to the perturbation, but a transition to another steady state is observed. This new steady state with a weakened oceanic heat transport and enhanced atmospheric heat transport is described in section 10.4. Models using other types of boundary conditions will be shortly described in section 10.5. It it shown the the response of the system is determined by the atmospheric model. A discussion of the feedback mechanisms will be given in section 10.6.

10.1 Thermodynamic sea ice model

The thermodynamic sea ice model regulates surface heat and salt fluxes for the ocean when the energy balance at the atmosphere-ocean interface produces sea surface temperatures at the freezing point 271 K. The temperature profile in the sea ice is assumed to be linear, so that the conductive heat flux F_c through the sea ice is

$$F_c = \frac{D}{H_{ice}} \cdot (T_{ice} - T_O) \quad , \tag{10.1}$$

where $D = 2.16 \frac{W}{mK}$ is the conductive heat coefficient for ice. T_O, T_{ice} and H_{ice} denote the temperature of the oceanic mixed layer, ice surface temperature and mean ice thickness, respectively. The ice surface temperature is determined such that the conductive heat flux and the heat flux at the atmosphere-ice surface F_{ai} balance each other:

$$F_c + F_{ai} = 0 \quad . \tag{10.2}$$

The heat flux at the atmosphere-ice surface is approximated in a pragmatic way by a Newtonian law. It is assumed that the sum of various thermodynamic processes at the atmosphere-ice interface are proportional to the temperature difference between ice surface and atmospheric temperature T_A at 1000 mb:

$$F_{ai} = \gamma_2 \ (T_{ice} - T_A) \quad , \tag{10.3}$$

where γ_2 is a constant heat flux rate of $-16 \ W\, m^{-2}\, K^{-1}$. The atmospheric fresh water flux is not transformed into snow, and the fresh water is directly added into the oceanic mixed layer. This approximation which has to be modified in a improved sea ice model has also been used by Zhang et al. (1995). The change of sea ice height follows from the energy balance:

$$\rho_{ice} L_f \ \frac{dH_{ice}}{dt} = -F_c + Q_{ocean} \quad , \tag{10.4}$$

where ρ_{ice} is the density of sea ice, L_f is the latent heat of freezing and Q_{ocean} is the oceanic heat flux, computed by the ocean model. The sea ice model predicts additional fresh water fluxes S_f due to melting and freezing:

$$S_f = -[S_{ocean} - S_{ice}] \cdot \frac{dH_{ice}}{dt} = -30 \text{ psu} \cdot \frac{dH_{ice}}{dt} \quad , \tag{10.5}$$

where S_{ocean} and S_{ice} are reference salinities in the ocean and sea ice, respectively. The dynamics of sea ice are not considered here.

10.2 Experimental setup

The domain of the ocean circulation model is a 70^0 wide sector from 66^0 S to 80^0 N including an idealized Greenland-Scotland ridge. Otherwise, the ocean model is the same as described in section 5. The steady state ocean circulation for subsequent experiments is reached after 4000 years of integration, about 2600 years of the integration was done with the accelerated time stepping technique (Bryan, 1984).

During the spin up the fresh water flux is diagnosed from the salt flux due to a restoring boundary conditions on salinity. Surface salinity is restored to climatological salinities from Levitus (1982) which were zonally averaged over the Atlantic basin. The diagnosed fresh water flux is used for the mean latent heat transport in the atmospheric model. Because zonal mean temperatures (Oort, 1983) have been taken, the model ocean produces too cold surface temperatures compared to the present Atlantic. The atmospheric model is that of chapter 3 with fixed climatological wind stress. The transient eddy fluxes of heat and moisture provide (along with SST) changes in heat and fresh water fluxes for the ocean.

Figure 10.1 shows the stream function for the zonally integrated mass transport at the end of the spin up. The deep water formation takes place north of 55^0 N with a maximum overturning rate of 22 Sv. The stream function of the vertically integrated transport (figure 10.2 right) is determined by the wind stress curl and topography showing the tropical, subtropical and subpolar gyres.

The ice margin (about 68^0 N) is determined by the oceanic heat flux and the atmospheric temperature. Due to the lack of any sea ice dynamics the ice edge is zonally distributed. If sea ice is present, the heat loss out of the ocean is strongly reduced (figure 10.2 left). The heat flux out of the ocean is large at the western boundary and close to the sea ice edges.

Without any perturbation, the coupled system is integrated further 110 years from the spin up state. No significant change in the circulation is observed. As in chapter 6, the spin up will therefore be used as the reference case for subsequent experiments.

A perturbation in salinity of 0.5 psu between $50^0 - 70^0$ N is added to the surface level. This salt deficit is ca. 12 times larger than that of the Great Salinity Anomaly, observed in the northern North Atlantic (Dickson et al., 1988). The sensitivity of the THC with respect to this perturbation is investigated for different types of boundary conditions.

In the coupled experiment, denoted by cHF in chapter 6, heat and fresh water flux are coupled in the atmosphere-ocean system which will be be discussed in the next section.

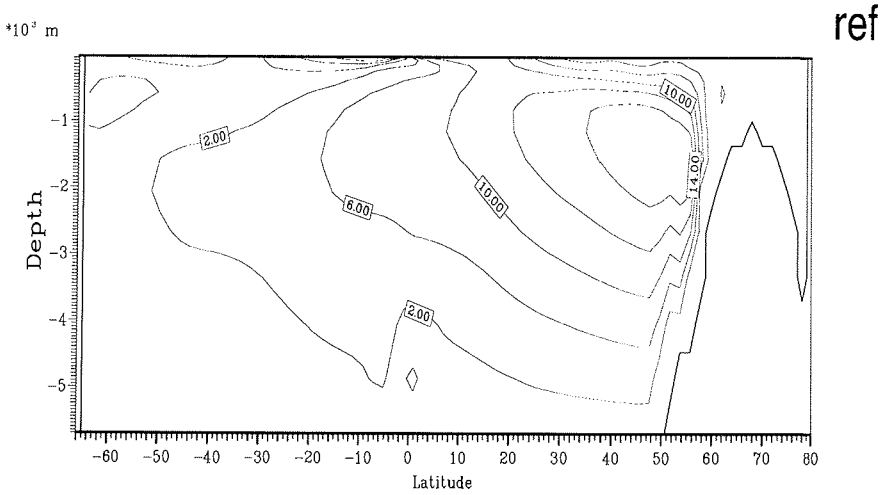

Figure 10.1: Stream function for the zonally integrated transport at the end of the spin up in Sv ($10^6 \frac{m^3}{s}$) which is taken as the reference state for subsequent experiments. The maximum overturning rate is about 22 Sv.

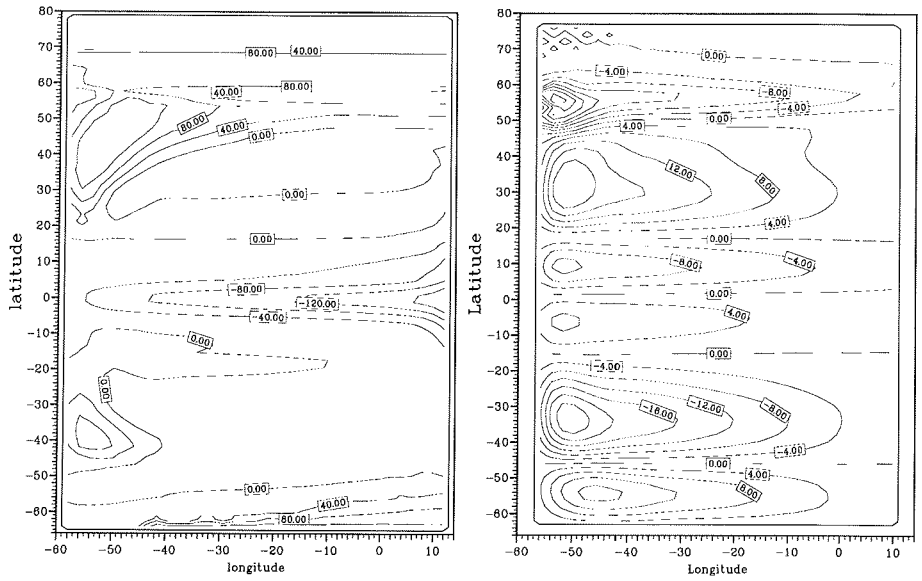

Figure 10.2: Initial state of the stream function of the vertically integrated transport (right). The upward heat flux from the ocean-ice system (left) is strongly reduced when sea ice is present (sea ice edge at about 68^0 N and 64^0 S). The contour interval for the stream function is 4 Sv and for the heat flux is $40\,Wm^{-2}$.

10.3 Coupled experiment

The time series of the maximum overturning stream function on the northern hemisphere (figure 10.3) shows that the strength of the meridional overturning recovers after a few decades. Afterwards, the circulation is in a shallow mode. The depth of deep water formation is reduced from 5 km to 3 km seen in the snap shots for 110 years after perturbation (figure 10.5) and at equilibrium (figure 10.6) after 890 years.

Deep water formation is slightly enhanced in the new equilibrium compared to the reference case (figure 10.1). Furthermore, a deep water cell with a reversed circulation of about -4 Sv is present in the deeper layers. The total mean kinetic energy divided by the volume of the ocean (figure 10.4) shows that the new state after 600 yrs of integration has more kinetic energy than the reference state. We will see that this new mode of circulation is connected with an increased atmospheric heat transport, decreased oceanic heat transport and nearly unchanged oceanic salt transport.

To investigate the transition of the system to the new equilibrium, model states at three different times are analyzed:

- 14 yrs after the perturbation when the overturning and the northward oceanic heat and salt transport are at the minimum.
- 110 yrs after perturbation as an intermediate state. In that phase the meridional mass transport reestablishes.
- The new equilibrium at 890 years after perturbation.

Figures 10.7, 10.8 and 10.9 show the response of the coupled system for these different times. The response of the coupled system to that perturbation is a combination of different mechanisms. The large fresh water perturbation weakens initially the overturning. This abrupt reduction of the THC to less than 50% of its original value is combined with a cooling at high latitudes on both the northern and southern hemispheres (figure 10.7 a). The atmospheric temperature drops due to a reduction in heat flux out of the ocean (figure 10.7 b). There are local mechanisms affecting the decrease in heat flux:

- Fresh water added to the surface stabilizes the water column to the extent that convection as a mixing process is shut off. Such interruption decreases the mixed layer depth which further freshens the water column. This mechanism seems to dominate at year 14 after the perturbation because the reduction in heat flux (figure 10.7 b) is strong where the sea surface salinity anomaly has been imposed.
- Another mechanism reducing the heat flux out of the ocean is due to sea ice. The sea ice edge expands equatorward hindering the atmosphere-ocean heat

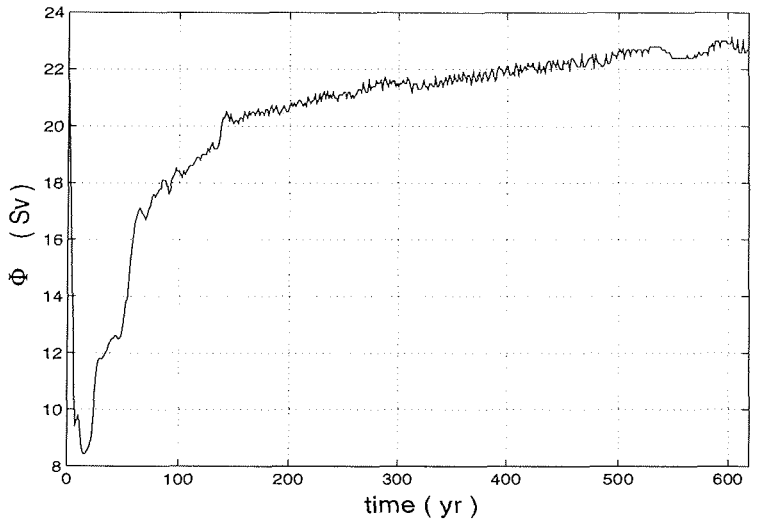

Figure 10.3: Time series of the maximum overturning stream function in the northern hemisphere for experiment cHF after perturbation in high latitude salinity.

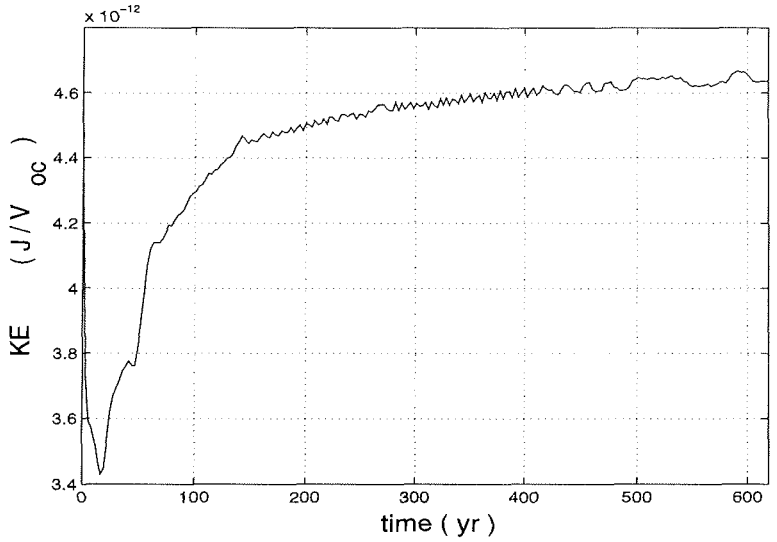

Figure 10.4: Time series of the mean kinetic energy divided by the ocean volume. The new mode with shallower deep water formation has more kinetic energy.

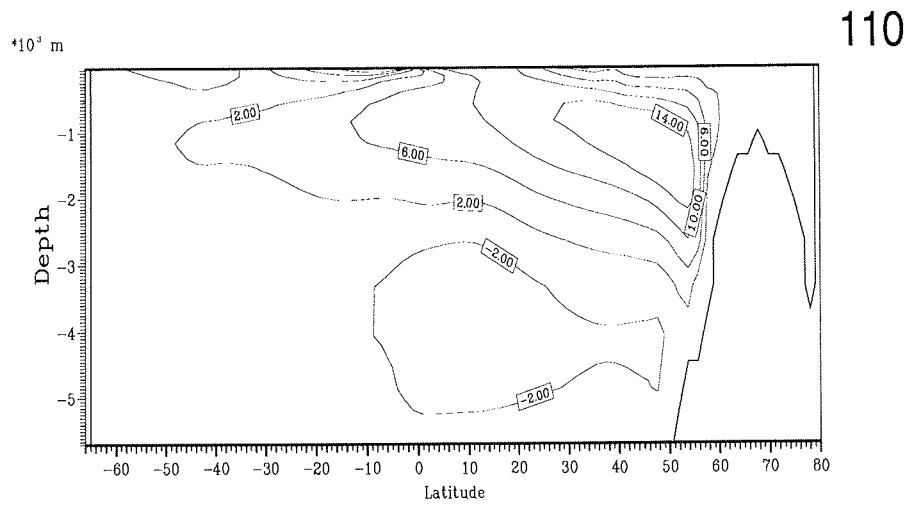

Figure 10.5: Stream function for the zonally integrated transport in the coupled system 110 yrs after the perturbation at high latitudes. The maximal overturning rate is about 18 Sv.

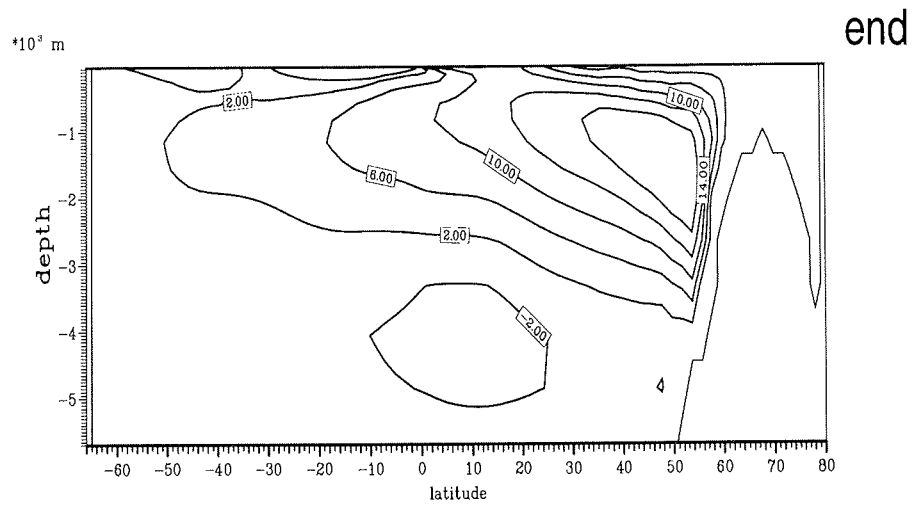

Figure 10.6: Stream function for the zonally integrated transport in the coupled system 890 years after the perturbation at high latitudes. A new equilibrium with a shallower deep water formation is reached.

exchange. This effect dominates poleward of the new ice edge (figure 10.7 b) at 64^0 N and 60^0 S, respectively. Interestingly, the sea ice change on the southern hemisphere remains constant in time for the three different phases. It is conceivable that the positive feedback (decreased temperature-more ice) is responsible for increasing the sea ice (figures 10.7 a and b).

A colder climate produces more snow which increases the surface albedo. This effect is included in the atmospheric model within an ice-albedo feedback factor (see sections 3.1 and 4.2). Decreased temperatures may amplify formation of sea ice which is a positive feedback.

- Furthermore, the latent heat flux at the ocean-atmosphere interface depends on temperature and is reduced by decreased temperatures.

The response of the atmospheric variables to the reduction in heat flux is similar to the behavior of the atmospheric EMB to a long-lived SST anomaly in section 4.1. The northward atmospheric heat transport is strengthened (figure 10.8) warming the air at high latitudes. This warming pushes the ice edge poleward partly compensating the positive feedback (more sea ice - cold air) discussed above. We will see in section 10.5 that the atmospheric heat transport is crucial for the stability of the "salinity conveyor belt".

In the phase where the THC is minimal (14 years after perturbation), the fresh water flux is increased up to $28\,mm\,yr^{-1}$ at mid-latitudes and decreases up to $-31\,mm\,yr^{-1}$ at high latitudes (figure 10.7 c). Interestingly, the effects of temperature and temperature gradient are competing effects for the latent heat transport (see also chapter 7, equation (7.14)). A decrease of temperature (figure 10.7 a) reduces the saturation mixing ratio whereas the increased temperature gradient (seen in the same figure) favors baroclinic instability and accelerates latent heat transport. These effects partially balance such that the anomalous latent heat transport (figure 10.8 b) is small compared to the sensible heat transport (figure 10.8 a). This finding partial is in contrast to results of box models (Nakamura et al., 1994; chapters 7, 8) where the latent heat transport is calculated at mid-latitudes (e.g. 40^0 N) thus overestimating the hydrological cycle.

When the THC is at its minimum, the anomalous latent heat transport is directed southward at the northern hemisphere south of 40^0 N. The change is only a fifth of the sensible heat transport change. After the second phase (110 years after perturbation) the fresh water flux northward of 50^0 N remains almost constant. The moisture convergence and the enhanced sensible heat transport in figure 10.8 qualitatively agree with figures 4.2 and 4.3 where a long lived SST-anomaly has been imposed. The anomalous transport is directed towards the temperature anomaly reducing the mean meridional temperature gradient.

In contrast to the stand alone experiment in section 4.1, the northward oceanic heat and salt transport are affected by the changed surface fluxes. A reduced heat flux out of the ocean leads to a reduction of northward oceanic heat transport cooling high latitudes. However, even in this cold period the THC did not stop completely, although the oceanic heat transport (figure 10.8 c) is remarkably reduced.

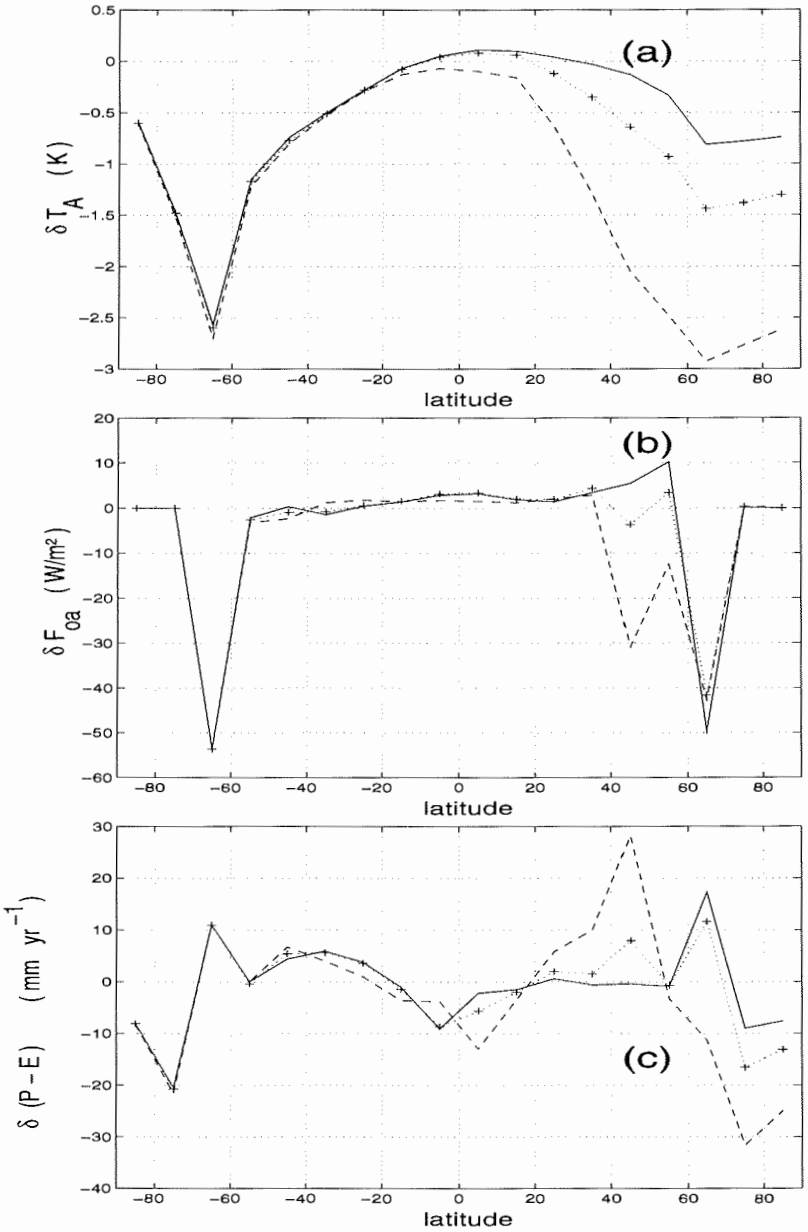

Figure 10.7: Change of atmospheric surface temperature (a), heat flux (b) and fresh water flux (c) at the ocean surface. The solid line denotes the new equilibrium. The dashed line is for 14 yrs after the perturbation where the overturning and the northward heat and salt transports are at the minimum. The dotted line with plus signs stands for an intermediate state 110 yrs after perturbation.

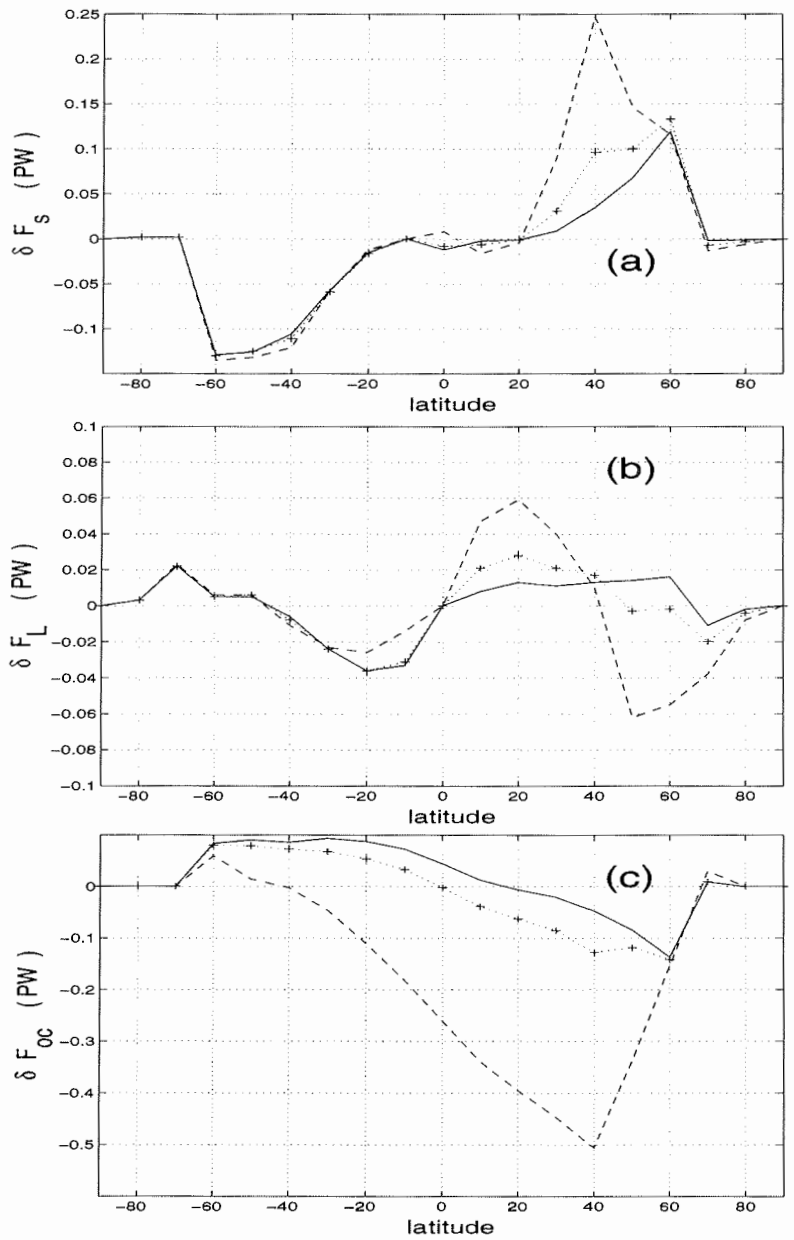

Figure 10.8: Change of sensible (a), latent (b) and oceanic (c) heat transports for: New equilibrium $(-)$, 14 yrs after the perturbation $(- -)$ and 110 yrs after perturbation $(\cdot + \cdot)$. Note that through the non-linear dependence of the water vapor mixing ratio on temperature the change of latent heat transport is higher in low latitudes than sensible heat transport.

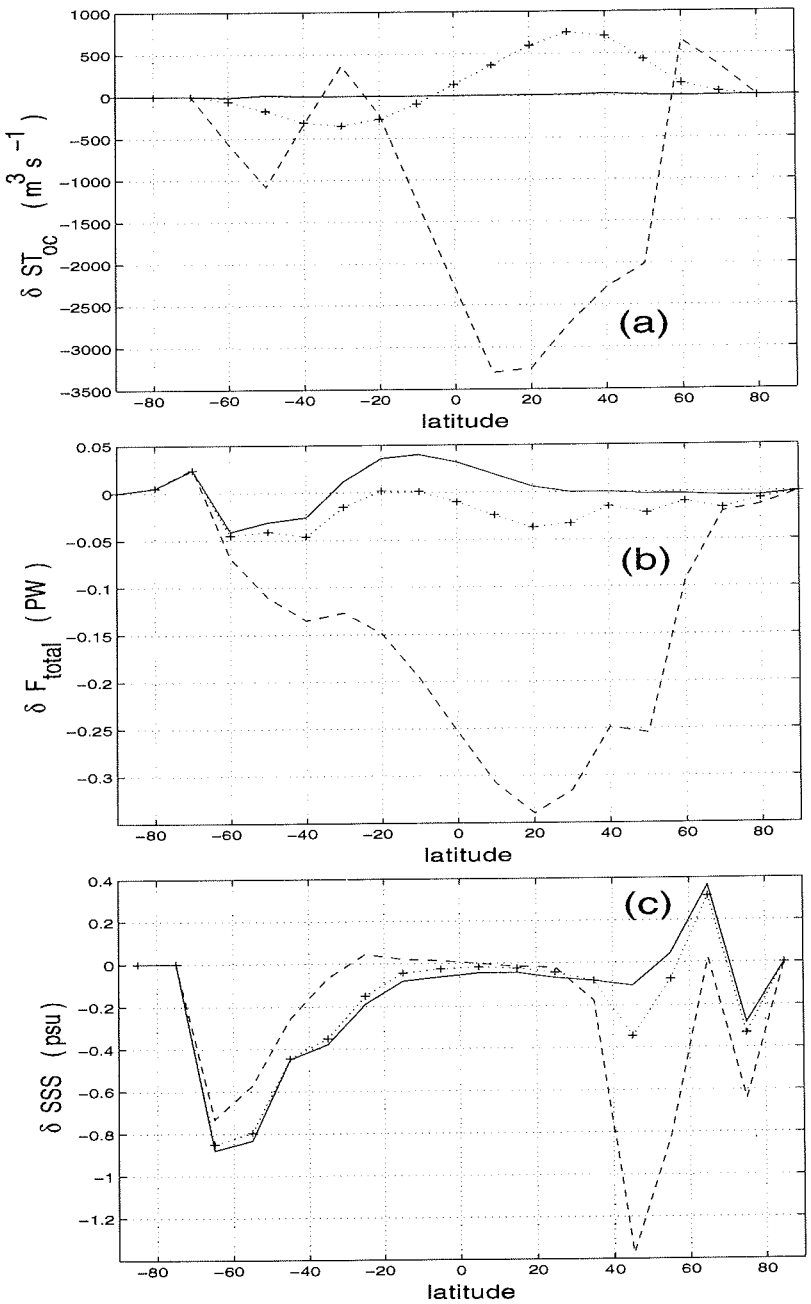

Figure 10.9: Change of northward salt transport in the ocean (a) measured as a negative fresh water transport. Change of total (atmosphere + ocean) northward heat transport (b). Change of sea surface salinity (c). The notation for 14, 110 yrs after the perturbation and equilibrium are the same as in figure 10.8.

At 40^0 N, the heat transport is reduced by 0.50 PW to the value of 0.37 PW which reduces oceanic temperatures at high latitudes. At the same time the oceanic northward salt transport is reduced (figure 10.9 a). At 40^0 N, the salt transport of 13175 $m^3 s^{-1}$ is reduced by 2293 $m^3 s^{-1}$ (figure 10.9 a). The vertically integrated oceanic salt transport is drastically reduced when mass transport is at minimum (figure 10.9 a). However, in the phase of reestablishing meridional mass transport (110 years after perturbation), the anomalous salt transport is directed northward on the northern hemisphere. This stabilizing effect on the THC is induced by colder temperatures (figure 10.7 a) enhancing the meridional velocities in the upper ocean layers. This phenomenon may be seen by comparing the zonally averaged meridional mass transport of the reference case (figure 10.1) and 110 years after perturbation (figure 10.5).

In equilibrium, the anomalous salt transport is close to zero (figure 10.9 a). This finding is consistent with the equilibrium salt balance (6.2) from the relatively small change in surface fresh water flux (figure 10.7 c):

$$\delta ST_O(\phi) = \frac{1}{\cos(\phi)} \int_{-90^0}^{\phi} a \cos(\phi') \frac{S_0}{\rho_w} \delta (P - E)(\phi') \, d\phi' \quad , \tag{10.6}$$

where ρ_w and S_0 are the density of fresh water and a reference salinity, respectively.

The sea surface salinity (SSS) distribution has a strong minimum between $40^0 - 60^0$ N 14 years after perturbation (figure 10.9 c). After that time, the minimum vanishes due to enhanced salt transport at the surface from regions of high salinity. The anomalous sea surface salinity in equilibrium results from less advection of salt in the surface layers north of 70^0 N. This decreases SSS north of 70^0 N and increases SSS south of 70^0 N.

The change of total heat transport (atmosphere+ocean) is shown in figure 10.9 b. This graph could also be obtained by adding the anomalous northward heat transport of figure 10.8. The total heat transport is not constant in time. The strong decrease of oceanic heat transport is only partly balanced by the atmospheric heat transport 14 years after perturbation. Therefore, fixing the total heat transport and calculating the latent as the residuum from sensible and oceanic as in Tang and Weaver (1995) or in model version 1 of Chen et al. (1995) overestimates the latent heat transport in a transient run. Such models produce therefore too high fresh water fluxes thus destabilizing the THC.

However, in the second phase and in equilibrium, the change of total heat transport is small (less than 0.05 PW). The change of total heat transport is determined by the radiation on top of the atmosphere. Changes due to increased albedo are partly balanced by less outgoing longwave radiation. In equilibrium, the anomalous oceanic heat transport is therefore balanced by anomalous atmospheric transport. An anomalous northward oceanic heat transport is observed south of 20^0 N due to changed oceanic circulation in the deep ocean layers (figure 10.8 c). This is compensated at high latitudes on the southern hemisphere by anomalous southward sensible heat transport by transient eddies (figure 10.8 a). The new equilibrium will be discussed in more detail in the next section.

10.4 New equilibrium

The two solutions obtained from the coupled experiments (reference case and the end of the perturbation experiment) represent two different climatic states. In the reference climate the sea margin is about four degrees further poleward than in the new climate. The perturbation in high latitude salinity caused transition from one climate to another. In the second equilibrium, deep water formation in the northern North Atlantic is shallower and the sites of deep water formation areas have shifted southward. The deep water sinks only to intermediate depth because the density is less than in the reference case. It is surprising that the deep water is about 1 K warmer in the new equilibrium (figures 10.11 A and 10.11 B: 15^0 E section) although the atmospheric temperatures at high latitudes (10.7 a) is about 0.8 K colder. Therefore, the heat flux close to the sea ice edge is stronger but more confined than in the reference case (compare figures 10.2 and 10.10). Furthermore, the heat loss at the southern boundary of the ocean basin is almost shut off. In the spin up (figure 10.11 C) an antarctic intermediate water is observed whereas in the new equilibrium (figure 10.11 D) very fresh water is responsible for a halocline on the northern and southern hemisphere. In the regions of deep water formation the thermohaline structure in the 15^0 E section is very different influencing the convection sites and deep water (figure 10.11). In the reference circulation the 2^0C isotherm is located at 60^0 N and the 0^0C isotherm is found at 64^0 N. In this region deep water is formed sliding down the ridge. In the new equilibrium the 3^0C isotherm is found at 58^0 N whereas the 1^0C isotherm is part of the thermocline found north of the ridge (figure 10.11 B).

The warming of the deep ocean in the new equilibrium is due to more equatorward convection sites. The density of the water which forms the sinking is decreased and deep penetration is reduced. Deep antarctic bottom water is not observed in both states. This is due to the low salinities in the boundary conditions of the spin up. The second cell underneath the North Atlantic deep water cell with maximal 4 Sv (figure 10.6) shows a downwelling in the south-eastward part of the ocean basin and upwelling in the northwestern side.

The horizontal transport is also affected by changes in the THC. Matching with the changed overturning of the new equilibrium, the subpolar gyre in the stream function of the vertically integrated transport is strongly reduced according to figure 10.10 right. In a flat-bottom model as in chapters 6, 9 or in the southern hemisphere (figure 10.10 right) the equilibrium stream function would be given by the fixed wind stress curl. The anticyclonic gyre between 20^0 and 50^0 N of figure 10.10 right intensifies and moves further northward than in the reference case.

The weaker cyclonic cell is combined with a sea ice edge at 62^0 N. However, the sea ice thickness is reduced from maximal 20 cm to 10 cm in the North Atlantic. This sea ice thickness seems to be of minor importance compared to the sea ice extent because the reduction of heat loss (figure 10.10 left) from the ocean surface is mainly determined by the larger sea ice extent.

In the new equilibrium found here, the recirculation in the subarctic gyre is weakened (figure 10.10 right) and the surface transport of relatively fresh water at high

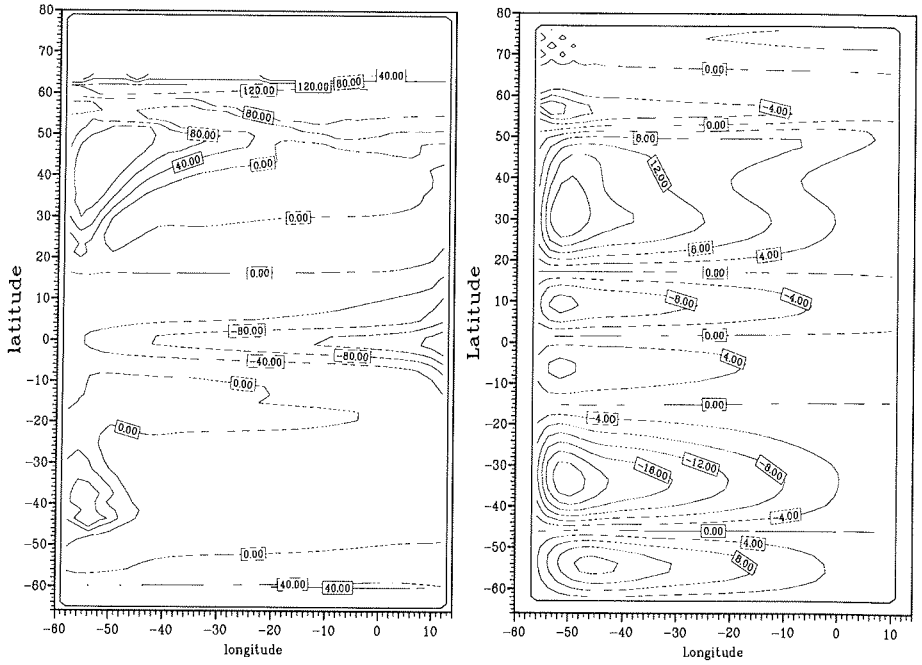

Figure 10.10: Heat flux out of the ocean-sea ice system (left) and stream function of the vertically integrated transport (right) in the new equilibrium. Compared to the initial state the subpolar gyre is weakened (right figure). The contour interval is 4 Sv. The sea ice extent is more southward compared to the reference case (figure 10.2 left) reducing the heat flux for the atmosphere.

latitudes is reduced. The zonally averaged sea surface salinity is increased between 60^0 and 70^0 N but reduced north of 70^0 N because of the new circulation (figure 10.10 right) with sinking further southward. Therefore, the difference in the sea surface salinity between the two equilibria can be attributed to a changed circulation of surface water and not to a difference in the fresh water flux at the atmosphere-ocean interface which is positive between $55^0 - 70^0$ N.

What is shown here, is that sea ice changes have considerable influence on the climate state and cannot be neglected in sensitivity studies any more. The presented second mode of circulation can cause a temperature drop in the northern North Atlantic without switching the conveyor off. This can be viewed in terms of paleoclimatic changes of the THC.

Paleoclimatic interpretation

In nature, several water masses contribute to the North Atlantic Deep Water (Dietrich et al., 1975), viz Labrador Sea Water, overflow water of intermediate waters from the Nordic Sea, salty subtropical water penetrating into the central northern Atlantic, and water which is formed in the open areas of the North Atlantic. Paleoclimatic studies (e.g. Imbrie et al., 1992) suggest that if one of these sources is shut off, e.g. due to meltwater or anomalous ice, the conveyor switches into a different mode. Indeed, biogeochemical proxies in marine sediments confirm this idea (Bond, 1995). It is only recently that variations in the relative strength of deep and intermediate currents in the North Atlantic have been analyzed over the past 25000 years (McCave et al., 1995). There is strong evidence that speeds of deep and intermediate water masses are inversely related. According to McCave et al. (1995), deep water current decreases while intermediate water increases during the well documented climate shifts as the Younger Dryas (11000 yrs B.P), Older Dryas (=Heinrich event 1, 19000 yrs B.P.), and the Last Glacial Maximum (27000 yrs B.P.).

This finding is consistent with our model results: A fresh water release to the surface ocean (as in the Younger and Older Dyras) decreases the density of the surface water sufficient to cause cessation of deep convection and forming of intermediate water only.

10.5 Other types of boundary conditions

The sensitivity of the circulation to freshening at high latitudes depends on processes including sea ice and atmosphere. Considering the sources of feedback in the atmosphere-ocean-sea ice system, different boundary conditions will be used to investigate stabilizing and destabilizing effects for the THC.

To isolate the effect of the atmospheric heat transport, an experiment with Schopf's

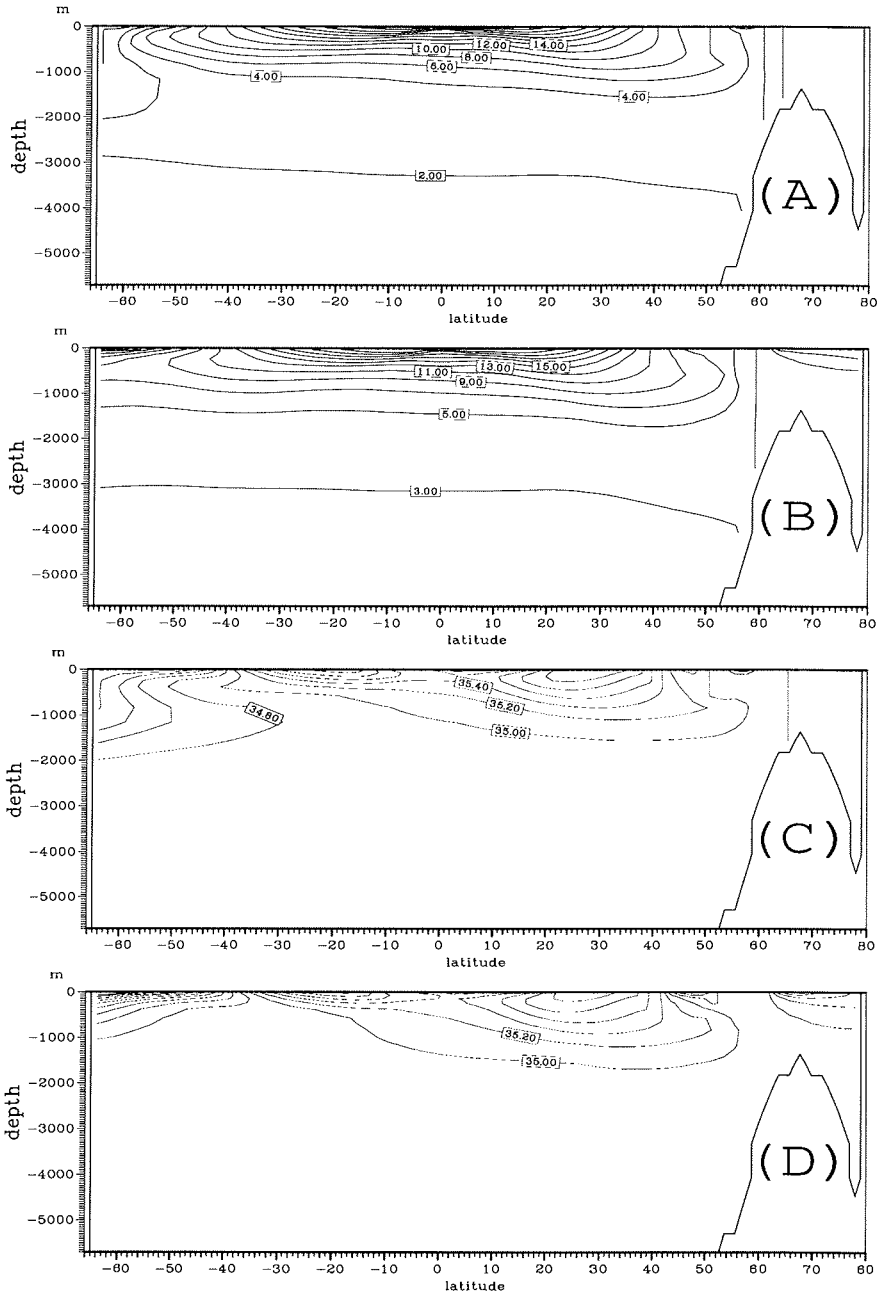

Figure 10.11: Comparison of temperature and salinity in a section at 15^0 east for both steady states (initial condition, equilibrium after perturbation in salinity). Temperature and salinities in the spin up steady state (figures A and C). Temperature and salinities in the new equilibrium (figures B and D). The units are ${}^0C$ and psu, respectively.

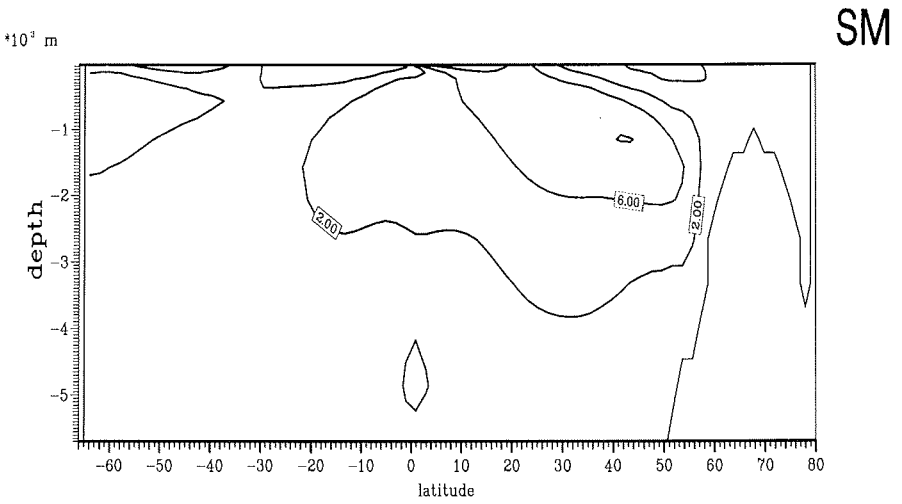

Figure 10.12: Stream function for the zonally integrated transport for the experiment where no anomalous atmospheric transport is allowed. Deep water formation does not takes place any more 200 years after perturbation.

(1983) atmospheric model (denoted by SM in chapter 6) as the thermal boundary condition is performed. In this model the meridional heat transport is held constant. Therefore, the temperature is only determined by the local heat balance in the vertical air column. Furthermore, the fresh water flux is held fixed in this model.

In contrast to the experiment in chapter 6, the THC collapses. The more equatorward sea ice extent reduce the heat flux out of the ocean. The poleward heat and salt transports and the THC will break down completely (figure 10.12) after a few years. The NADW formation does not take place any more 200 years after the perturbation.

Because changes in atmospheric heat transport are neglected, this model produces too low temperatures over the anomalous sea ice. The breakdown of the THC is induced by the insulating effect of sea ice and by the ice-albedo effect. Both effects amplify the formation of sea ice and reduce further the heat loss of the ocean. As a consequence, northward heat and salt transports in the Atlantic basin are strongly reduced.

This atmospheric model is not appropriate as a boundary condition because temperature changes are only determined by a radiation balance and heat flux changes (up to $-75\,W\,m^{-2}$ in the experiment SM). This system is integrated over 200 years model time which produces an unrealistic atmospheric temperature profile with equatorward temperature gradients at 70^0 N.

In a further experiment, mixed boundary conditions (fixed atmospheric temperature and surface fresh water flux) are used as the atmospheric model in the coupled system. Under this boundary conditions, the system is more stable than the system with SM because the atmospheric temperature is fixed which determines the sea ice

extend. As we have seen in the previous chapters, this boundary condition implies strong atmospheric heat transport to keep the atmospheric temperature. However, a large perturbation in high latitude salinity can induce a breakdown of the THC using mixed boundary conditions.

Because the sea ice edge is affected by the fixed atmospheric temperature T_A^*, the sea ice edge is further poleward than in the experiment SM with fixed atmospheric heat transport. The local heat flux change due to freshening of the oceanic surface layers induces the reduction of the mass transport.

The density of the water at high latitudes is reduced further through a reduced northward mass transport which leads to the shut down of the THC ("polar halocline catastrophe"). This collapse of the THC is similar but not identical to the "polar haline catastrophe", originally observed by Bryan (1986) without sea ice. The main deficiency of the mixed boundary conditions is that the atmospheric temperature is held fixed although the air-sea heat flux is strongly reduced.

A further coupled experiment is performed to investigate the effect of changed fresh water flux In the experiment the fresh water flux to the ocean surface is fixed (analogous to cH in chapter 6). This experiment is integrated over 110 years. The circulation is nearly the same as in cHF which is not shown here because this finding is close to that of chapter 6. Note, that the anomalous fresh water flux $P - E$ in the coupled experiment (figure 10.7 c) looks similar to figure 4.3. In the model precipitation is not transformed into snow which could be another important positive feedback (Ledley, 1991) affecting the heat and fresh water balance.

To investigate the effect of the additional fresh water flux due to freezing and melting, the coupled model is integrated with switched off additional fresh water flux for the ocean surface. This experiment shows a non significant stabilizing effect for the THC. The results show nearly identical patterns to experiment cHF and therefore are not shown here. The effect of fresh water due to sea ice is probably more important in a model which includes the seasonal cycle and sea ice transport.

10.6 Discussion of feedback mechanisms

The feedback mechanisms for the coupled ocean-atmosphere-sea ice system are schematically shown in figure 10.13. As in figure 2.1, positive (+) and negative (−) feedback must be multiplied to get the effective negative or positive feedback mechanism. In addition to figure 2.1 the thermodynamic properties of sea ice are included.

Sea ice insulates the colder atmosphere from the warmer ocean. Furthermore, in a colder atmosphere the albedo is increased. One important negative feedback stabilizing the climate system is due to large-scale eddies in the atmosphere: A colder atmosphere at high latitudes coincides with large sea ice extent. The air is heated and the ice edge is shifted poleward due to enhanced eddy activity. The experiment with no anomalous atmospheric heat transport in section 10.5 shows the importance

of variable atmospheric heat transport.

If sea ice melts the surface water is freshened and a decrease in sea surface density and vertical ocean heat flux is expected. This would prevent further sea ice melting. On the other hand, if sea ice volume increases, brine release increases SSS and thus vertical ocean heat flux which reduces sea ice. This loop is a negative feedback. However, the effects due to additional surface fresh water flux from ice are of minor importance in the experiments.

A reduced oceanic poleward heat transport brings less warm water to high latitudes which favors the formation of sea ice. More sea ice increases the density of the mixed layer which increases the poleward heat transport and reduces sea ice.

The schematic picture of the feedbacks affecting the THC helps to understand sensitivity studies which include sea ice. The results presented indicate that sea ice may be responsible for changes in the meridional heat and mass transport of the Atlantic. This has also been found for different CO_2-scenarios in the coupled GCM model of Manabe and Bryan (1985). They found that the THC is very sensitive to a reduction of 50% in the CO_2 content in the atmosphere and relatively insensitive to a doubled CO_2 content. In the reduction case, the poleward mass transport decreases which further decreases SST and air temperature, owing to the influence of sea ice upon the THC. The poleward salt transport is reduced and the surface density on high latitudes decreases as a net-effect. The latent heat decreases due to colder temperatures whereas the sensible heat transport is amplified. In their experiment the sensible heat transport contributes not as much as in the presented experiment to shift the ice edge northward.

An interesting ice-ocean-atmospheric model is the simple box model of Saltzmann (1978, in the appendix) and Moritz (1979) where only the mass-averaged ocean temperature and sea ice edge are considered as the variables. Atmosphere and ocean temperature are calculated by a linear decrease in temperature from the equator to the ice edge. The SST at the ice edge is fixed. All interactions with the salt are neglected in this model. The net surface energy fluxes into the ocean are integrated from the equator to the sea ice edge. The mass-averaged ocean temperature depends on the sea ice edge in a non-linear way due to the latitude dependent solar radiation intensity. The sea ice edge, on the other hand, depends on the ocean temperature (melting of ice) and on the ice-albedo feedback. This mechanism may lead to damped oscillations in the system of two ordinary differential equations. A warm ocean melts ice, the heat loss of the ocean causes colder temperatures and more ice. Therefore, this model shows the insulating effect of sea ice, preventing a large heat loss out of the ocean. This model neglects the atmospheric heat transport effects. Furthermore, the oceanic region interacting with the sea ice is an uncertain parameter in the model. In reality, this would depend on the properties of the oceanic circulation.

A similar effect is reported by Zhang et al. (1995) using an ocean circulation model including a thermodynamic sea ice model. Their ice-albedo effect is incorporated by an ad hoc assumption about the atmospheric temperature T_A differing from the climatological temperature T_A^*: $T_A = T_A^* + T_i + T_s$, where $T_i = -4\,K$ if $H_{ice} > 10$ cm, and $T_s = -2K$ if $H_{snow} > 8$ cm. This neglects the change of the atmosphere temperature due to eddy activity. and the atmospheric temperature

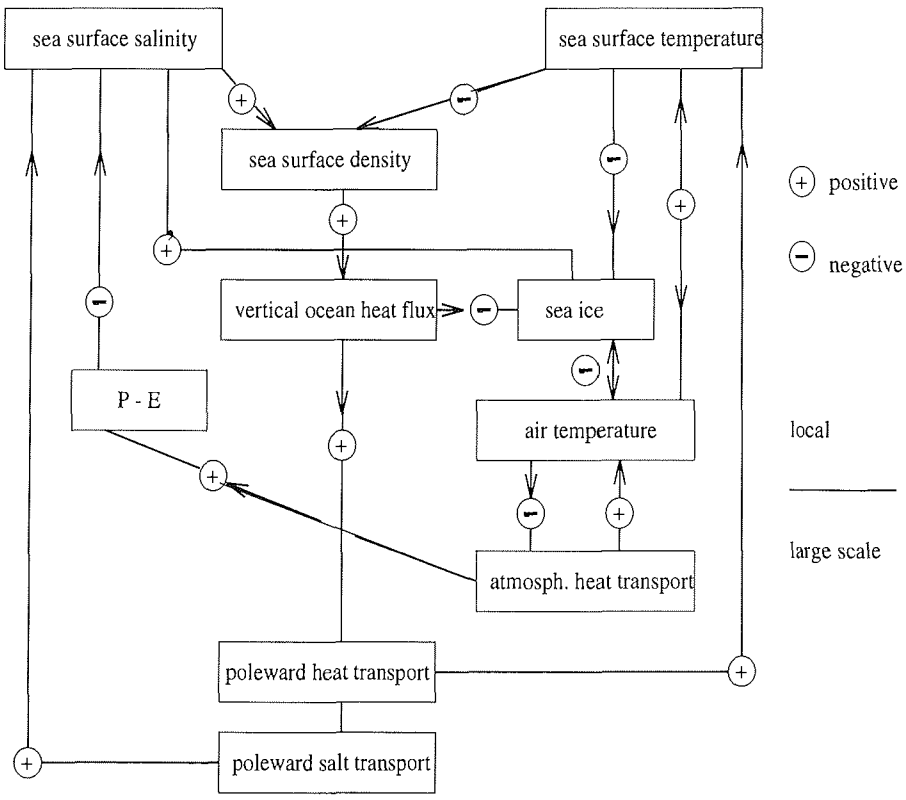

Figure 10.13: Feedback mechanisms in the coupled ocean-atmosphere-sea ice system. Positive (+) and negative (−) feedbacks must be multiplied to get the effective mechanism. On large scales the oceanic heat and salt transports determine sea surface temperature and salinity. The present salinity conveyor belt depends strongly on the positive loop (SSS, density, vertical mixing, poleward transport) because the salinity at high latitudes is relatively weakly influenced by surface fluxes. In contrast, the SST at high latitudes is strongly coupled to the air temperature. Reduced oceanic poleward transports decrease SST and air temperature and are connected with a larger sea ice extent. Sea ice insulates the atmosphere from the warmer ocean and has a high albedo compared to water. Salt brine release (SSS, density, vertical mixing, sea ice) is a negative feedback of minor importance in our experiments. An important negative feedback stabilizing our climate system is the enhanced atmospheric heat transport which warms the air and shifts the ice edge poleward.

changes only locally.

They found self sustained oscillations of the THC and sea ice extent which are linked to a negative feedback between poleward oceanic heat transport and sea ice extent. The thermal insulation of ice cover reduces the surface heat loss and vertical mixing. Furthermore, the thermal insulation allows the ocean to warm up. Strong poleward transport leads to an onset of deep convection which melts ice. In Zhang et al.'s (1995) experiments, the period of oscillation (amplitude about 5 Sv) is governed by the heat flux rate at the ice-atmosphere surface, which is far too strong ($50\,W\,m^{-2}\,K$).

Their feedback mechanism is observed in our coupled model (cHF), too. Small fluctuations of less than 0.01 PW at 60^0 N are seen in the first 60 years of integration. At that time the sea ice thickness is reduced and large-scale leads occur stochastically which influence the heat flux out of the ocean. Due to the topographic barrier, the poleward mass transport has no chance to push to the northern boundary of the basin as in Zhang et al. (1995). The effect of brine rejection during ice formation has no influence on the model results of Zhang et al. (1995) which is in agreement with our result.

Recently Yang and Neelin (1993) found that in an idealized two dimensional ocean model under mixed boundary conditions the negative feedback between poleward heat advection and salt brine release induces oscillations with a period of 13.5 years (reduced THC, more formation of sea ice, salt brine release, vertical mixing, enhanced THC). As in the coupled model presented the sea ice model is thermodynamic whereas the ocean model is a zonally averaged model. Furthermore, they used mixed boundary conditions without a seasonal cycle. The oscillation time is governed by the sea ice-ocean coupling and is not associated with any oceanic time scale. Their simplified ocean-sea ice model suggests that the negative feedback (sea ice melting-freezing process) may not be neglected in the coupled system.

However, the constant atmospheric temperature implies an atmospheric heat transport to keep the atmospheric temperature. The process of salt brine release is not important in model results (cHF), but could be relevant in studies including the seasonal cycle and dynamic processes of sea ice. In the real ocean, salt brine release is one of the main mechanisms affecting high latitude salinity and thus deep water formation.

The results of previous studies (Zhang et al., 1995; Yang and Neelin, 1993) should be questioned in terms of the coupled system because none of them included an interactive atmosphere model. The experiments, documented here, have shown that the stability of the THC depends on the formulation of the atmospheric model. It is concluded that the atmospheric heat transport in connection with sea ice has a stabilizing effect on the circulation in the coupled model.

Sea ice transport and snow affect the THC in an important way. One preliminary run with a dynamic sea ice model (velocity of sea ice is equal to the velocity in the upper ocean) has indicated that the sensitivity is reduced compared to the purely thermodynamic sea ice model. Therefore, a simple dynamical sea ice model should be applied in further sensitivity studies. The transport of low salinity water and sea ice through the Fram Strait (see e.g. Aargaard and Carmack, 1989) is left out. The transport from the Arctic to the North Atlantic is thought to be important

but poorly understood. The influence of sea ice variability for the North Atlantic ciculation is an important task for future model studies.

Furthermore, snow, leads and a seasonal cycle should be incorporated in a more complex system. Snow and leads have significant effects on the thermal properties of the atmosphere-sea ice interface (Ledley, 1991, 1988). The introduction of leads will reduce the insulating effect of sea ice. Effects of snow on sea ice, e.g. changed albedo, insulating properties, specific heat and heat of fusion would complicate this simplified approach and will be left to further investigations.

Chapter 11

Summary and Conclusions

A principal understanding of feedback mechanisms in the coupled ocean-atmosphere-sea ice system is obtained by a stability analysis using analytical and numerical models. Different types of boundary conditions have been used to study the sensitivity of the thermohaline circulation (THC). An energy balance model (EBM) has been presented which was designed to be a useful upper boundary condition for the ocean. The dynamics of the atmosphere is simplified to the change in the transport due to large-scale eddies. The atmospheric model responds to sea surface temperature anomalies and external forcing in such a way that it is consistent with complex atmospheric models. The experiments performed explore the mechanisms included in the EBM, e.g. the effect of latent and sensible heat transport.

Coupled models have been presented in which either the atmosphere or both atmosphere and ocean are simplified in their dynamics. The analysis shows that atmospheric transport of heat and moisture do influence the large-scale heat exchanges at the air-sea interface and thus affect the stability of the THC.

The local change of atmospheric temperature is a stabilizing effect for the THC since it tends to keep the heat flux at the sea-air interface nearly unchanged. However, if sea ice is present, a local formulation of the atmospheric heat budget allows sea ice to move equatorward such that northward oceanic heat and salt transport are strongly reduced. As a result, the heat flux at the upper ocean surface is reduced in regions of deep water formation by sea ice.

The coupled atmospheric energy balance - oceanic circulation model (EBM-OGCM) experiments point to the meridional transport in the ocean which can be amplified by a perturbation due to a positive feedback in the salt transport. An enhanced northward salt transport intensifies the transport of more dense water to high latitudes which further amplifies the meridional transport. This destabilizing feedback is partly balanced by the effect of oceanic heat transport which is underestimated if the atmospheric temperature is held fixed. Numerical experiments and theoretical analysis have shown that the boundary conditions imply an atmospheric model with meridional transports of heat and moisture.

The coupled experiments indicate that the meridional atmospheric heat transport

is the most important atmospheric feedback while the effect of moisture transport seems to be of minor importance. This finding is partly in contrast to the box model presented in section 7 where the effect of fresh water acts as a strong destabilizing feedback. Thus, the box model is more sensitive to perturbations in surface salinity at high latitudes than the coupled EBM-OGCM. The coarse resolution of the box model and simplified physics are responsible for the greater sensitivity.

The feedback mechanisms in the coupled ocean-atmosphere system are shown by a linear stability analysis in a simple coupled model. The atmospheric transport due to large-scale eddies is parameterized as diffusion, whereas the oceanic THC is approximated by a non-linear box model. The advective mechanisms in the ocean transporting heat and salt are included in the box model whereas effects of mixing and localized sinking are not represented. In this coupled model, the qualitative effects of heat and fresh water fluxes on the THC are explored.

A strong, thermally-dominated deep water formation favors stability of the circulation with respect to salinity perturbations. The atmospheric transport of heat and moisture destabilize the THC, partly compensating for the stabilizing effect of a local atmospheric cooling due to reduced heat flux from the ocean to the atmosphere. In the linearly stable parameter region of the box model, there is a threshold of critical salinity perturbation beyond which the non-linear system becomes unstable. Feedback related to the transport of salt, heat and moisture in the box model are thought to qualitatively reflect the processes weakening the THC through freshening events at high latitudes, such as the GSA and meltwater events. Furthermore, the analysis indicates how flux corrections may enter into the sensitivity of the THC.

Simplified models have been shown to be a useful tool in studying stability and variability of the THC (chapters 7 and 8). The restriction of no zonal extent and crude vertical and meridional resolution can be relaxed (Maas, 1994). Maas (1994) has shown how the dynamics of box models can be derived rigorously from vorticity equations. Therefore, these simplified vorticity equations may be a possible way of understanding the behavior of the THC from the dynamical system perspective.

The simple coupled model given in chapter 8 is the numerical counterpart of the analytical investigation of chapter 7. The coupled model is used to study the time dependent response of an increased CO_2 content in the atmosphere. A polar amplification of surface temperature and intensification of the hydrological cycle are observed which is consistent with earlier studies. A reduced oceanic heat transport brings less warm water to high latitudes. This is a stabilizing feedback of the THC due to changes in fresh water flux in the more humid climate. However, it remains an open question as to how sensitive the circulation is to changes in the surface water and atmospheric tracer gas concentrations in complex climate models.

A stochastic box model suggests that variability on decadal time scales may be induced by fluctuations in the atmosphere. The ocean works as an integrator of the atmospheric noise. The power spectra of the oceanic transport depend on the parameterization of meridional mass transport. The low frequency variability is stronger the more sensitive the THC is.

Estimating natural variations within the Earth's climate system, mechanisms should be isolated when exploring variability of a coupled model. One possible mechanism was found in chapter 9 where horizontal salinity gradients affect the motion such

that the gradients move with the horizontal motion. This phenomenon can be induced by very strong gradients in salinity which might be caused by melt water release.

The coupled experiments show (chapters 7 and 9) that the sensitivity of the circulation increases for stronger salinity contrasts between high and mid latitudes. One could speculate that meltwater events, calving icebergs or anomalous sea ice, might have a stronger influence on the THC under glacial conditions when compared to today's conditions the sea surface at low latitudes was about one psu saltier combined with a slightly fresher ocean surface at high latitudes. Therefore, the stability of other climatic states with respect to perturbations should be analyzed in detail, e.g. the oscillator-ocean or the new equilibrium found in chapter 10.

Chapter 10 has shown that the presence of sea ice affects the sensitivity of the THC in an important way. The main influences of sea ice in the climate system are the insulation between the ocean and atmosphere and the high albedo compared to water. The upward oceanic heat flux over the region covered by ice is strongly reduced thereby cooling the atmosphere. The experiments documented in chapter 10 have again shown that the stability of the THC depends on the formulation of the atmospheric model. It is concluded that the atmospheric heat transport in connection with sea ice has a stabilizing effect on the circulation in the coupled model. Due to perturbation in high latitude salinity a different steady state has evolved with a more equatorward sea ice edge and a shallower deep water formation in the North Atlantic. Because of the sea ice covered areas, the atmosphere is colder and convection sites move southward. These shifts in convection sites are important for changes in the THC related with changed atmospheric conditions. A reduced oceanic northward heat transport is balanced by enhanced eddy activity in the atmosphere in the northern hemisphere.

More complex sea ice models must be applied to investigate the feedbacks identified in our model. A simple, computer-inexpensive dynamical sea ice model is in preparation which is similar to the cavitating fluid model (Flato and Hibler, 1992).

Zonally averaged EBMs (Stocker et al., 1992; Nakamura et al., 1994; the presented one) overestimate the zonal and meridional transport, because they implicitly assume a zonally homogeneous atmosphere. In Rahmstorf and Willebrand's model (1995), on the other hand, the meridional heat transport is underestimated by assuming that anomalous atmospheric transport takes place only over ocean surfaces. The local atmospheric response in zonally averaged models is less than in a model with longitudinal resolution. Therefore, the resulting anomalous atmospheric transport is underestimated partly compensating for the above effect.

Thus, a 2-dimensional $(x, y)-$ EBM including transport over land and catchment areas for run off should be applied to an ocean model. The transport of heat and moisture may be related to the local temperature gradients at the surface. Such a formulation for the temperature was used by Kleeman and Power (1995) in their EBM without moisture. Including precipitation on land surfaces would require a runoff scheme, e.g. a bucket model (Manabe, 1969), and a horizontal routing scheme (e.g. Miller et al., 1994).

However, it is inconsistent to model the effects of horizontal heat flux and neglect the vertical stabilization caused by vertical heat transport. Ignoring feedback in-

volving vertical fluxes of baroclinic eddies is a simplification often made in one-level models (Branscome, 1983). The importance of the vertical resolution might be seen in the necessary condition for baroclinic instability which depends on the vertical stratification (Holton, 1979). The formulation of the vertical and horizontal heat transport given by Stone and Yao (1990) may be used for the transient eddies. A correct description of the transports would require a model with vertical resolution (see for EBMs e.g.: Peng et al., 1982, 1987; Chan et al., 1995; Lohmann, 1995).

An alternative to the EBM-approach is a non-linear long wave model (e.g. White and Green, 1982) based on quasi-geostrophy. They parameterized baroclinic instability, but considered both zonal and longitudinal fields. Generally such models neglect transport of moisture. A diagnostic formulation of the mixing ratio of water vapor depending on climatological relative humidity and water vapor saturation could introduce a hydrological cycle in the model. The advantage of a non-linear long wave model compared to an EBM is its better physical justification. Furthermore, the dynamics are explicitly calculated which is probably necessary when dealing with the seasonal cycle. Lorenz (1979) has shown that the diffusive parameterization is justified from measurements for seasonal averaged models only.

The statistical approach described in section 3.6 might also be a promising way because the statistics of a highly complex atmospheric model is included in the diagnostic atmospheric model. Furthermore, there is a need for computer inexpensive atmospheric circulation models which can be used for coupled models.

A model of the world ocean is the natural extension of the idealized geometries of the Atlantic ocean used. This model should simulate today's deep water formation and the overflow over topographic barriers correctly. The transport of water between the Atlantic and Pacific basins is a task for further coupled ocean-atmosphere models. It is not clear whether today's fresh water export from the North Atlantic (Wijffels et al., 1992; Chen et al., 1994; Peixoto, 1995) will change under different climate conditions. An enhanced export would change the haline forcing stabilizing the THC in contrast to the anomalous meridional water vapor transport (chapters 6 and 7). The geographic location of changed precipitation, evaporation and runoff may influence the sensitivity.

We have seen that the model behavior and the stability properties of the THC depend on the model components included with its feedback mechanisms, viz the representation of the atmospheric heat transport, the basic state of the THC, and the representation of sea ice. In the thesis presented, only first steps in looking for mechanisms of the coupled atmosphere-ocean (-sea ice) system have been done. Much more work is needed to understand the interrelation of the climate components. This will lead to further discussion, where I agree with a comment of Boyle and Weaver (1994) : "As we advance our understanding through a series of progressively more complex models, how many more new model behaviors will we discover, and are any of them truly related to the behavior of the real ocean ?"

However, the mechanisms described in this thesis should be found in more complex coupled models. If not, one must have good arguments why a process does not affect the sensitivity of the THC. Therefore, a logical next step would be to study more complex coupled climate models to investigate the feedback mechanisms identified in the presented models.

Bibliography

[1] Aagaard, K., and Carmack, E.C., 1988: The role of sea ice and other fresh water in the Arctic circulation. J. Geophys. Res. 94,14485-498.

[2] Augustsson, T., and Ramanathan, V., 1977: A radiative-convective model study of the CO_2 climate problem. J. Atm. Sci. 34,448-451.

[3] Barnett, T.P., Latif, M., Graham, N., Flügel, M., Pazan, S., and White, W., 1993: ENSO and ENSO-related predictability. Part I: Prediction of equatorial Pacific sea surface temperature with a hybrid coupled ocean-atmosphere model. J. Climate 4,1545-1566.

[4] Berger, A., 1978 : Long time variations of daily insolation and quaternary climate changes. J. Atm. Sci. 13,2362-2367.

[5] Birchfield, G.E., 1989: A coupled ocean-atmosphere climate model: temperature versus salinity effects on the thermohaline circulation. Climate Dynamics 4,57-71.

[6] Bolton, D., 1980: The computation of equivalent potential temperature. Month. Weath. Rev. 108,1046-1053.

[7] Bond, G.C., 1995: Climate and the conveyor. Nature 377,383-384.

[8] Boyle, E.A., and Keigwin, L.D., 1987: North Atlantic thermohaline circulation during the past 20,000 years linked to high latitude surface temperature. Nature, 330,35-40.

[9] Boyle, E.A., and Weaver, A., 1994: Conveying past climates. Nature, 372,41-42.

[10] Branscome, L.E., 1983: A Parameterisation of transient eddy heat flux on a beta plane. J. Atm. Sci. 40,2508-2521.

[11] Bretherton, F.P., 1982: Ocean climate modeling. Prog. Oceanog., 11, 93-129.

[12] Broecker, W.S., Bond, G., Klas, M., Bonani, G., and Wolfi, W., 1990: A salt oscillator in the glacial Atlanic? 1. The concept. Paloeoceanogr. 5,469-477.

[13] Broecker, W.S., Peteet, D.U., and Rind, D., 1985: Does the ocean-atmosphere system have more than one stable mode of operation. Nature 315,21-26.

[14] Bryan, F., 1986: High latitude salinity effects and inter hemispheric thermohaline circulations. Nature 323,301-304.

[15] Bryan, F., 1987: Parameter sensitivity of primitive equation ocean general ciculation models. J. Phys. Oceanogr. 17,970-985.

[16] Bryan, K., 1969: A numerical method for the study of the circulation of the world ocean. J. Comput. Phys. 4,347-376.

[17] Bryan, K., 1984: Accelerating the convergence to equilibrium of ocean-climate models. J. Phys. Oceanogr. 14,666-673.

[18] Budyko, M.I., 1969: The effect of solar radiation variations on the climate of the Earth. Tellus 21,611-619.

[19] Cai, W., Greatbatch, R.J., and Zhang, S., 1995: Interdecadal variability in an ocean model driven by a small, zonal redistribution of the surface buoyancy flux. J. Phys. Oceanogr. 25,1998-2010.

[20] Cessi, P., and Young, W.R., 1992: Multiple equilibria in two-dimensioal thermohaline circulation. J. Fluid Mech. 241,291-309.

[21] Cess, R.D., Ramanathan, V., and Owen, T., 1980: The Martian paleoclimate and enhanced atmospheric carbon dioxide. Icarus 41,159-165.

[22] Chan, D., Higuchi, K., Lin, C.A., 1995: The sensitivity of the simulated normal and enhanced CO_2 climates to different heat transport parameterizations in a 2-dimensional multilevel energy balance model. J. Climate 8(4),844-852.

[23] Charney, J.G, 1947: The dynamics of long waves in a baroclinic westerly current. J. Meteor. 4,135-162.

[24] Chen, F., and Ghil, M., 1995: Interdecadal variability of the thermohaline circulation and high-latitude surface fluxes. J. Phys. Oceanogr. (submitted).

[25] Chen, D., Gerdes, R., and Lohmann, G., 1993: A 1-D energy balance atmospheric model applied to ocean modelling, Technical Report 44, AWI.

[26] Chen, D., Gerdes, R., and Lohmann, G., 1995: A 1-D atmospheric energy balance model developed for ocean modelling. Theor. Appl. Climatol. 51, 25-38.

[27] Chen, T.-C., Pfaendtner, J., and Weng, S.-P., 1994: Aspects of the hydrological cycle in the atmosphere-ocean system. J. Phys. Oceanogr. 24,1827-1833.

[28] Chou, M., Peng, L., and Arking, A., 1982: Climate studies with a multi-layer energy balance model. Part II: The role of feedback mechanisms in the CO_2 problem, J. Atm. Sci. 39,2657-2666.

[29] Chu, S., and Ledley, T.S., 1995: Hydrological cycle parameterization for energy balance climate models. J. Geophys. Res. 100(D8),16289-303.

[30] Courant, R., Friedrichs, K., and Lewy, H., 1928: Über die partiellen Differentialgleichungen der mathematischen Physik. Math. Ann. 100,32-74.

[31] Cox, M.D., 1984: A primitive equation,3-dimensional model of the ocean. GFDL Techn. Report 1, Princeton University.

[32] Cubasch, U., Hegerl, G.C., Hellbach, A., Höck, H., Mikolajewics, U., Santer, B.D., and Voss, R., 1995: A climate change simulation starting from 1935. Climate. Dynamics 11,71-84.

[33] Danabasoglu, G., and McWilliams, J.C., 1994: Sensitivity of the global ocean circulation to parameterizations of mesoscale tracer transports. J. Climate (submitted).

[34] Dickson, R.R., Meincke, J., Malmberg, S.A., and Lee, A.J., 1988: The "Great Salinity Anomaly" in the northern Atlantic 1968-1982. Prog. Ocean. 20,103-151.

[35] Dickson, R.R., and Brown, J., 1994. The production of North Atlantic Deep Water: Sources, rates and pathways. J. Geophys. Res. 99 (C6),12319-12341.

[36] Dietrich, G., Kalle, K., Krauss, W., Siedler, G., 1975: Allgemeine Meereskunde - Eine Einführung in die Ozeaneographie. Borntaeger, Berlin Stuttgart, 3. Auflage, 593 pp..

[37] Delworth, T., Manabe, S., and Stouffer, R.J., 1993: Interdecadal Variations of the thermohaline circulation in a coupled ocean-atmosphere model. J. Climate 6,1993-2011.

[38] Deser, C., and Blackmon, M.L., 1993: Surface Climate Variations over the North Atlantic Ocean during Winter: 1900-1989. J. Climate 6,1743-1753.

[39] Flato, G.M., and Hibler, W.D. III, 1992: Modeling pack ice as a cavitating fluid. J. Phys. Oceanogr. 22,626-651.

[40] Frankignoul, C., 1985: Sea surface temperature anomalies, planetary waves, and the air-sea feedback in middle latitudes. Rev. Geophys. 23 (4),357-390.

[41] Gent, P.R., McWilliams, J.C., 1990: Isopycnal mixing in ocean circulation models. J. Phys. Oceanogr. 20,150-155.

[42] Gerdes, R., Köberle, C., and Willebrand, J., 1991: The influence of numerical advection schemes on the results of ocean circulation models. Climate Dynamics 5,211-226.

[43] Ghil, M., 1976: Climate Stability for a Sellers-Type model. J. Atm. Sci. 33,3-20.

[44] Ghil, M., and Vautard, R., 1991: Interdecadal oscillations and the warming trend in global temperature time series. Nature 350,324-327.

[45] Greatbatch, R.J., and Zhang, S., 1994: An interdecadal oscillation in an idealized ocean basin forced by constant heat flux. J. Climate 8(1),81-91.

[46] Green, J.S.A., 1970: Transport properties of large-scale eddies and the general circulation of the atmosphere. Q. J. Roy. Meteor. Soc. 96,157-185.

[47] Griffel, D.H., and Drazin, P.G., 1981: On diffusive climatological models. J. Atm. Sci. 38,2327-2332.

[48] Griffies, S.M., and Tziperman, E., 1995: A linear thermohaline oscillator driven by stochastic atmospheric forcing. J. Climate (in press).

[49] Haney, R. L., Surface thermal boundary conditions for ocean circulation models. J. Phys. Ocean. 1, 241-248, 1971.

[50] Hasselmann, K., 1976: Stochastic climate models, Part 1, Theory. Tellus 28,289-485.

[51] Held, I.M., and Hou, A.Y., 1980: Nonlinear axially symmetric circulations in a nearly invicid atmosphere. J. Atm. Sci. 37,515-533.

[52] Held, I.M., 1978: The vertical scale of an unstable baroclinic wave and its importance for eddy heat flux parameterizations. J. Atm. Sci. 35, 572-576.

[53] Hellerman, S, and M. Rosenstein, 1983: Normal monthly wind stress over the world ocean with error estimates. J. Phys. Oceanogr. 13,1093-1104.

[54] Hibler, W.D. III, 1979: A dynamic thermodynamic sea ice model. J. Phys. Oceanogr. 9(4),815-846.

[55] Hibler, W.D. III, and Johnsen, S.J., 1979: The 20-yr cycle in ice core records. Nature 280,481-483.

[56] Holton, J. R., 1979: An Introduction to Dynamical Meteorology. Int. Geophysics. Ser., Vol. 23. Academic Press, 391 pp.

[57] Imbrie, J., Boyle, E.A., Clemens, S.C., Duffy, A., Howard, W.R., Kukla, G., Kutzbach, J., Martinson, D.G., McIntyre, A., Mix, A.C., Molfino, B., Morley, J.J., Peterson, L.C., Pisias, N.G., Prell, W.L., Raymo, M.E., Shackelton, N.J., and Toggweiler, J.R., 1992: On the structure and origin of major glaciation cycles. 1. Linear response to Milankovitch forcing. Paleoceanogr. 7(6),701-738.

[58] Jentsch, V., 1991: An energy balance climate model with hydrological cycle: 1. Model description and sensitivity to internal parameters. J. Geophys. Res. 96, 17,169-17,179.

[59] Jentsch, V., 1991: An energy balance climate model with hydrological cycle: 2. Stability and sensitivity to external forcing. J. Geophys. Res. 96, 17,181-17,193.

[60] Kann, D.M., Yang, S.-K., and Miller, A.J., 1994: Mean meridional transport of energy in the earth-atmosphere system using NMC global analyses and ERBE radiation data. Tellus 46A,553-656.

[61] Keigwin, L.D., Jones, G.A., Lehmann, S.J., and Boyle, E.A., 1991. Deglacial meltwater discharge, North Atlantic deep circulation, and abrupt climate change. J. Geophys. Res. 96,16811-16826.

[62] Keith, D.W., 1995: Meridional energy transport: uncertaity in zonal means. Tellus 47A,30-44.

[63] Kleeman, R., and Power, S.B., 1995: A simple atmospheric model of surface heat flux for use in ocean modeling studies. J. Phys. Oceanogr. 25(1),92-105.

[64] Kushnir, Y., 1994: Interdecadal Variations in North Atlantic Sea Surface Temperature and Associated Atmospheric Conditions. J. Climate 7,141-157.

[65] Lal, M., and Ramanathan, V., 1984: Effects of moist convection and water vapour radiative processes on climate sensitivit. J. Atm. Sci. 41, 2238-2249.

[66] Landau, L.D., and Lifschitz, 1970: Lehrbuch der Theoretischen Physik VI, VII. Akademie-Verlag.

[67] Latif, M. and Barnett, T.P., 1994: Causes of Decadal Climate Variability over the North Pacific and North America. Science 266,634-637.

[68] Ledley, T.S., 1988: A coupled energy balance climate-sea ice model: Impact of sea ice and leads on climate. J. Geophys. Res. 93 (D12),15919-15932.

[69] Ledley, T.S., 1991: Snow on sea ice: Competing effects in shaping climate. J. Geophys. Res. 96 (D9),17185-17208.

[70] Lehmann, S.J., and Keigwin, L.D.,1982: Sudden changes in North Atlantic circulation during the last deglaciation. Nature 356,757-762.

[71] Lemke, P., 1977: Stochastic climate models, Part 3, Application to zonally averaged energy models. Tellus 29,385-392.

[72] Lenderink, G., and Haarsma, R.J., 1994: Variability and multiple equilibria of the thermohaline circulation associated with deep-water formation. J. Phys. Oceanogr. 24,1480-1493.

[73] Leovy, C.B. 1973: Exchange of water vapour between the atmosphere and the surface of Mars. Icarus 18,120-125.

[74] Levitus, S., 1982: Climatological atlas of the world ocean. NOAA Professional paper 13, US Dept. of Commerce, NOAA, Washington DC, 172 pp.

[75] Lindzen, R.S., and Hou, A.Y., 1988: Hadley Circulation for Zonally Averaged heating Centered off the Equator. J. Atm. Sci. 45,2416-2427.

[76] Lindzen, R.S., and Ferrel, B., 1980: The Role of polar regions in global climate, and a new parameterization of global heat transport. Month. Weather Rev. 108,2064-2079.

[77] Lohmann, G., 1992: Stabilität stochastischer dynamischer Systeme, Diplom Thesis. Philipps-Universität Marburg, 146 pp..

[78] Lohmann, G., 1995: Stabilität der thermohalinen Zirkulation. DAAD Report, 88 pp..

[79] Lohmann, G., Gerdes, R., and Chen, D., 1994: Feedback mechanisms affecting the thermohaline circulation. Proceedings of WCRP Conference on the Dynamics of the Arctic Climate System, Gothenburg, Sweden.

[80] Lohmann, G., Gerdes, R., and Chen, D., 1995 a: Sensitivity of the thermohaline circulation in coupled oceanic GCM-atmospheric EBM experiments. Climate Dynamics (in press).

[81] Lohmann, G., Gerdes, R., and Chen, D., 1995 b: Stability of the thermohaline circulation in a simple coupled model. Tellus (in press).

[82] Lorenz, E.N., 1979: Forced and free variations of weather and climate. J. Atm. Sci. 36,1367-1376.

[83] Maas, L.R.M., 1994. A simple model for the three-dimensional thermally and wind-driven ocean circulation. Tellus 46A,671-680.

[84] Manabe, S., 1969: Climate and the ocean circulation 1. The atmospheric circulation and the hydrology of the earth's surface. Mon. Wea. Rev 97,739-774.

[85] Manabe, S., and Bryan, K., 1985: CO_2-induced change in a coupled ocean-atmosphere model and its paleoclimatic implications. J. Geophys. Res. 90, 11,689-11,707.

[86] Manabe, S., and Wetherald, R.T., 1967: Thermal equilibrium of the atmosphere with a given distribution of relative humidity. J. Atm. Sci. 24,241-259.

[87] Manabe, S., and Wetherald, R.T., 1980: On the distribution of climate change resulting from an increase in the CO_2 content of the atmosphere. J. Atm. Sci. 37, 99-118.

[88] Manabe, S., and Terpstra, T., 1974: The effects of mountains on the general circulation of the atmosphere as identified by numerical experiments. J. Atmos. Sci. 37,3-42.

[89] Manabe, S., and Stouffer, R.J., 1988: Two stable equilibria of a coupled ocean-atmosphere model. J. Climate 1,841-863.

[90] Manabe, S., and Stouffer, R.J., 1993: Century-scale effects of increased atmospheric CO_2 on the ocean-atmosphere system. Nature 364,215-218.

[91] Maier-Reimer, E., Mikolajewicz, U., Hasselmann, K., 1993: Mean circulation of the Hamburg LSG OGCM and its sensitivity to the thermohaline surface forcing. J. Phys. Ocean. 23,731-757.

[92] Marotzke, J., 1990: Instabilities and multiple equilibria of the thermohaline circulation. Ph.D. Thesis, Kiel University, 126 pp.

[93] Marotzke, J. and Willebrand, J., 1991: Multiple equilibria of the global thermohaline circulation, J. Phys. Oceanogr.21, 1372-1385.

[94] Marotzke, J., 1994: Ocean models in climate problems. In: Ocean processes in climate dynamics: Global and mediterranean examples, 79-109. P. Malanotte-Rizzoli and A.R. Robinson (eds.), Kluwer, Amsterdam.

[95] Marotzke, J. and Stone, P.H., 1995: Atmospheric transports, the thermohaline circulation, and flux adjustments in a simple coupled model. J. Phys. Oceanogr. 25,1350-1364.

[96] Matteucci, G., 1989: Orbital forcing in a stochastic resonance model of the Late-Pleistocene climate variations. Climate Dynamics 3,179-190.

[97] McCave, N., Manighetti, B., and Beveridge, N.A.S., 1995: Circulation in the glacial North Atlantic inferred from grain-size measurements. Nature 374(9),149-151.

[98] Mikolajewicz, U., Maier-Reimer, E., 1994: Mixed boundary conditions in ocean general circulation models and their influence on the stability of the model's conveyor belt. J. Geophys. Res. 99 (C11),22633-22644.

[99] Miller, J.R., Russel, G.L., and Calisi, G., 1994: Continental-scale river flow in climate models. J. Climate 7(6),914-928.

[100] Moritz, R.E., 1979: Nonlinear analysis of a simple sea ice-ocean temperature oscillator model. J. Geophys. Res. 84 (C8),4916-4920.

[101] Nakamura, M., Stone, P.H., and Marotzke, J., 1994: Destabilization of the thermohaline circulation by atmospheric eddy transports. J. Climate 7,1870-1882.

[102] Nicolis, C., 1979: The effect of solar output, infrared cooling and latitudinal heat transport on the evolution of the earth's climate. Tellus 31,193-198.

[103] North, G. R., 1975 a: Analytical solution of a simple climate model with diffusive heat transport. J. Atm. Sci. 32, 1300-1307.

[104] North, G. R., 1975 b: Theory of energy-balance climate models. J. Atm. Sci. 32, 2033-2043.

[105] Oberhuber, J.M., 1988. An atlas based on the COADS data set: The budgets of heat, buoyancy and turbulence kinetic energy at the surface of the global ocean. Max-Planck-Institute for Meteorology, Report No. 15.

[106] Olbers, D.J., Wenzel, M., and Willebrand, J., 1985: The inference of North Atlantic circulation patterns from climatological hydrographic data. Rev. Geophys. 23(4),313-356.

[107] Oort, A. H., 1983: Global atmospheric circulation statistics, 1958-1973. NOAA Prof. Pap. No. 14, Govt. Printing Office, Washington, D.C., 180 pp+microfiches.

[108] Oort, A.H., Peixoto, J.P., 1983: Global angular momentum and energy balance requirements from observations. Adv. Geophys. 25,355-490.

[109] Pacanowski, R.K., Dixon, K., Rosati, A., 1991,1993: The GFDL modular ocean model user's guide. GFDL Techn. Report 2, Princeton University.

[110] Peixoto, J.P., 1995: The role of the atmosphere in the water cycle. In: The role of water and the hydrological cycle in global change. H.D. Oliver, and S.A. Oliver (eds.), Springer, Berlin Heilberg New York Tokyo.

[111] Peng, L., Chou, M., and Arking, A., 1982: Climate studies with a multi-layer energy balance model. Part I: Model description and sensitivity to the solar constant. J. Atm. Sci. 39,2639-2656.

[112] Peng, L., Chou, M., and Arking, A., 1987: Climate warming due to increasing atmospheric CO_2: Simulations with a multilayer coupled atmosphere-ocean seasonal energy balance model. J. Geophys. Res. 92 (D5),5505-5521.

[113] Power, S.B., and Kleeman, R. , 1994: Surface heat flux parameterizations and the response of OGCMs to high latitude freshening. Tellus, 46A,86-95.

[114] Power, S.B., Kleeman, R. , Colman, R.A., and McAvaney, B.J., 1995: Modeling the surface heat flux response to long-lived SST anomalies in the North Atlantic. J. Climate 8,2161-2180.

[115] Rahmstorf, S., 1994: Rapid climate transitions in a coupled ocean-atmosphere model. Nature 372,3,82-85.

[116] Rahmstorf, S., 1995 a: Multiple convection patterns and thermohaline flow in an idealized OGCM. J. Climate (in press).

[117] Rahmstorf, S., 1995 b: Sensitivity of the North Atlantic circulation to changes in the hydrological cycle. Nature 378(9),145-149.

[118] Rahmstorf, S. and Willebrand, J., 1995: The role of the temperature feedback in stabilizing the thermohaline circulation. J. Phys. Oceanogr. 25,787-805.

[119] Rennick, M. A., 1977: The parameterization of tropospheric lapse rates in terms of surface temperature. J. Atm. Sci. 34, 854-862.

[120] Reverdin, G., Cayan, D., Dooley, H.D., Ellet, D.J., Levitus, S., Penhoat, Y., and Dessier, A., 1994: Surface salinity of the North Atlanic: Can we reconstruct its fluctuations over the last hundred years ? Prog. Oceanog. 33,303-346.

[121] Rieckers, A. and Stumpf, H., 1977: Themodynamik Bd. 2. Vieweg, 385 pp.. Rind, D., Peteet, D., Broecker, W., McIntyre, A., and Ruddiman, W., 1986: The impact of North Atlanic sea surface temperatures on climate: Implications for the Younger Dyras cooling (11-10k). Climate Dynamics 1,3-33.

[122] Saltzmann, B., 1978: A survey of statistical-dynamical models of the terrestrial climate. Adv. Geophys. 20,183-304.

[123] Sander, J., Wolf-Gladrow, D., and Olbers, D., 1995: Numerical studies of open ocean deep convection. J. Geophys. Res. 100(C10),20579-600.

[124] Sarntheim, M., Winn, K., Jung, S.J.A., Duplessy, J.-C., Labeyrie, L., Erlenkeuser, H., and Ganssen, G., 1994: Changes in east Atlantic deep water circulation over the last 30,000 years: Eight time slice reconstructions. Palaeoceanogr. 9 (2),209-267.

[125] Sausen, R., Barthels, R.K., and Hasselmann, K., 1988: Coupled ocean-atmosphere models with flux correction. Climate Dynamics 2,154-163.

[126] Schmetz, J., and Raschke, E., 1979: An Application of a Two-Stream Approximation to calculations of the Transfer of Solar Radiation in an Atmosphere with Fractional Cloud Cover. Contr. Atmosph. Phys. 52,151-160.

[127] Schmetz, J., 1984: On the parameterisation of the radiative properties of broken clouds. Tellus 36A,417-432.

[128] Schneider, S.H., 1972: On the carbon dioxide-climate confusion. J. Atmos. Sci. 32,2060-2066.

[129] Schopf, P.S., 1983: On equatorial waves and El Nino. II: Effects of air-sea thermal coupling. J. Phys. Oceanogr. 21,1725-1739.

[130] Sellers, W.D., 1969: A global climate model based on the energy balance of the earth-atmosphere system. J. Appl. Meteorol. 8, 392-400.

[131] Sellers, W.D., 1973: A new global climate model. J. Appl. Meteorol. 12, 241-254.

[132] Send, U., and Marshall, J., 1995: Integral effects of deep convection. J. Phys. Oceanogr. 25,855-872.

[133] Shepherd, T.G., 1989: Nonlinear saturation of baroclinic instability. Part II: Continuously statified fluid. J. Atm. Sci. 46,888-907.

[134] Shepherd, T.G., 1993: Nonlinear saturation of baroclinic instability. Part III: Bounds on the energy. J. Atm. Sci. 50,2697-2709.

[135] Shutts, G.J., 1978: Quasi-geostrophic planetary forcing. Q.J.R. Meteorol. Soc. 104,331-350.

[136] Stocker, T.F., and Wright, D.G., 1991: A zonally averaged ocean model for the thermohaline circulation. Part II: Interocean circulation in the Pacific-Atlantic system. J. Phys. Oceanogr. 21,1725-1739.

[137] Stocker, T.F., Wright, D.G., and Mysak, L.A., 1992: A zonally averaged, coupled ocean-atmosphere model for paleoclimate studies. J. Climate 5,773-797.

[138] Stommel, H.M., 1961: Thermohaline convection with two stable regimes of flow. Tellus 13,224-230.

[139] Stommel, H.M., 1993: A conjectural regulating mechanism for determining the thermohaline structure of the oceanic mixed layer. J. Phys. Oceanogr. 23,142-148.

[140] Stone, P.H. and Miller, D.A. , 1980: Empirical relations between seasonal changes in meridional fluxes of heat. J. Atm. Sci. 37,1708-1721.

[141] Stone, P.H. and Yao, M.S., 1990: Development of a two-dimensional zonally averaged statistical-dynamical model. Part III: The parametrisation of the eddy fluxes of heat and moisture. J. Climate 3,726-740.

[142] Tang, B., and Weaver, A.J., 1995: Climate stability as deduced from an idealized coupled atmosphere-ocean model. Climate Dynamics 11,141-150.

[143] Trefethen, L.N., Trefethen, A.E., Reddy, S.C., and Driscoll, T.A., 1993: Hydrodynamic stability without eigenvalues. Science 261,578-584.

[144] Vallis, G.K., 1982: A statistical-dynamical climate model with a simple hydrological cycle. Tellus 34,211-227.

[145] Warren, B.A., 1983: Why is no deep water formed in the North Pacific? J. Mar. Res. 41,327-347.

[146] Warren, S. G. and S. H. Schneider, 1979: Seasonal simulations as a test for uncertainties in the parameterizations of a Budyko-Sellers zonal climate model. J. Atm. Sci. 36, 1377-1391.

[147] Washington, W.M., and Meehl, G.A., 1983: General circulation model experiments on the climatic effects due to a doubling and quadrupling of carbon dioxide concentration. J. Geophys. Res. 88, 6600-6610.

[148] Washington, W.M., and Meehl, G.A., 1984: A seasonal cycle experiment on the climatic sensitivity due to a doubling of CO_2 with an atmospheric general circulation model coupled to a simple mixed layer ocean model. J. Geophys. Res. 89, 9475-9503.

[149] Weaver, A.J. and Sarachick, E.S., 1991: Evidence for decadal variability in an ocean general circulation model: An advective mechanism. Atmosph.-Ocean 29,197-231.

[150] Weaver, A.J., Sarachick, E.S., and Marotzke, J., 1991: Freshwater flux forcing of decadal and interdecadal oceanic variability. Nature 353,836-838.

[151] Weaver, A. J., Marotzke, J., Cummins, P.F., and Sarachik, E.S., 1993: Stability and variability of the thermohaline circulation. J. Phys. Oceanogr.23, 39-60.

[152] Welander, P., 1986: Thermohaline effects in the ocean circulation and related simple models. In: Large-scale transport processes in oceans and atmosphere, J. Willebrand and D.T.A. Anderson, eds., Reidel, 163-200.

[153] White, A.A., and Green, J.S.A., 1982: A non-linear atmospheric long wave model incorporating parameterizations of transient baroclinic eddies. Quart. J. R. Met. Soc. 108,55-85.

[154] Wijffels, S.E., Schmitt, R.W., Bryden, H.L., and Stigebrandt, A., 1992: Transport of fresh water by the oceans. J. Phys. Oceanogr. 22,155-162.

[155] Willebrand, J., 1993: Forcing the ocean with heat and fresh water fluxes. In: Energy and water cycles in the climate system, E. Raschke, ed., Springer, Berlin Heilberg New York Tokyo.

[156] Winton, M., 1994: On the role of horizontal boundaries in parameter sensitivity and decadal-scale variability of coarse-resolution ocean circulation models. J. Phys. Oceanogr. (submitted).

[157] Winton, M., 1995: Why is deep sinking narrow ? J. Phys. Oceanogr. 25(5),997-1005.

[158] Winton, M., and Sarachik, 1993: Thermohaline oscillations induced by strong steady salinty forcing of ocean general circulation models. J. Phys. Oceanogr. 23(7),1389-1410.

[159] Wright, D.G., and Stocker, T.F., 1991: A zonally averaged ocean model for the thermohaline circulation. Part I: Model development and flow dynamics. J. Phys. Oceanogr. 21,1713-1724.

[160] Yang, J. and Neelin, J.D., 1993: Sea-ice interaction with the thermohaline circulation. Geophys. Res. Lett., Vol.20(2),217-220.

[161] Zaucker, F. and Broecker, W.S. 1992: The influence of atmospheric moisture transport on fresh water balance of the Atlantic drainage basin: General circulation model simulations and observations. J. Geophys. Res. 97, 2765-2773.

[162] Zhang, S., Greatbatch, R.J., and Lin, C.A., 1993: A reexamination of the polar halocline catastrophy and implications for coupled ocean-atmosphere modeling. J. Phys. Oceanogr. 23,287-299.

[163] Zhang, S., Lin, C.A., and Greatbatch, R.J., 1995: A decadal oscillation due to coupling between an ocean circulation model and a thermodynamic sea-ice model. J. Mar. Res. 53,79-106.

Acknowledgments

I would like to thank Dr. Rüdiger Gerdes, Dr. Deliang Chen, and Prof. Dr. Dirk Olbers for their support and many helpful suggestions improving the manuscript. Dr. Chris Dodge, Cornelia Köberle, and Dr. Rebecca Woodgate are gratefully acknowledged for reading parts of the thesis and clarifying the language.

I would like to acknowledge the great help and advice during the research of Dr. Rüdiger Gerdes without whom this work would not have been successful, as well as Dr. Deliang Chen for teaching me about energy balance climate models and supporting a friendly stay at his department at Göteborg's University. Furthermore, I appreciate the constructive suggestions of Prof. Dr. Dirk Olbers who initiated the present work.

Thanks go to the Alfred Wegener Institute (AWI) computer group for their help and to Cornelia Köberle for sharing me her post-processing program. Many thanks are due to the members of the Physics department of the AWI for creating a stimulating working environment. Finally, Anne Heilemann is acknowledged for her support during writing the thesis.